WARM GAS TVC DESIGN STUDY

Final Technical Report
Contract NAS8-28651

September 1973

OR 12,796 Copy

by

Seth B. Moorhead, Jr.

Prepared for

George C. Marshall Space Flight Center
National Aeronautics and Space Administration

Martin Marietta Aerospace
Orlando Division
Post Office Box 5837
Orlando, Florida 32805

PRECEDING PAGE BLANK NOT FILMED

PRECEDING PAGE BLANK NOT FILMED

TABLE OF CONTENTS

Preface v

1.0 Summary 1

2.0 Warm Gas TVC System 3

- 2.1 Injection Geometry Analysis 3
- 2.2 Material Selection. 9
- 2.3 Performance Analysis 9
- 2.4 Structural Analysis 23
- 2.5 Valve Torque Analysis 27
- 2.6 Thermophysical Analysis 28

3.0 High Contaminant Direct Drive Servovalve 37

- 3.1 Torque Motor Design Analysis 37
- 3.2 Spool Valve Design Analysis 39
- 3.3 Performance Analysis 47
- 3.4 Layout 51
- 3.5 Design Critique 56

4.0 Conclusions 59

5.0 Appendix 61

- 5.1 References 61
- 5.2 Glossary of Symbols 62
- 5.3 Detail Drawings - Gas Injection TVC System 63
- 5.4 Detail Drawings - High Contaminant, Direct Drive Servovalve 73

ILLUSTRATIONS

2.1-1 Injection Flow Rate versus Location 4
2.1-2 Control Flow Rate versus Location 5
2.1-3 Injection Flow Rate versus Angle. 7
2.1-4 Control Flow Rate versus Angle. 8
2.3-1 Conditions for Maximum Interaction Side Force 11
2.3-2 Comparison of Predicted and Experimental Side Force Coefficients, Injection of Air into Air 12
2.3-3 Comparison of Specific Impulse Ratio for Hot Air Injection H_2O_2 Decomposition Product. 13
2.3-4 Comparison of Predicted and Experimental Side Force Coefficients, Injection of Ar and He into H_2O_2 Decomposition Products. 14
2.3-5 Side Force Coefficient versus Momentum Ratio. 16
2.3-6 Side Force Coefficient versus Momentum Ratio. 17
2.3-7 TVC Angle versus Injection Position 19
2.3-8 TVC Angle versus Injection Mach Number. 20
2.3-9 TVC Angle versus Injection Angle. 21
2.3-10 TVC Angle versus Injection Location 22
2.3-11 Variation of TVC Angle with Injection Mach Number 24
2.3-12 Variation of TVC Angle with Injection Angle 25
2.4-1 Warm Gas TVC Design Study 29
2.6-1 L-605 Thermophysical Properties (Actuator Shaft, Tube). 31
2.6-2 4130 Steel Thermophysical Properties. 32
2.6-3 C-103 Thermophysical Properties (Butterfly Valve) 33
2.6-4 Components Growth Comparison. 34
3.1-1 Schematic Diagram of Permanent Magnet Torque Motor. 37
3.2-1 Schematic of Spool Valve. 40
3.2-2 Schematic of Valve-Actuator-Mass-Spring-Dashpot System. 41
3.2-3 Flow Paths. 46
3.2-4 Geometry for Determining X_{1d}. 47
3.2-5 Geometry for Determining X_{2d}. 47
3.3-1 Block Diagram Representation of the Electro-Hydraulic Servo-Actuator. 48
3.3-2 Simulated Valve Step Responses. 52
3.3-3 Predicted Frequency Responses 54
3.4-1 Finalized Layout of Valve 55

TABLES

2.2-I High Temperature Materials - Properties Comparison. 10
2.3-I Comparison of Predicted and Experimental Results. 18
2.4-I Summary of Design Configuration Structural Study. 26
2.6-I Component Thermophysical Properties 30
3.3-I Block Diagram Nomenclature. 49

PRECEDING PAGE BLANK NOT FILMED

PREFACE

Maneuvering control of rocket powered vehicles can be efficiently achieved through angular deflection of the thrust vector. These deflections can be obtained either by mechanical means (deflecting the engine or nozzle) or by secondary injection. In the secondary injection system, the nozzle is held fixed while the thrust vector is deflected by injecting a secondary flow of liquid or gas through the nozzle wall. Although liquid secondary injection systems are in common use on several vehicles, gaseous injection systems are theoretically more efficient, especially in cases where the gas is bled directly from the main thrust chamber. Recent progress in the development of hot gas valves and ducts together with analysis and test data on the forces generated by intersecting flows indicates that a chamber bleed gaseous secondary injection thrust vector control system is feasible.

The objectives of Contract NAS8-28651, "Warm Gas TVC System Design Study" were to optimize the injection geometry for a specific engine configuration and to design an injection valve capable of meeting the baseline requirements. To optimize injection geometry, studies were made to determine the performance effects of varying injection location, angle, port size, and port configuration. Having minimized the injection flow rate required through this study, a warm gas valve was designed to handle the required flow.

An additional objective was to analyze and design a direct drive hydraulic servovalve capable of operating with highly contaminated hydraulic fluid. The valve is sized to flow 15 gpm at 3000 psia and the direct drive feature is capable of applying a spool force of 200 pounds.

The baseline requirements are the development of 6° of thrust vector control utilizing 2000°F (total temperature) gas for 180 seconds on a 1.37 million pound thrust engine burning LOX and RP-1 at a chamber pressure of 250 psia with a 155 inch long conical nozzle having a 68 inch diameter throat and a 153 inch diameter exit.

1.0 SUMMARY

1.1 Thrust Vector Control Valve

For developing 6° of thrust vector control by injecting 2000°F gas, the injection geometry was optimized through an analytical study resulting in selection of an injection point at 60% of the distance from the nozzle throat to the nozzle exit (X/L = .6), an injection Mach number of 1.5 and an injection angle of 50° upstream from the nozzle wall using multi-point injection of 3 ports per quadrant. The analysis showed that a flow rate of 6.9% of the main engine flow would be required. Accordingly, for the 1.37 million pound thrust engine burning LOX and RP-1 at a chamber pressure of 250 psia, a set of 3 injection valves capable of flowing 425 pounds per second per quadrant was designed to operate for the 180 second flight time. The valve is a rotary butterfly type, each valve having a 12.19 inch diameter inlet, a plenum in which the gas is turned through 127°40', a butterfly valve forming the sonic throat, and an exit of 11.140 inch diameter. The material selected was Haynes 25 (L-605) alloy internally lined with rubber modified silica phenolic. The valve was specifically designed to be attached to the 155 inch long conical nozzle having a 68 inch diameter throat and a 153 inch diameter exit. Detail drawings were made suitable for fabrication of prototype valves for use in demonstration tests.

1.2 Direct Drive Hydraulic Servovalve

A direct drive hydraulic servovalve sized for a flow rate of 15 gallons per minute at 3000 psia and capable of supplying a spool force of 200 pounds was analyzed and designed. The computed performance analysis indicates a settling time to a step input of 6 to 19 milliseconds with 90° phase lag occurring at 117 cycles per second. The valve design provides for operating with highly contaminated fluid by using a spool diametral clearance of 0.0005 inch and a slightly underlapped spool and sleeve. The valve employs .014 inch diameter orifices for damping.

PRECEDING PAGE BLANK NOT FILMED

2.0 WARM GAS TVC SYSTEM

2.1 Injection Geometry Analysis

Injection of a gas or fluid into the side of a main thrust nozzle produces a localized flow disturbance resulting in a high pressure region inside the nozzle. Control of this injection flow can be used to control the magnitude of the localized pressure and the resulting side force on the vehicle. To obtain the optimum design, consideration must be given to injection angle and axial location.

Figure 2.1-1 plots the ratio of injection flow rate to main engine flow rate versus the axial location in the nozzle (test data in Reference 3). The data shows that for gaseous injection into a nozzle with a cone 1/2 angle of 10°, the optimum location from an injection flow rate standpoint is 66.5 percent aft of the nozzle throat for all thrust vector control angles from 3° to 10°. The empirically derived formula which fits the data shown is:

$$M_j/M_a = .25\ (X/L-.665)^2 + .0085\ (\Theta^\circ)$$

where

M_j = main engine flow rate

X = distance from nozzle throat to injection point

L = length of nozzle (from throat to exit)

Θ = TVC angle (angle whose tangent is the side force/ engine thrust).

The data shown in Figure 2.1-1 addresses the problem of optimizing the injectant flow only (i.e., minimizing the size and weight of the valves and ducts required) without accounting for the thrust variation that occurs at the different injection locations. In a chamber bleed thrust vector control system, the flow rate of gas needed for control purposes represents a loss in engine thrust efficiency. As the gas is injected into the nozzle, an increase in thrust occurs depending on the location of the injection point. After accounting for this change in thrust (which was also measured), the curves shown in Figure 2.1-2 were plotted to show the ratio of control flow rate to main engine flow rate versus axial injection location. The term "control flow" (M_C) is defined as that portion of the injectant flow which produces no thrust. The curves of Figure 2.1-2 show that the optimum injection

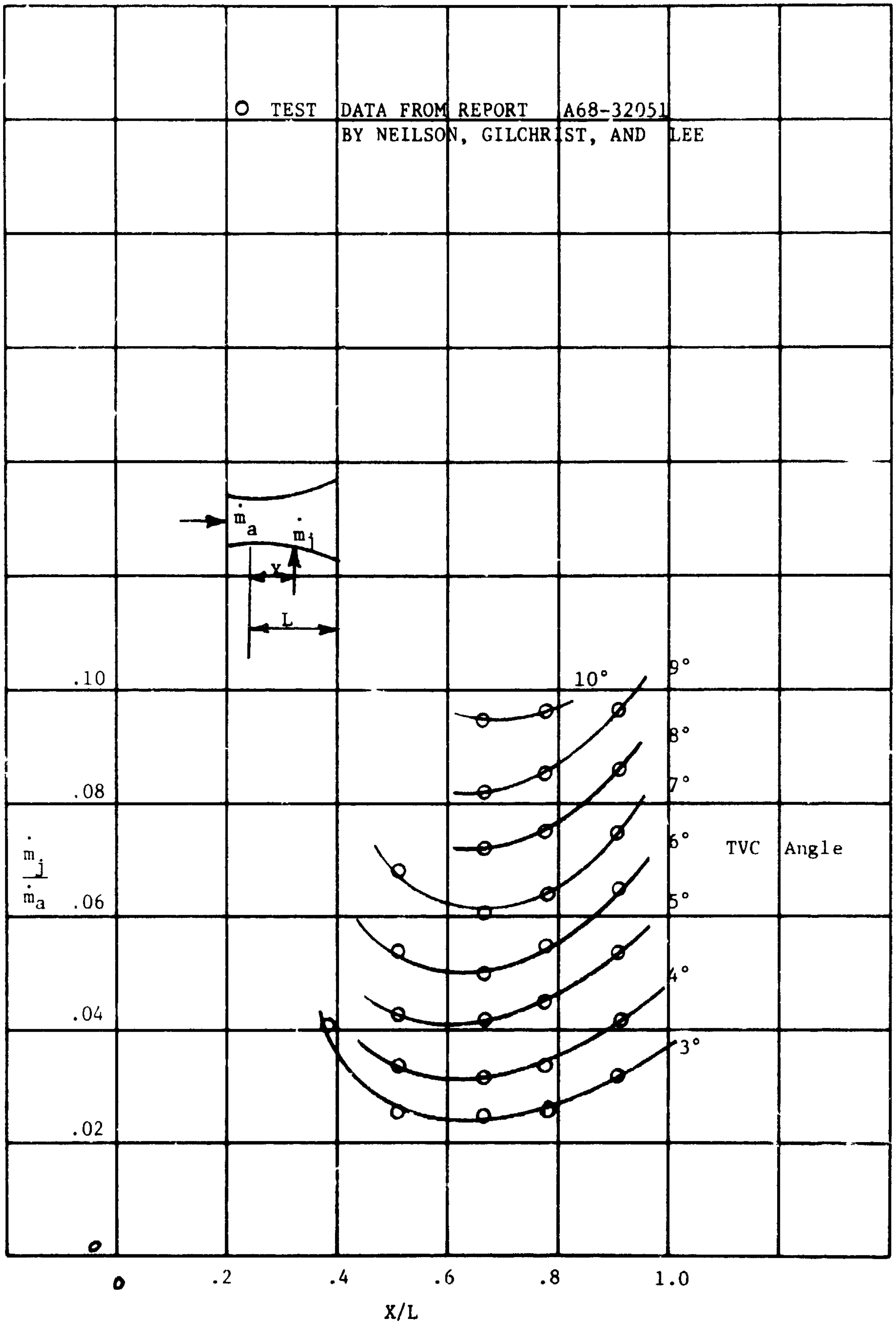

Figure 2.1-1. Injection Flow Rate versus Location

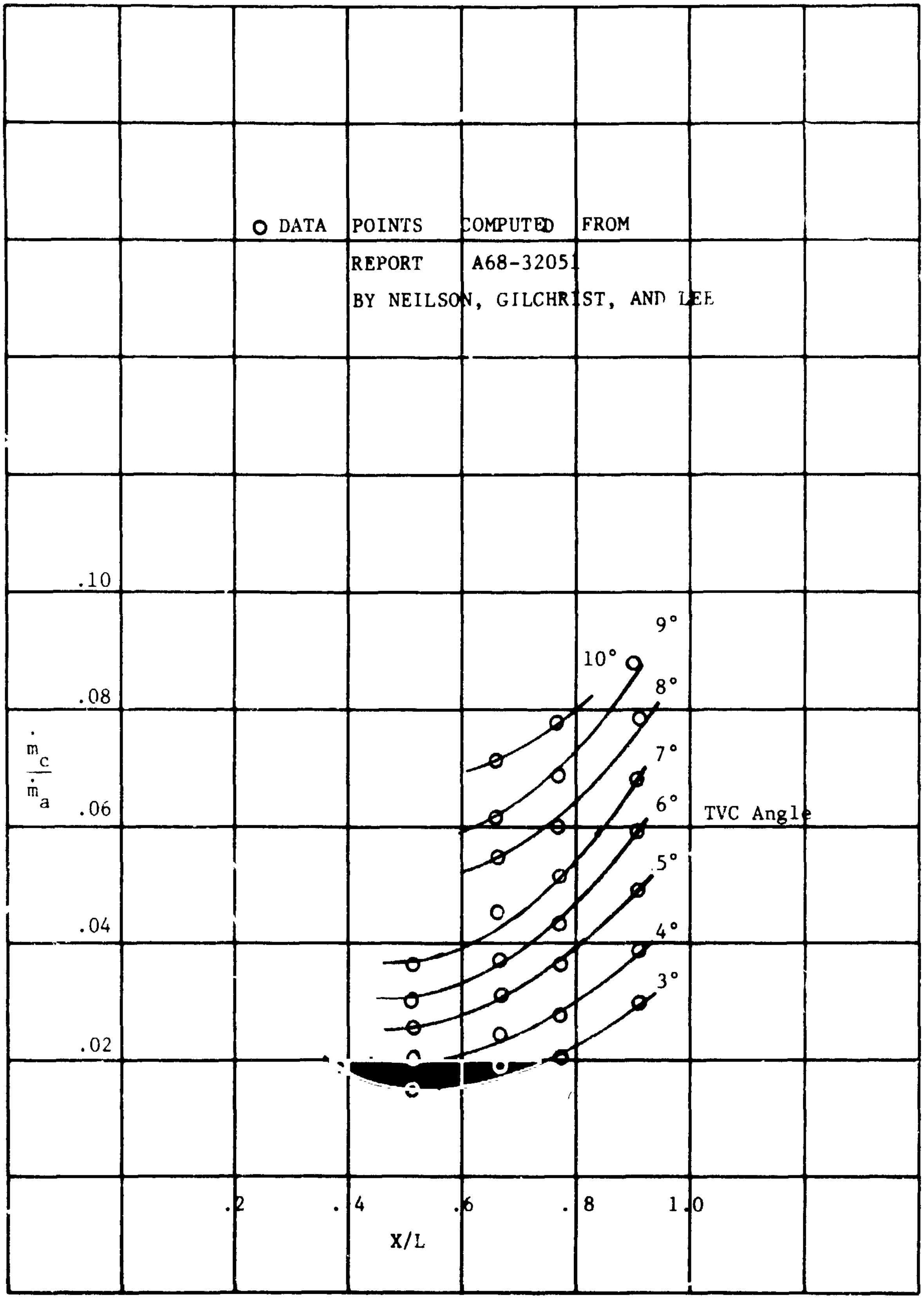

Figure 2.1-2. Control Flow Rate versus Location

location (from a standpoint of minimum thrust loss) is 51 percent aft of the nozzle throat. The empirically derived formula which fits the data shown is:

$$\dot{M}_c/\dot{M}_a = .18\ (X/L-.51)^2 + .005\ (\Theta^\circ).$$

As an example of how to apply Figure 2.1-2, a need is assumed to minimize the size and weight of a TVC valve capable of 6° TVC. Figure 2.1-1 shows the minimum required injection flow rate is 5 percent of main engine flow, using a single port normal sonic injector located 66.5 percent aft of the throat. Figure 2.1-2 shows propellant flow required for control producing no thrust is 3.7 percent of main engine propellant flow.

For a second example, a need is assumed to minimize thrust penalty to the engine while obtaining 6° TVC. Figure 2.1-2 shows minimum control flow to be 3 percent of the main engine flow with the injection point located 51 percent aft of throat. Figure 2.1-1 indicates that TVC duct and valve assemblies installed at that location must be sized to accommodate 5.4 percent of main engine flow. This assumes a single port, sonic injection with injector orientation normal to the main nozzle centerline, the main nozzle having a cone 1/2 angle of 10° with a throat to exit area ratio of 1.95.

For any vehicular application, TVC valve and duct hardware weight needs to be traded against propellant weight. From this, optimum injection point location must fall between 51 and 66.5 percent aft of the throat, depending on the control duty cycle. Where a 100 percent duty cycle and maximum burnout velocity are required, the performance penalty of fixed hardware weight is approximately twice that of expendable propellant weight. This makes an optimum injection point 2/3 of the distance back from the 51 percent point, 61.3 percent aft of the throat.

Figures 2.1-3 and 2.1-4 show the effect of varying the injection angle. The empirically derived expressions are:

$$\dot{M}_j/\dot{M}_a = 6.4 \times 10^{-6}\ (\varepsilon-30)^2 + .007\ (\Theta^\circ)$$

and

$$\dot{M}_c/\dot{M}_a = 3.2 \times 10^{-6}\ \varepsilon^2 + .0056\ (\Theta^\circ)$$

where ε is the angle between injection and a line perpendicular to the main nozzle centerline (in degree). Both curves and corresponding formulas show that the optimum injection angle for minimum valve and duct size is 30°, while the optimum angle for minimum fuel usage is 0°.

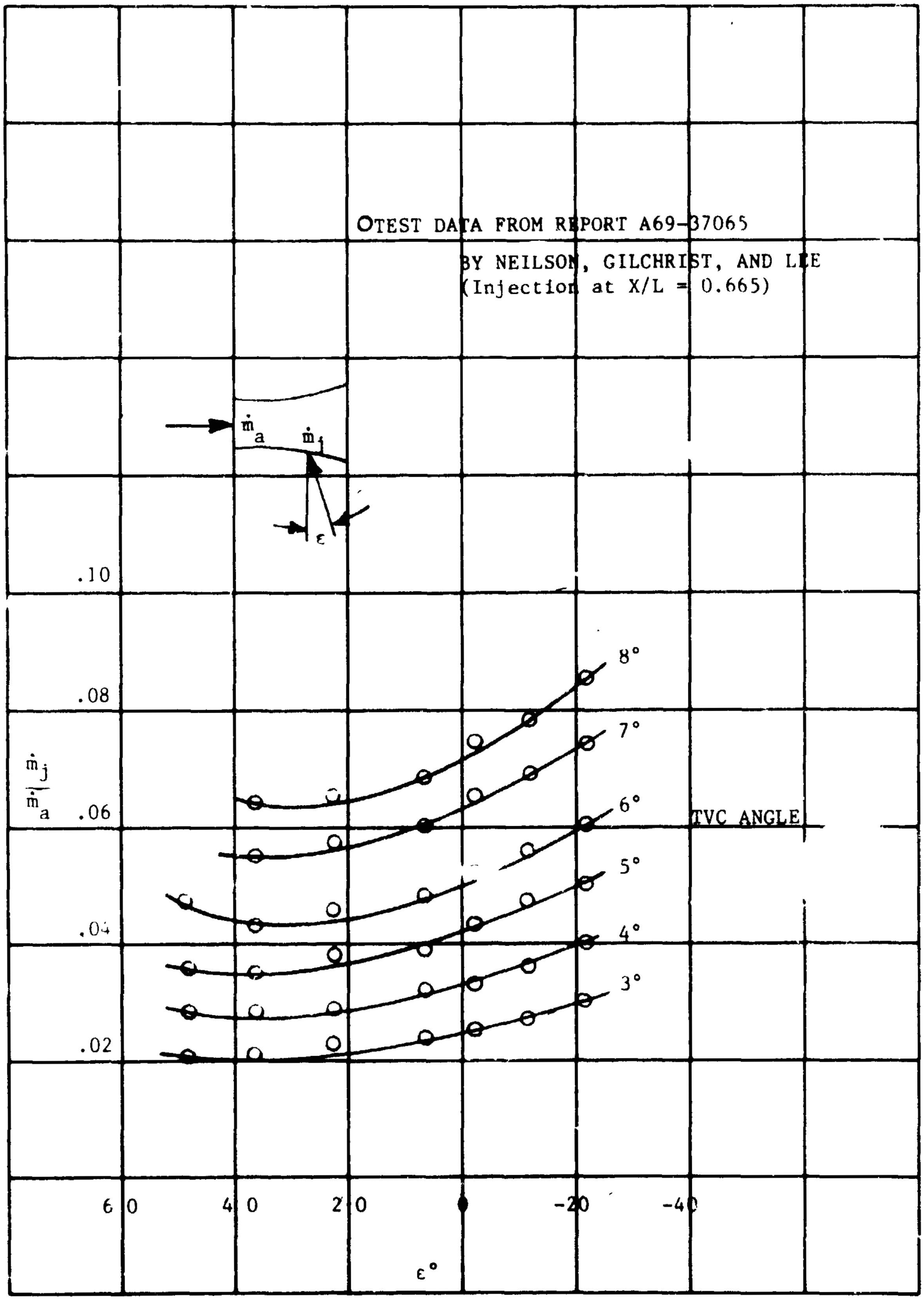

Figure 2.1-3. Injection Flow Rate versus Angle

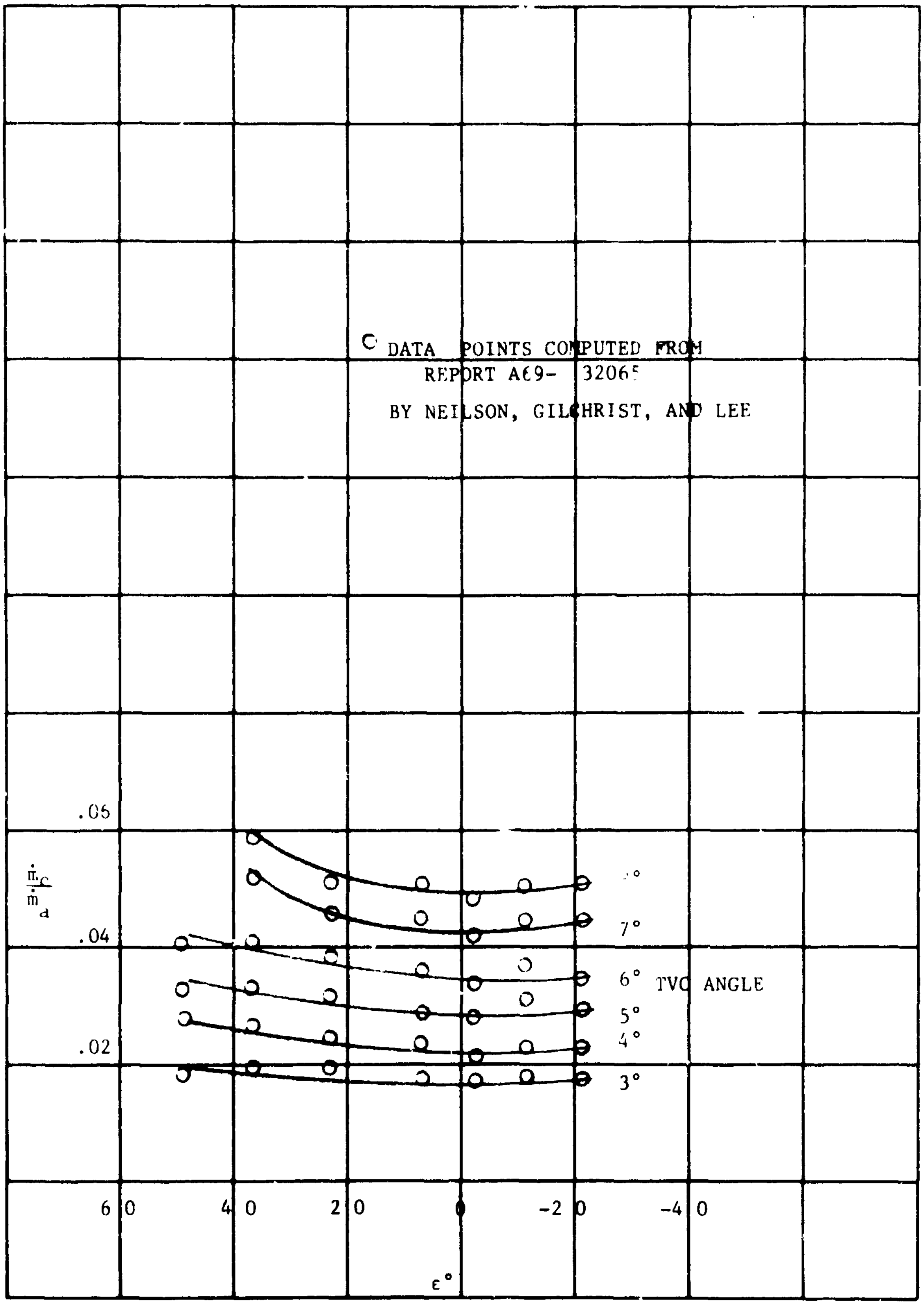

Figure 2.1-4. Control Flow Rate versus Angle

Again considering a 100 percent duty cycle and maximum burnout velocity as design criteria, overall system optimum injection angle should be 20°.

2.2 Material Selection

The materials selection study was completed with the candidates narrowed to two materials: 347 CRES and Haynes 25. The general requirement used were formability, weldability, weight, cost, and strength at 2000°F. Technical reports, manufacturer's literature and handbooks were reviewed for metals which would qualify as candidates. The literature survey revealed that a number of iron-, nickel-, cobalt-, and columbium-base alloys would qualify under the established requirements guidelines. The alloys selected as primary candidates were:

Iron-base:	347 CRES and N-155
Nickel-base:	Inconel X and Hastelloy X
Cobalt-base:	Haynes 25 (L-605)
Columbium-base:	C-103

The requirement for weldability (in anticipation of detailed design features) eliminates 316 CRES.

A summary of the mechanical and physical properties of the candidate materials are shown in Table 2.2-I. The low material cost of the 347 CRES coupled with its forming and welding qualities make it a primary candidate. The N-155, Inconel X and Hastelloy X alloys, although showing considerable strength advantages over 347 CRES at lower temperatures, indicate a negligible strength advantage at 2000°F which would not be worth the added cost. The Haynes 25 (L-605) has about twice the strength of 347 CRES at 2000°F which makes it also a primary candidate because of the lower weight design that would result. The C-103 alloy has a strength (weight) advantage at 2000°F but a very high cost and limited availability. The final selection between 347 CRES and Haynes 25 will be made during stress analysis of the design layout. The lower cost and ease of fabrication of the 347 CRES would be preferred; however, stress analysis may show that the higher strength of the Haynes 25 is required. Data from the stress analysis will also allow a cost versus weight tradeoff between these two materials.

2.3 Performance Analysis

The performance analysis was undertaken using a FORTRAN program on an IBM 360 computer. This program provided a baseline for performance of a gaseous secondary injection TVC. The program computes induced forces using blast wave theory for high secondary mass flow rates, and linearized supersonic flow theory coupled with one-dimensional analysis for low secondary flow rates. The program also computes side forces for both cases and selects the lower value. Inputs used include:

TABLE 2.2-I

High Temperature Materials - Properties Comparison

Material Designation	347 CRES Steel	N-155	Inconel X	Hastelloy X	Haynes 25(L-605)	C-103
Composition, % Primary Elements	18Cr-10Ni-0.7Cb .07C-BAL.Fe	21Cr-20Ni-20Co-3Mo-2W-BAL.Fe	15Cr-7Fe-2.5Ti 1Cb-0.7Al-BAL.Ni	22Cr-18Fe-9Mo-1.5Co-0.5W-BAL.Ni	20Cr-15W-10Ni-BAL. Co.	10Hf-1Ti-0.7Zr-BAL.Cb
Density, lbs./in^3	0.290	0.296	0.298	0.297	0.330	0.320
Melting Range, °F	2550-2600	2325-2475	2540-2600	2300-2470	2425-2570	4260
Coeff. Thermal Expansion, x10^{-6} in/in/°F	11.2(1800)	10.14(1800)	9.75(1800)	9.2(1800)	9.41(1800)	4.5(2200)
Modulus of Elasticity psi 70°F (°F)	29.0 x 10^6 18.7 x 10^6(1600)	29.3 x 10^6 20.8 x 10^6(1500)	31.0 x 10^6 18.5 x 10^6(1500)	28.3 x 10^6 18.3 x 10^6(1800)	34.2 x 10^6 21.5 x 10^6(1800)	13.1 x 10^6 12.3 x 10^6(2000)
Tensile Strength, ksi	90 @ 70°F 21 @ 1600°F 10 @ 2000°F	118 @ 70°F 39 @ 1600°F 13 @ 2000°F	130 @ 70°F 52 @ 1500°F 9 @ 1800°F	113 @ 70°F 37 @ 1600°F 13 @ 2000°F	146 @ 70°F 47 @ 1600°F 19 @ 2000°F	61 @ 70°F 27 @ 2000°F 13 @ 2500°F
Yield Strength, ksi	37 @ 70°F 16 @ 1600°F 6 @ 2000°F	58 @ 70°F 30 @ 1600°F 8 @ 2000°F	60 @ 70°F 44 @ 1500°F 6 @ 1800°F	52 @ 70°F 26 @ 1600°F 8 @ 2000°F	67 @ 70°F 35 @ 1600°F 12 @ 2000°F	42 @ 72°F 20 @ 2000°F 10 @ 2500°F
Elongation, Percent	50 @ 70°F 76 @ 1600°F 85 @ 2000°F	49 @ 70°F 15 @ 1600°F 38 @ 2000°F	40 @ 70°F 22 @ 1500°F 89 @ 1800°F	43 @ 70°F 51 @ 1600°F 40 @ 2000°F	64 @ 70°F 30 @ 1600°F 34 @ 2000°F	20 @ 70°F 45 @ 2000°F 70 @ 2500°F
Tensile Strength to Density Ratio	310 x 10^3 @ 70°F 34.5x10^3@ 2000°F	398x10^3 @ 70°F 43.9x10^3@2000°F	437x10^3 @ 70°F 30.2x10^3@2000°F	380x10^3 @ 70°F 43.7x10^3@2000°F	442x10^3 @ 70°F 57.6x10^3@2000°F	191x10^3 @ 70°F 84.4x10^3@2000°F
Modulus to Density Ratio	100x10^6 @ 70°F 64.5x10^6@1600°F	99x10^6 @ 70°F 70.2x10^6@1500°F	104x10^6 @ 70°F 62x10^6 @ 1500°F	95.2x10^6 @ 70°F 61.7x10^6 @ 1500°F	104x10^6 @ 70°F 65x10^6 @1800°F	41x10^6 @ 70°F 38.4x10^6@2000°F
Formability	Excellent	Good	Good	Good	Good	Good
Weldability	Good	Satisfactory	Satisfactory	Satisfactory	Satisfactory	Satisfactory
Availability	Excellent	Good	Good	Good	Good	Limited
Approx. Cost, $/Lb.	1.50	5.00	4.00	5.00	5.00	95.00
Remarks:	A stabilized 18-8 CRES steel used as the base line mtl.	Used extensively in the range of 1200 to 2000°F.	Excellent oxidation and corrosion resistance to 1800°F.	Excellent oxidation resistance up to 2200°F.	Used where high stresses exist in the range of 1700-2200°F.	Used in application where the temperatures may approach 2600°F.

pressure, temperature, molecular weight, Mach number, nozzle dimensions, injection location, and injection angle.

Using data reported by Walker, Stone, and Shander (Reference 1 and 2), program results were checked for agreement between predicted and measured side forces. Average error for 12 data points was 4.8 percent.

The analytical model for predicting the performance of gaseous secondary injection thrust vector control system performance was then modified to more realistically estimate the maximum pressure in the primary nozzle upstream of the secondary jet. Prediction of the secondary injection shock shape was also added to the program so that a physical interpretation of the program output could be made. This term serves as a maximum limiting condition for the blast wave model when the shock impingement on the primary nozzle crosses a position 90° from the secondary nozzle position. This is shown in Figure 2.3-1.

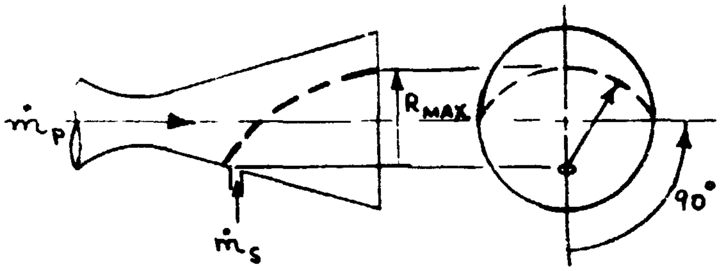

Figure 2.3-1. Conditions for Maximum Interaction Side Force

This limiting condition explains why the experimental data of Reference 3 fall off rapidly above mass flow ratios which are predicted to produce maximum interaction side force.

Comparisons of predicted side force coefficient and specific impulse ratio with experimental data for both cold and hot air are shown in Figures 2.3-2 and 2.3-3, respectively. Although there were some variations, the overall level of the predictions compared with experimental data within about 10-12 percent. Comparisons of argon and helium as secondary injection gases is shown in Figure 2.3-4. The blast wave prediction technique agrees quite well with the test data, except for the extremely low mass flow ratios for argon. These comparisons were adequate to conclude that the program was capable of predicting performance of gas injection TVC systems.

It is known that as momentum ratio increases, spreading the shock shape toward the maximum diameter of the main nozzle, the side

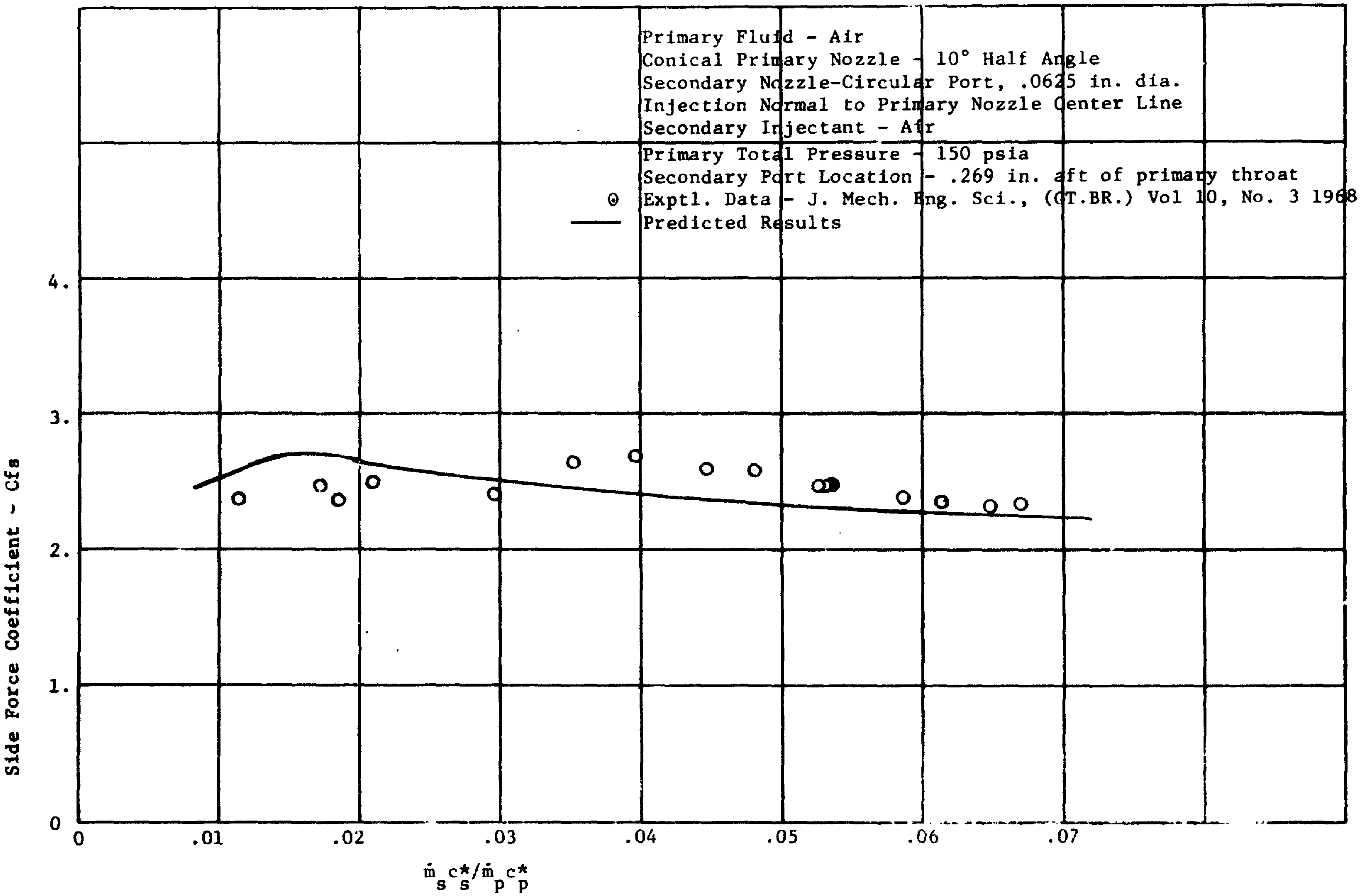

Figure 2.3-2. Comparison of Predicted and Experimental Side Force Coefficients, Injection of Air into Air P_p^T = 150, χ/L = 0.508, D_s^* = 0.0625

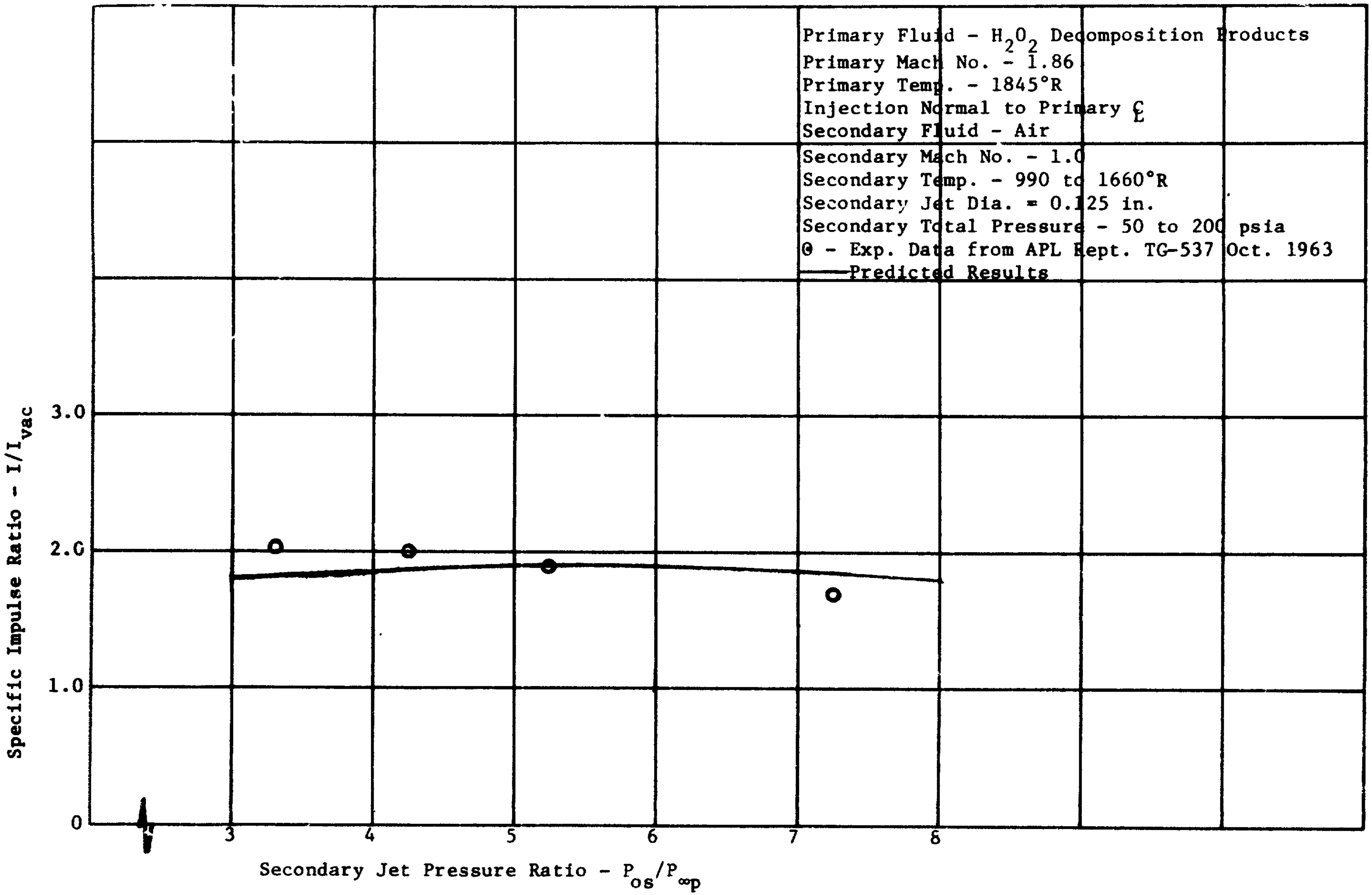

Figure 2.3-3. Comparison of Specific Impulse Ratio for Hot Air Injection H_2O_2 Decomposition Products

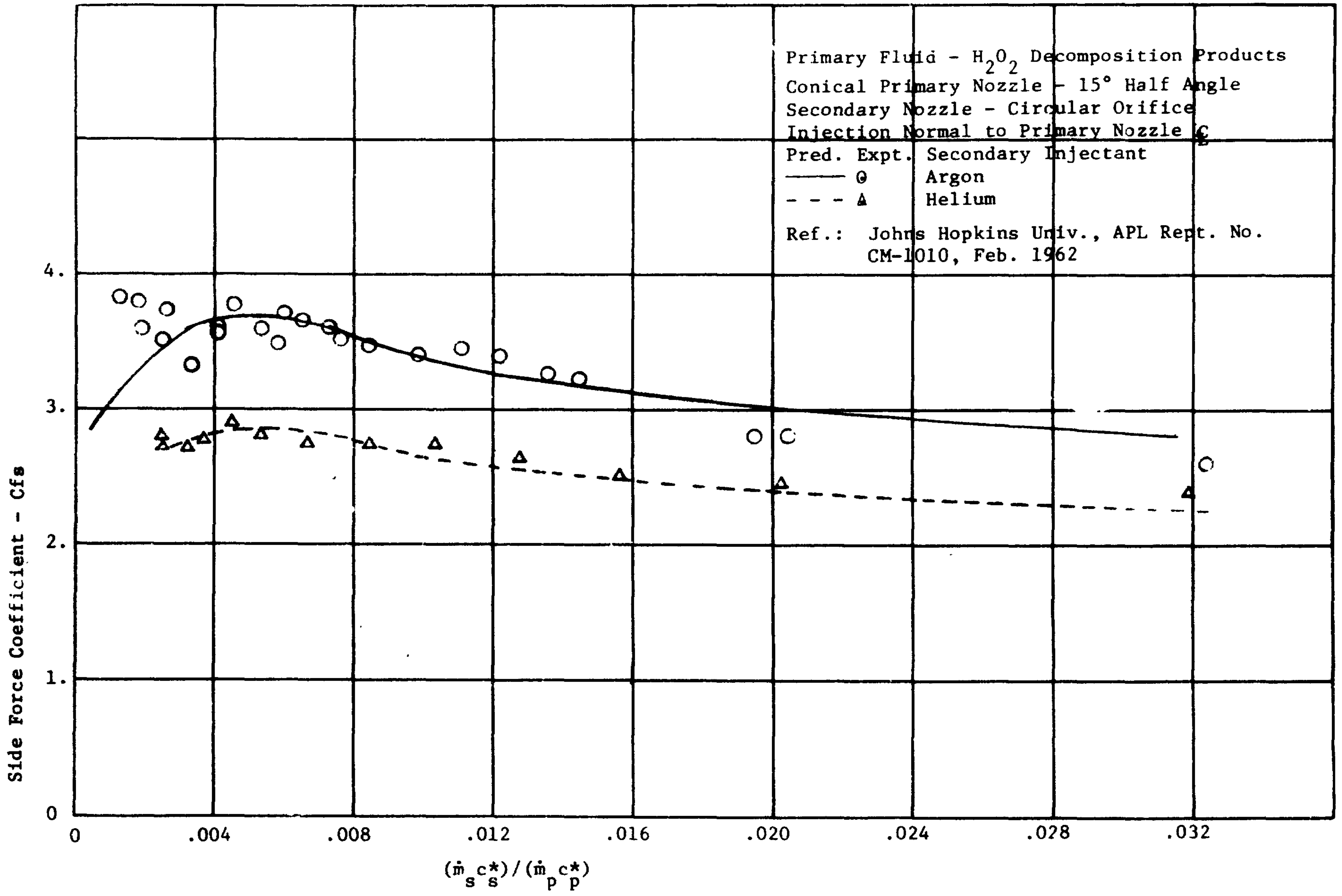

Figure 2.3-4. Comparison of Predicted and Experimental Side Force Coefficients, Injection of Ar and He into H_2O_2 Decomposition Products

force coefficient reaches a maximum value. Figures 2.3-5 and 2.3-6 illustrate the close correlation obtained between the predicted and actual momentum ratios to obtain peak side force coefficients. The experimental data shown is from two test conditions of Reference 3.

Results from the modified second-order blast wave shock shape prediction model were compared to experimental data from many sources over a wide range of test conditions, including both hot and cold gas injection. Table 2.3-I summarizes the results of these comparisons. The blast wave/shock shape prediction technique compared with experimental data within +10 to -25 percent for all 33 cases considered. The larger variations (up to -25%) were on the conservative side (i.e., lead to under-prediction of system performance).

Further refinements to the analytical model placed emphasis on 1) confirming the effects of the position and shape of the secondary shock on performance and 2) studying the sensitivities of injection position, Mach number, and angle. The model was used to study sensitivities, as shown in Figures 2.3-7, 2.3-8, and 2.3-9. These studies showed that the optimum injection parameters are approximately:

position (X/L) = 0.5, Mach No. = 1.5 and angle = 50 degrees.

These studies were preliminary because they considered a single circular injection port and an injection flow rate of 450 lb/second. Use of multiple ports or a slot was expected to reduce the required flow rate by approximately 25 percent. Therefore, a review was made of existing test data in which comparative studies were made between single point, multi-point and slot injection ports. Reference 7 indicated that three circular orifices with the same total mass flow as a single circular orifice could produce from 12 to 38 percent more TVC specific impulse, depending on the mass flow ratio. Reference 8 indicated that multiple orifices are better than slots for external jet interaction near the base of a cone. Jet interaction data on an ogive-cylinder model from Reference 9 indicated that a sonic slot with an aspect ratio of 8 positioned normal to the flow can produce about 23 percent more interaction force than a circular orifice with the same mass flow. From this data, it was concluded that a secondary jet exit configuration of three circular orifices spaced one diameter apart would produce near optimum system performance and would require approximately 25 percent less mass flow than a single orifice to obtain the design TVC angle of 6 degrees.

Using the computer programmed modified blast wave theory, studies were made of the variation in performance expected around the 6° TVC point when the several injection parameters were varied. Figure 2.3-10 shows the variation of TVC angle (θ) with the axial position of the secondary jet in the primary nozzle for several secondary to

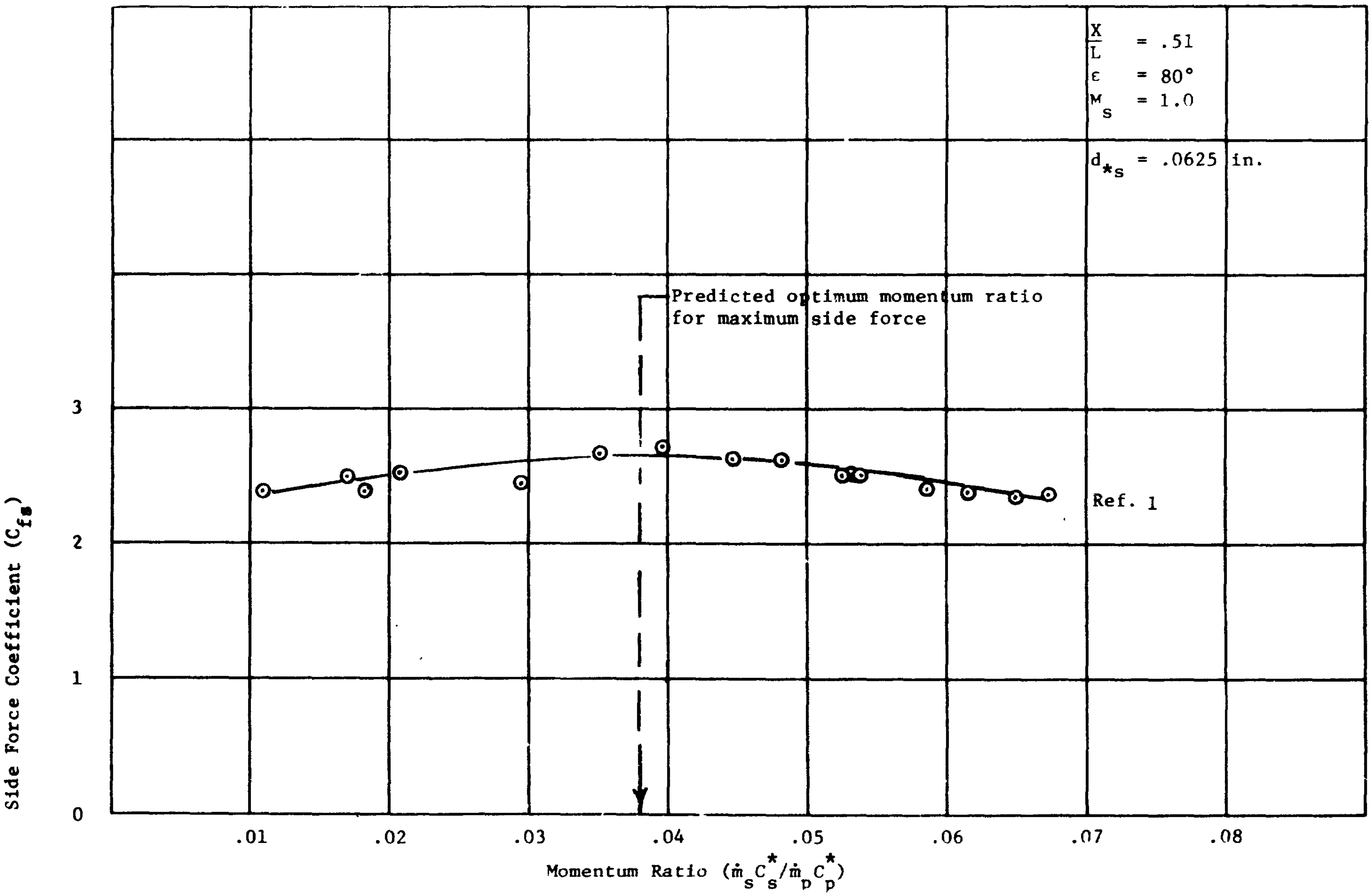

Figure 2.3-5. Side Force Coefficient versus Momentum Ratio

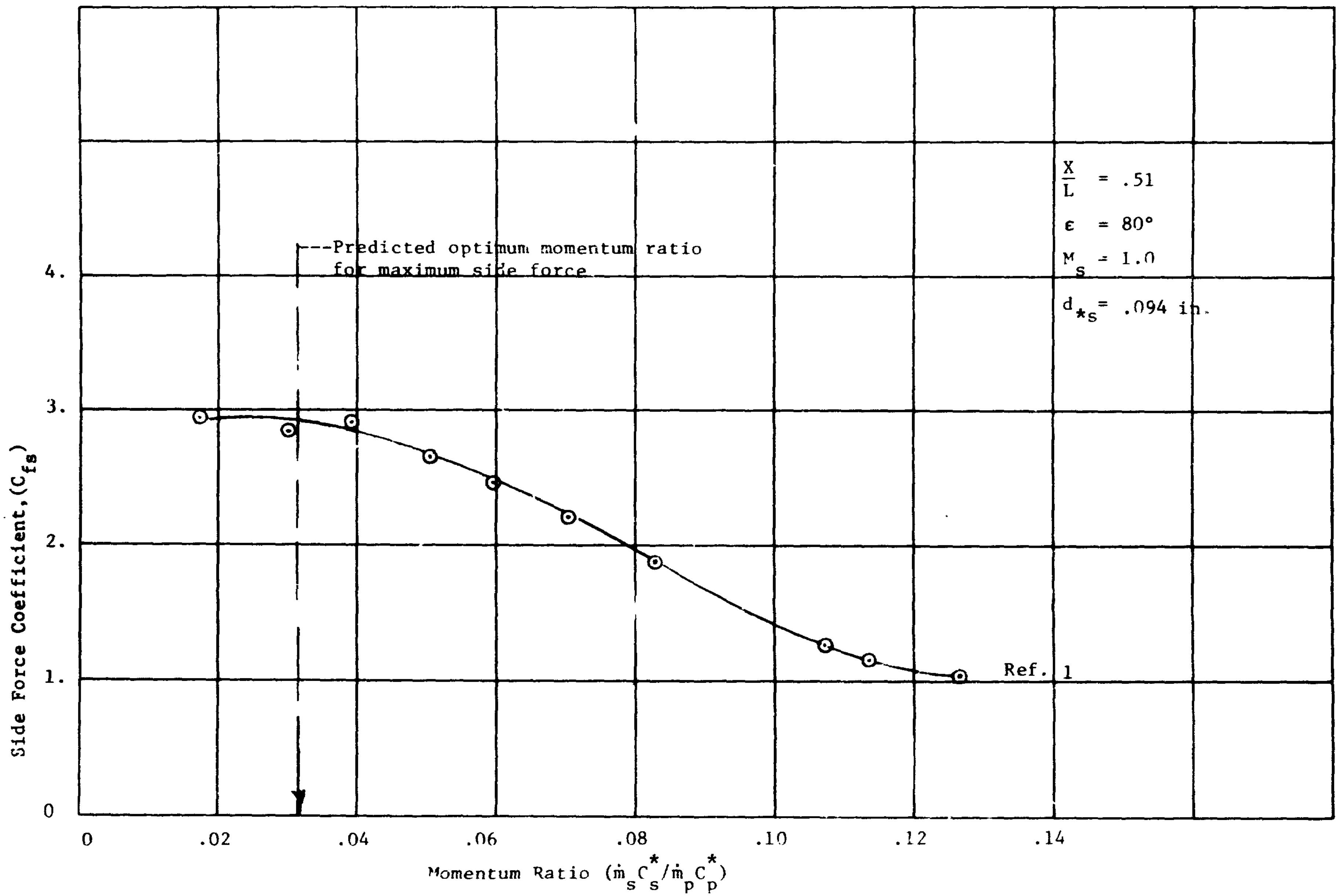

Figure 2.3-6. Side Force Coefficient versus Momentum Ratio

TABLE 2.3-I

Comparison of Predicted and Experimental Results

Reference	No. of Cases	Test Conditions			(All circular secondary nozzle exits)									Comparison Parameters	Prediction Variation from Experimental Results (%)
		α deg.	X/L -	ε deg.	Primary Gas	P_{op} psia	T_{op} °R	γ_p	Secondary Gas	P_{os} psia	T_{os} °R	γ_s	M_s		
1	6	10	.38-.66	80	Air	150	530	1.4	Air	0-150	530	1.4	1.0	Side force coefficient vs secondary to primary momentum ratio	+10 to -21.6
2	6	15	.5	75	H_2O_2 products	400	1845	1.266	N_2, H_2, CO_2, A, He	40-1000	530	1.3-1.67	1.0	Side force coefficient vs secondary to primary momentum ratio	+7.2 to -6.5
3	9	15	.46-.85	75	IRFNA/UDMH	1350	5760	1.15	IRFNA/UDMH	325-525	5350	1.17	1.0-1.95	Side to axial force ratio vs secondary to primary mass flow ratio	+9.2 to -16.3
4	3	0	.67	90	H_2O_2 products	155	1845	1.27	Air	50-200	900-1660	1.34-1.38	1.0	Specific impulse ratio vs pressure ratio	+8.8 to -12.2
5	6	15	.58-.75	55-75	Solid Propellant Gas Generator	523-645	6660	1.17	Solid Propellant Gas Generator	287-857	2090-2375	1.27	1.0-1.83	Side force vs secondary to primary mass flow ratio	0 to -25
6	3	12.5-20	.346-.714	90	LO_2/RP-1	232	5680	1.15	LO_2/RP-1	110-230	5680	1.15	1.0	Side force vs secondary to primary mass flow ratio	-13.7 to -17.3

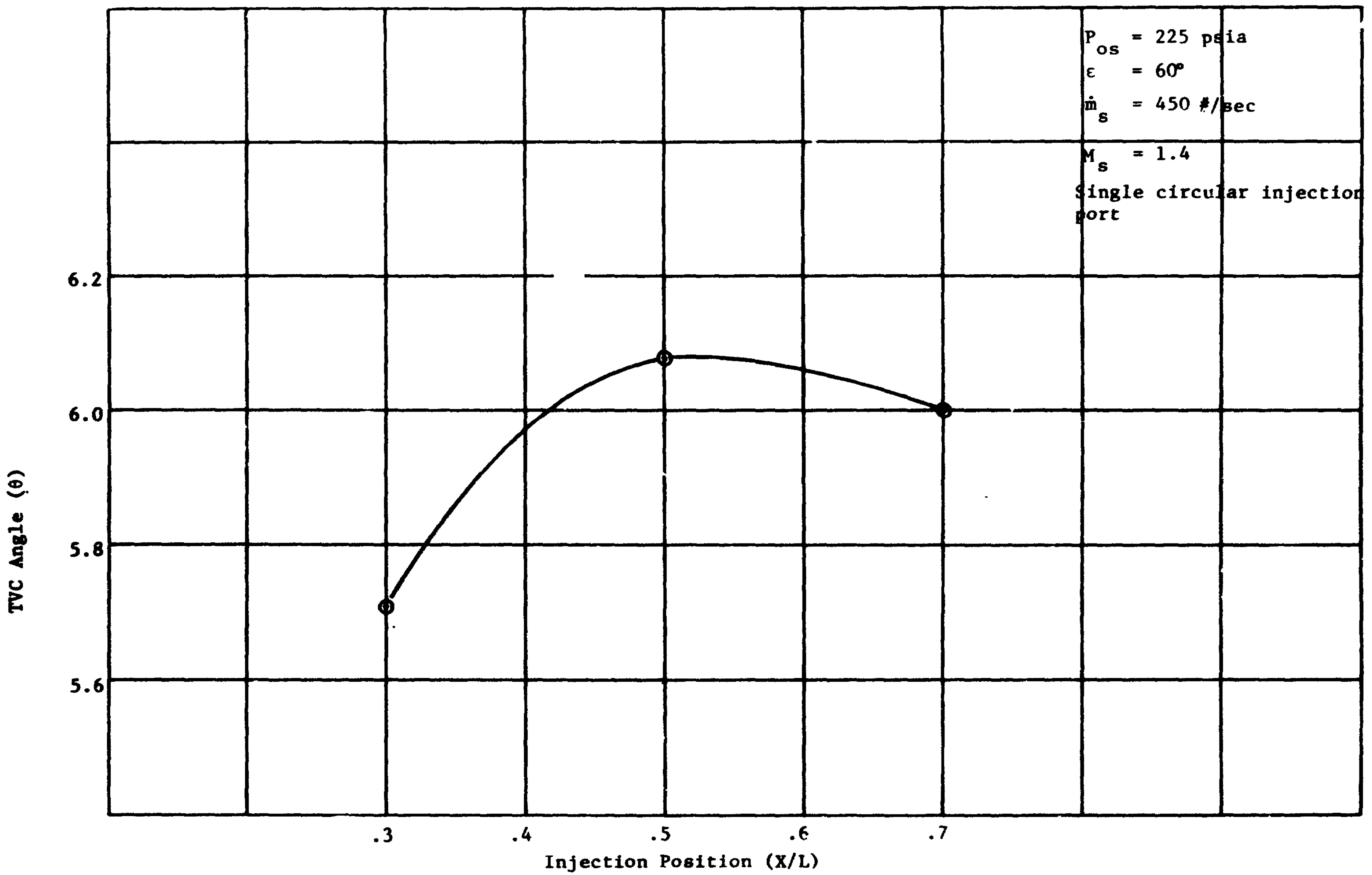

Figure 2.3-7. TVC Angle versus Injection Position

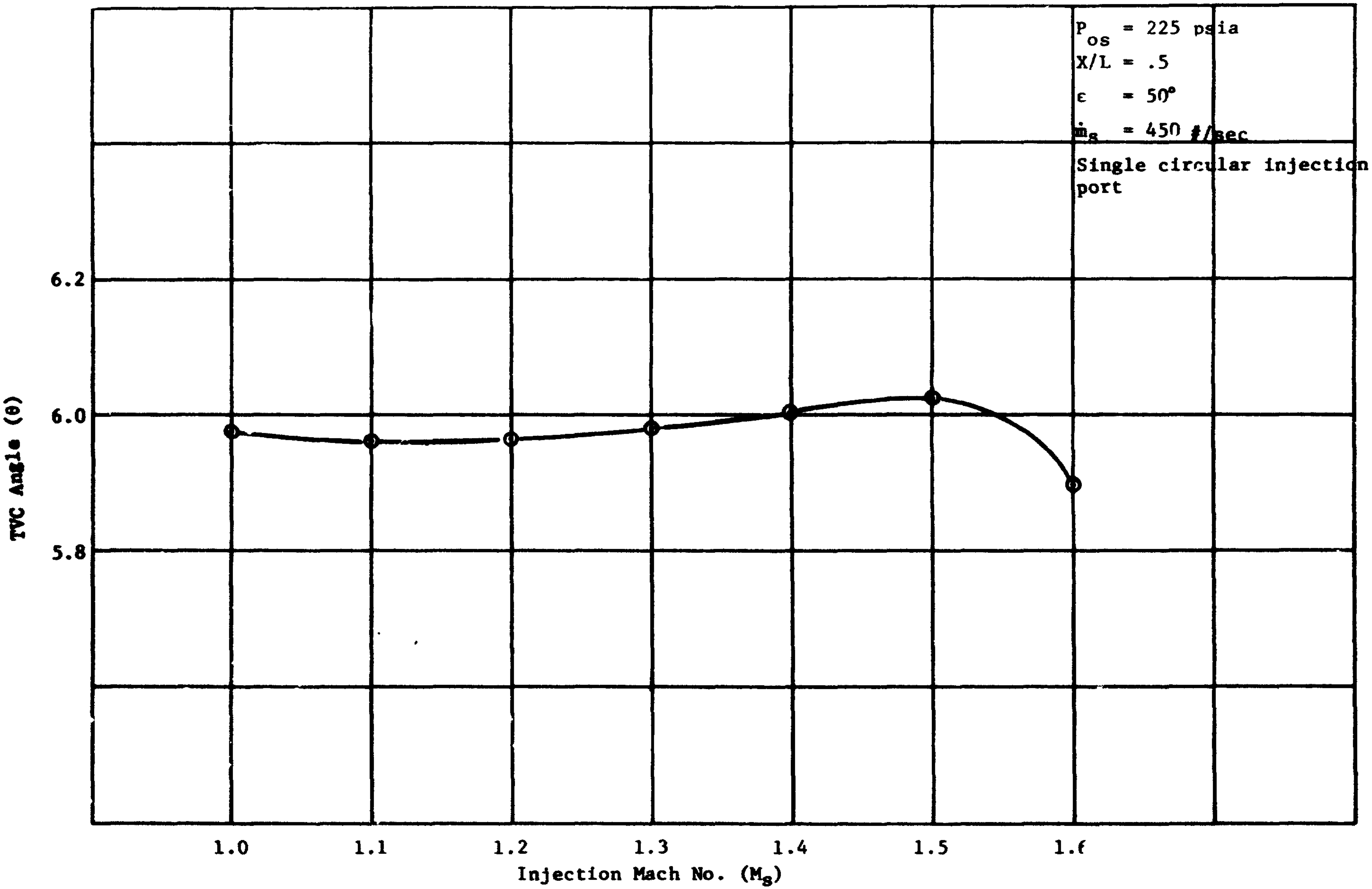

Figure 2.3-8. TVC Angle versus Injection Mach Number

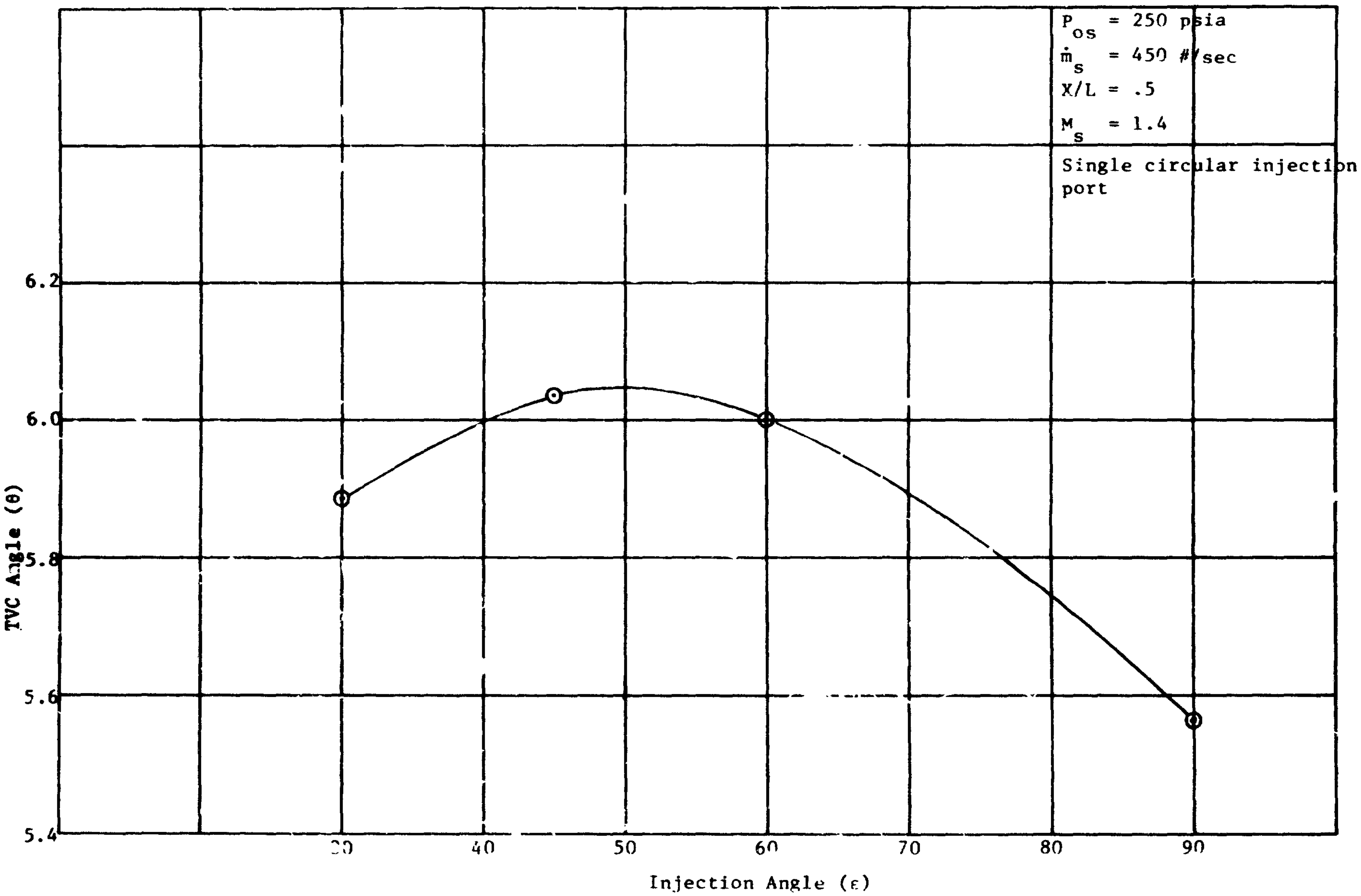

Figure 2.3.9. TVC Angle versus Injection Angle

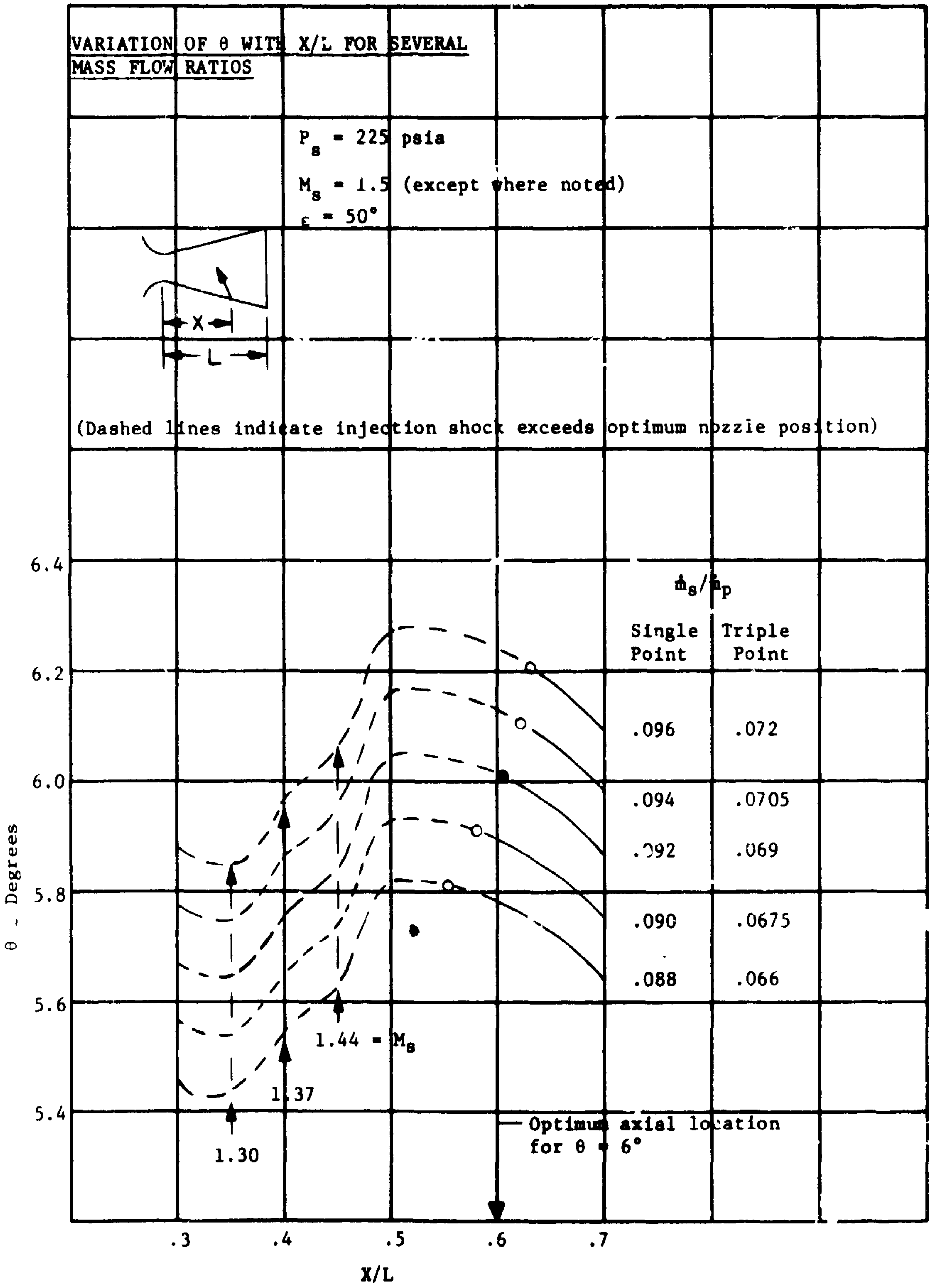

Figure 2.3-10. TVC Angle versus Injection Location

primary mass flow ratios. This considers a total secondary pressure of 225 psia, which is considered to be the basic design condition, assuming 10 percent duct losses from the primary nozzle total pressure of 250 psia. Thrust vector control angle is defined as Θ = arc tan (F_N/F_A) where F_N = total force normal to primary axis and F_A = total axial thrust. Variation of Θ with secondary injection Mach number is shown in Figure 2.3-11. Variation of Θ with secondary injection angle is shown in Figure 2.3-12. The figures illustrate that conditions producing maximum TVC angle for the lowest mass flow ratio are:

$X/L = 0.6$

$M_S = 1.50$

$\varepsilon = 50°$.

2.4 Structural Analysis

Two basic design concepts were evaluated. The first approach was to have a single valve per 90° of nozzle while the second approach was the utilization of a number of valves per nozzle quadrant. The results f the structural study indicated a significant weight savings could be realized by using the multi-valve approach.

The single valve design configuration is basically a cylindrical shell plenum with rectangular inlet and injection ports. The width of the unit was 32 inches and the total depth about 35 inches.

For the multi-valve approach, three units per quadrant were used. Two basic designs were considered. The first used a cylindrical plenum and the second a spherical plenum. For both these valves cylindrical ducts were used. The basic configuration of the several designs are shown in Table 2.4-I.

The stress analysis effort was confined to obtaining an objective weight evaluation for the valve design configurations. All valves were designed using L605 steel and for a pressure of 250 psia, a temperature of 500°F, and a factor of safety of 1.90. Normally a man rated system will only require a factor of 1.4; however, since this is a development type structure, engineering judgement was to use the 1.90. The weight results are shown in Table 2.4-I where it can be seen that Configuration IV is the lightest design.

In addition to the weight study, an evaluation was made for the selected design to determine the structural factor of safety as a function of structural temperature. These results are shown in Figure 2.4-1.

A preliminary thermal analysis was made to design the insulation for the inlet duct and valve housing. It was found that 0.3 inches thickness of integrally wrapped and bonded rubber base silica phenolic

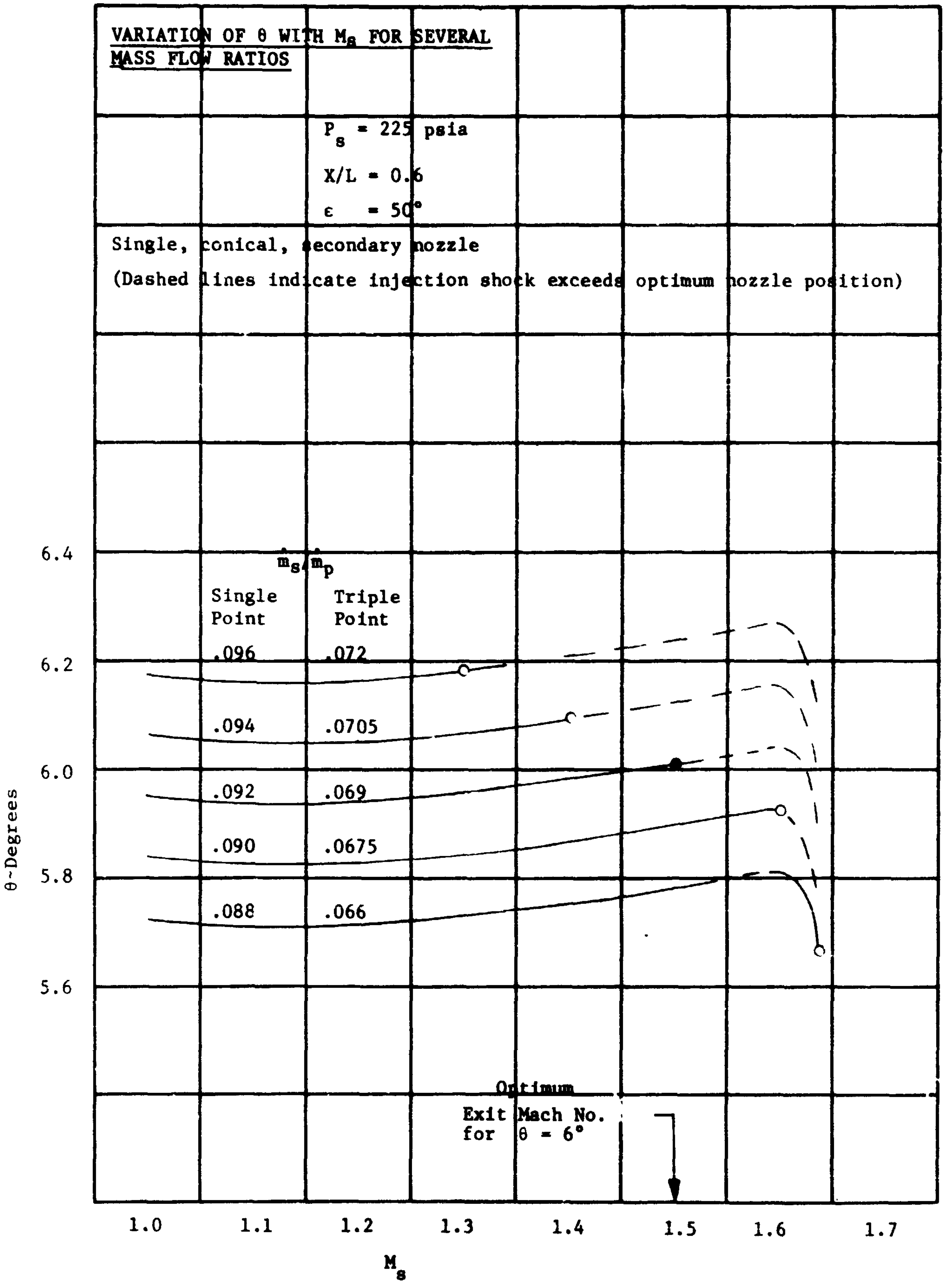

Figure 2.3-11. Variation of TVC Angle with Injection Mach Number

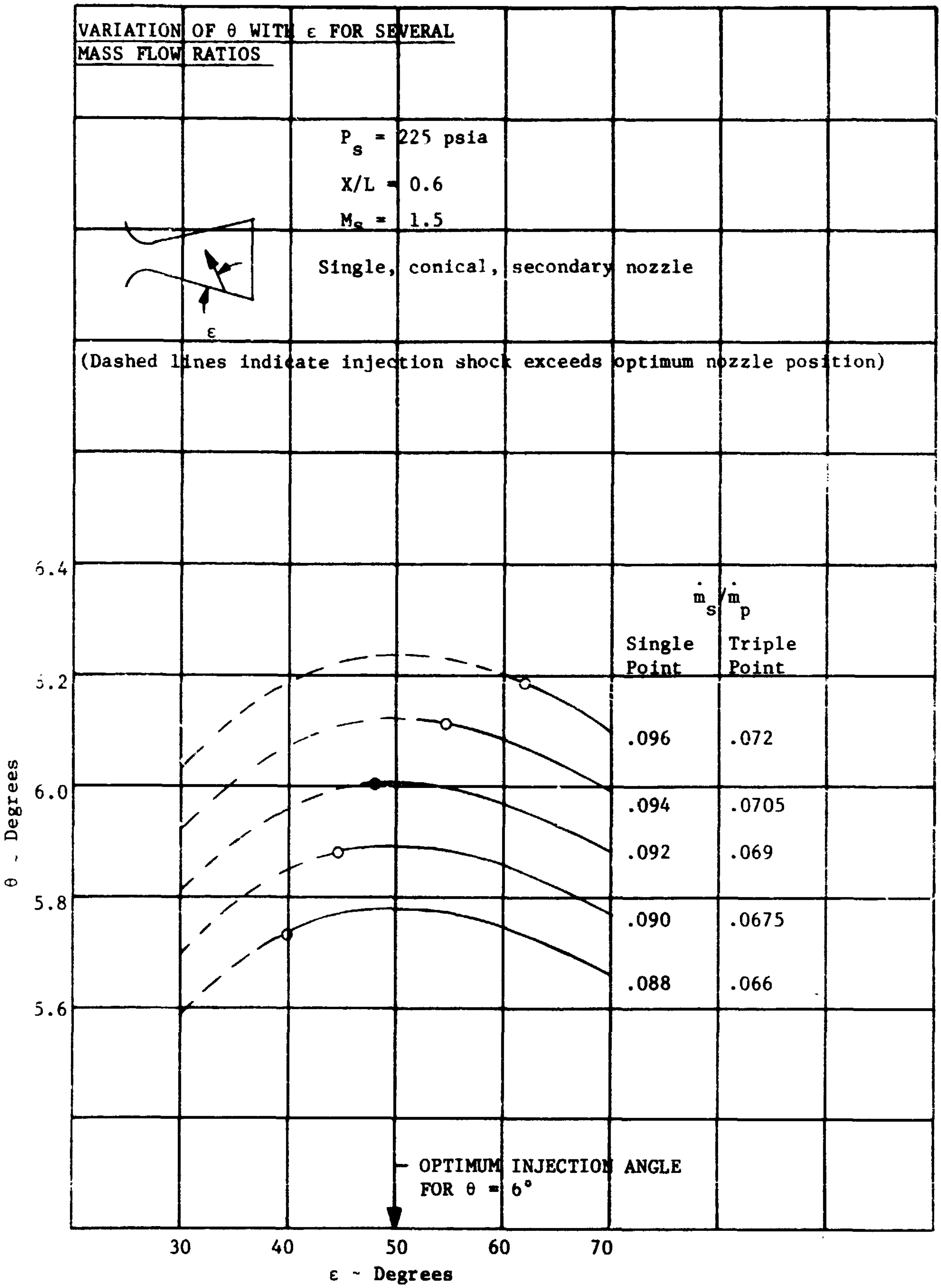

Figure 2.3-12. Variation of TVC Angle with Injection Angle

TABLE 2.4-˛

Summary of Design Configuration Structural Study

Configuration	General Description	Comments	Weight
I. 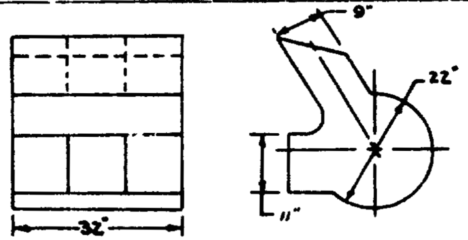	1. 3/4" end plates 2. 1/4" duct top & bottom with 1-1/2" high by 1/4 stiffener spaced at 4.3". 3. Two baffel plates with a thickness of .25" both ducts.	1. Many details to be welded which will lead to distortion. 2. Thermal mass concentrations which will lead to thermal stresses.	511#/quadrant
II. Same as above but utilizing honeycomb structure where possible.	Same as above except Item 2. 1/2" depth H/C with 10#/ft^3 1/4" cell and 020 faces.	Generally same as above plus the H/C edge detail problem.	473#/quadrant
III. 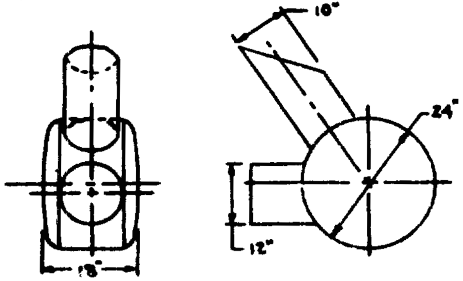	1. 12" dia. circular inlet duct t = .10". 2. 10" dia. circular injection duct t = .10" 3. Cylindrical plenum with torispherical ends t = .20.	1. Duct to cylinder joints straightforward approach. 2. Torispherical ends not the most optimum.	369#/quadrant
IV. 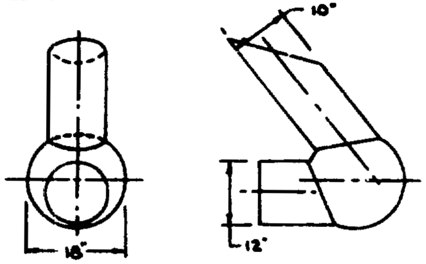	1. Same as above with sperical plenum t = .075"	1. Has least number of structural details. 2. Sphere is ideal pressure plenum.	249#/quadrant

would be adequate to maintain the metal structure temperature below 500°F. The predicted shear levels due to gas flow of 10 lbs/ft^2 are well below the minimum shear level of 60 lb/ft^2 required to cause ablation of the silica phenolic.

2.5 Valve Torque Analysis

The torque requirements for the butterfly valve were analyzed so that an actuator capable of meeting the performance requirements could be selected.

Using design data for butterfly valves obtained from Section 6.2.3 of "Aerospace Fluid Component Designer's Handbook," Volume I and applying characteristics of this proposed butterfly valve design. The coefficient was computed from the equation

$$C_1 = .01942\ (25.66\alpha - 13.43 - 11.25\alpha^2)$$

where α = opening angle in radians.

The fluid torque on the valve was then computed using the equation

$$T = P_1 d^3 C_1 C_2$$

where P_1 = 250 psi

C_1 = from above

$$C_2 = 1 - \left(\frac{\frac{P_1 P_2}{P_C P_1} - 1}{\frac{P_1}{P_C} - 1} \right)^2$$

P_C = static pressure downstream for critical flow

P_2 = static pressure downstream

d = valve effective diameter

The resulting torque curve showed a peak closing torque of 6500 in-lb at an opening angle of 80°. Sizing the actuator for some torque margin to provide acceleration capability it was decided to use an actuator with a stall torque rating of 9000 in-lb.

The valve configuration was then analyzed for rotational inertia. This information was combined with the actuator design data and the hydraulic natural frequency was estimated from:

$$F_n = 1/2\pi \sqrt{\frac{2B(dm)}{I\Theta m}}$$

where f_n = hydraulic natural frequency

B = 150,000 psi (MIL-H-5606 at 200°F)

dm = 9.0 in^3/radian displacement

Θm = $\pi/2$ radians (90°)

I = 3.2 in-lb-s^2

the resultant frequency was 116.6 Hz which is well above that required.

2.6 Thermophysical Analysis

The thermal model of the TVC valve mechanism was converted to the new computer program which employs a variable properties analysis and the data output checked against previous results of the old computer program which employed a constant properties analysis. The variable thermophysical properties presented in Figures 2.6-1 through 2.6-3 were added to the new version of the TVC valve thermal model. Analysis results are compared with the results of the constant properties analysis in Table 2.6-I. The variable properties analysis shows a sharper temperature gradient in the actuation shaft where it passes through the wall of the TVC tube. This is because the variable thermal conductivity data uses lower conductivity values at the lower temperature levels. The slight increase in bearing temperature is due to variable material specific heat data. The effects of variable thermophysical properties in this analysis are small and do not require any change in the valve design.

In addition, the TVC valve model was modified to include the calculation of component thermal expansion as a function of time for the major valve mechanism components. The results are plotted in Figure 2.6-4 in the form of component growth vs operating time. Figure 2.6-4 reaches its maximum growth (.095 inch) after 15 sec of operation while the duct tube which is internally insulated has not changed dimension within the first 15 sec of operation. Thus the valve design must allow for approximately 0.1 inch of butterfly valve expansion relative to the duct tube.

Figure 2.6-4 shows that the valve actuation half shaft will

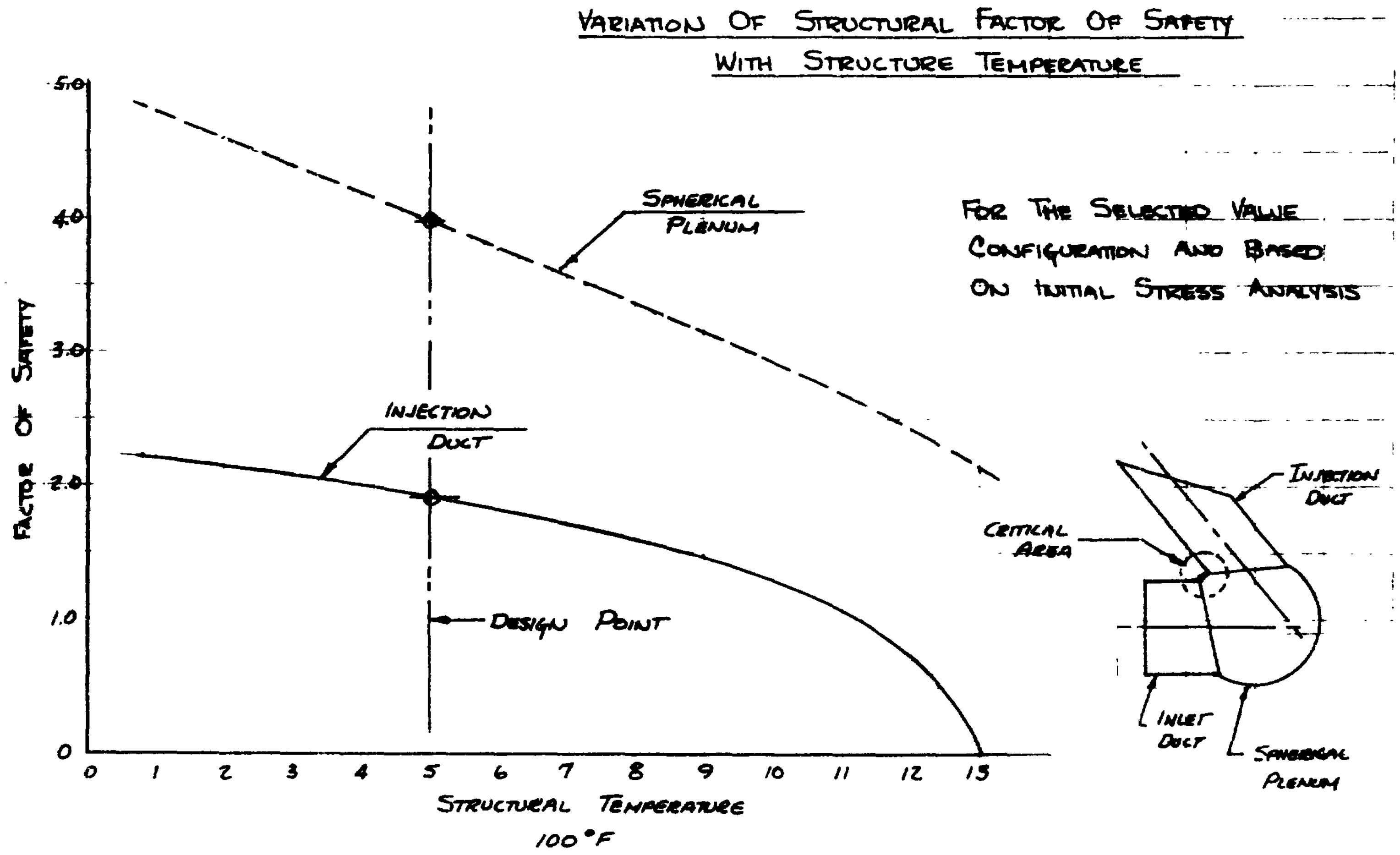

Figure 2.4-1. Warm Gas TVC Design Study

TABLE 2.6-I

Component Thermophysical Properties

Component	Temperature (°F) at the End of 3 Minutes Thermophysical Properties Constant	 Variable
Butterfly Valve	2000	2000
L-605 Shaft at Butterfly Valve	1972	1977
L-605 Shaft at Bearing	143	115
Bearing	80	84
L-605 Shaft at Universal Joint	123	97
Universal Joint	71	70

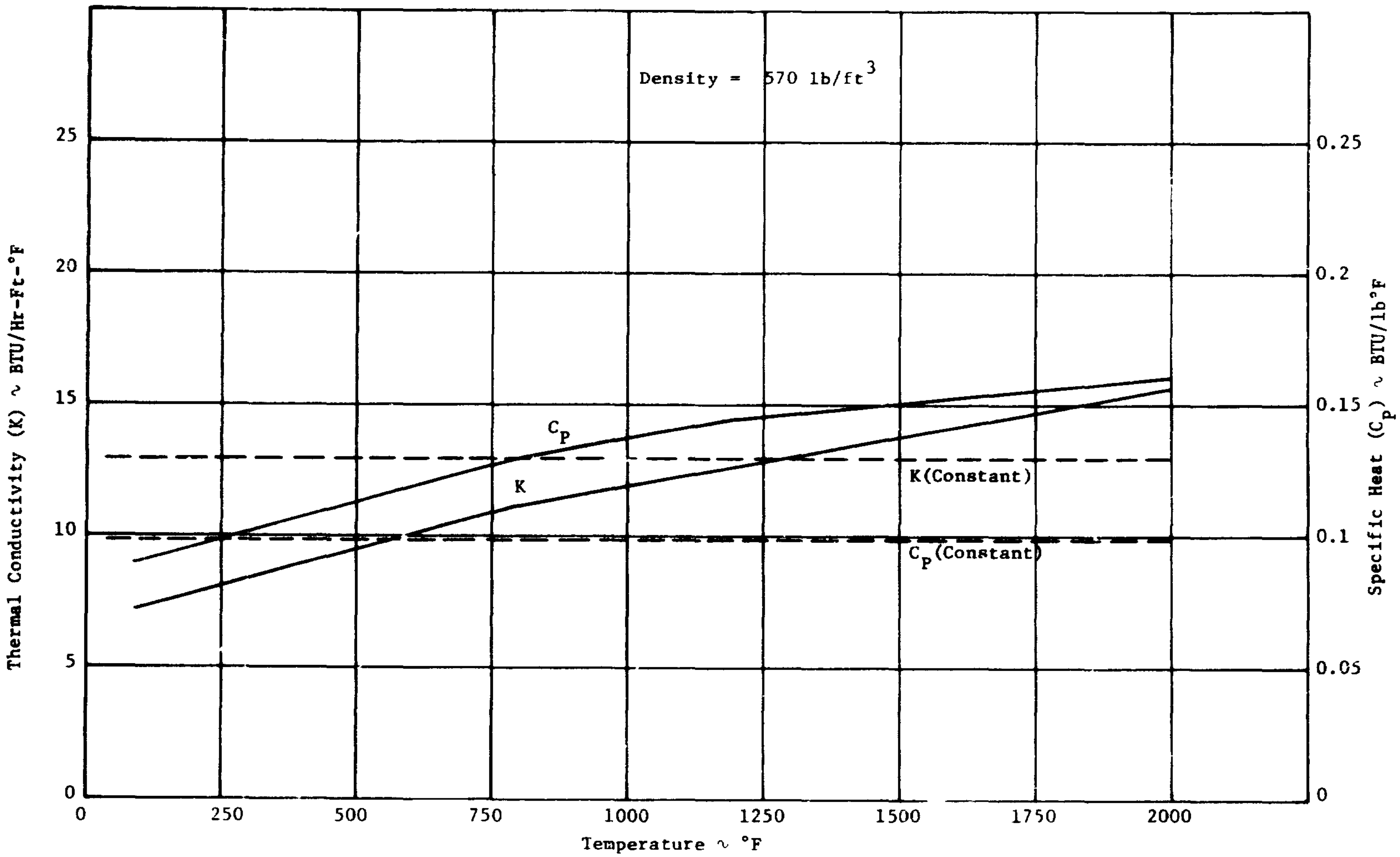

Figure 2.6-1. L-605 Thermophysical Properties (Actuator Shaft, Tube)

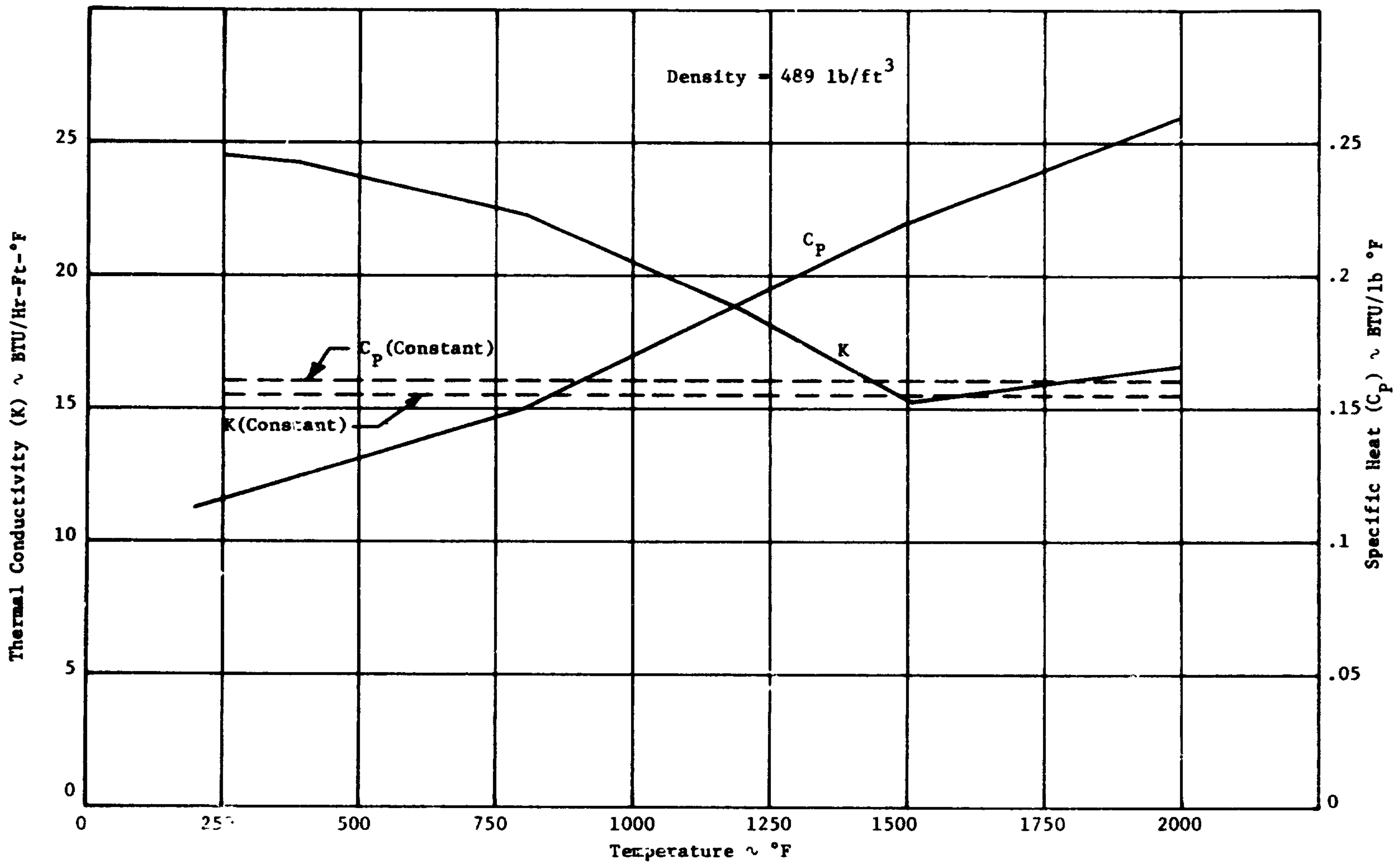

Figure 2.6-2. 4130 Steel Thermophysical Properties

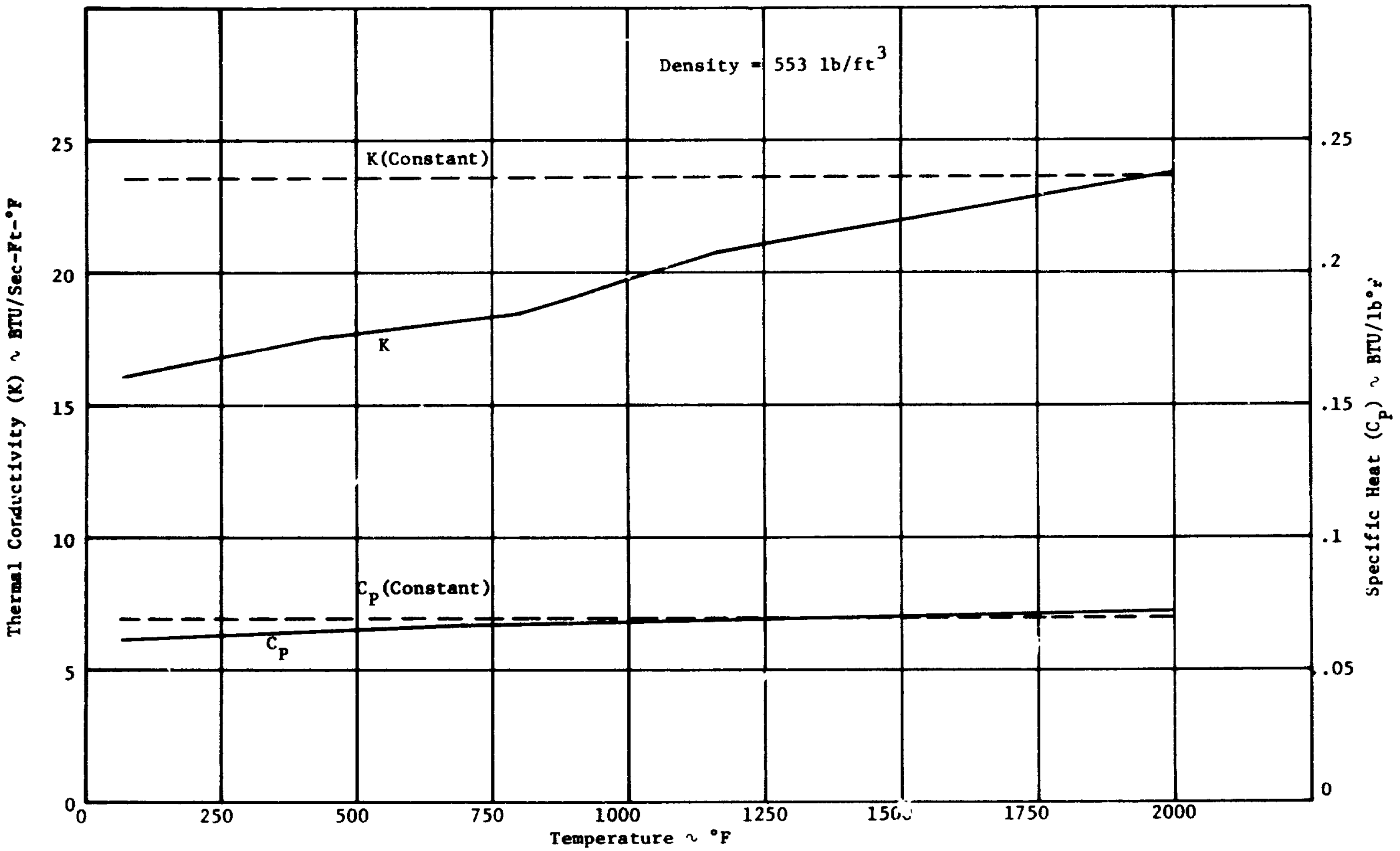

Figure 2.6-3. C-103 Thermophysical Properties (Butterfly Valve)

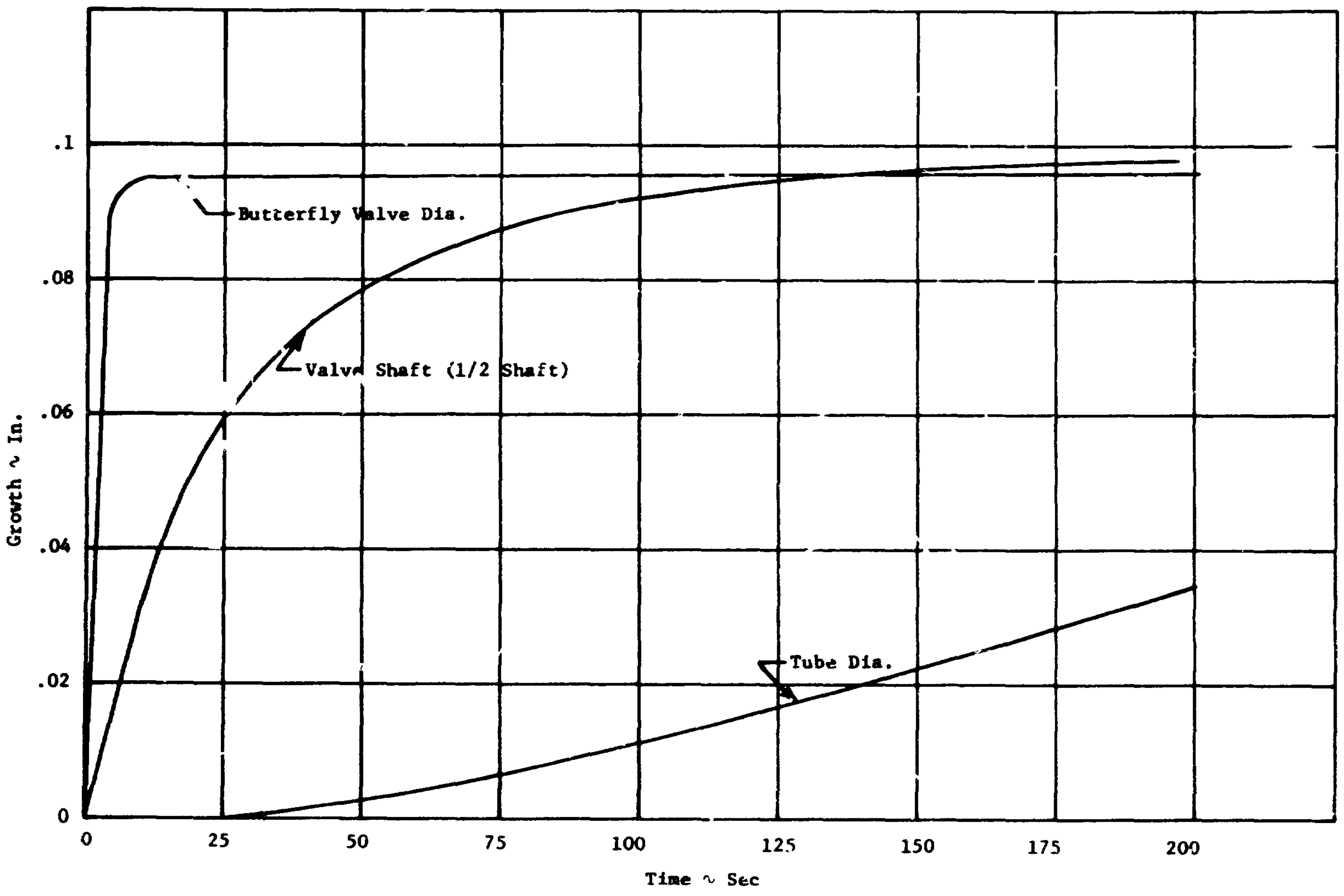

Figure 2.6-4. Component Growth Comparison

grow approximately 0.1 inch during operation. The butterfly valve growth based on the valve radius is 0.05 inch and is in the opposite direction to that of the actuation shaft. Thus the valve mechanism design must allow for 0.15 inch of relative expansion between the butterfly valve and the actuation shaft.

PRECEDING PAGE BLANK NOT FILMED

3.0 HIGH CONTAMINANT DIRECT DRIVE SERVOVALVE

3.1 Torque Motor Design Analysis

A conventional tee shaped armature with a permanent magnet field was selected as a baseline design because it is most widely used in two stage valve designs. Magnetic material advancements have extended the environmental and strength capabilities of permanent magnets, while the dual gap magnetic bridge offers maximum torque capability in minimum packaging volume.

A schematic of the torque motor arrangement and the equivalent magnetic circuit is shown in Figure 3.1-1.

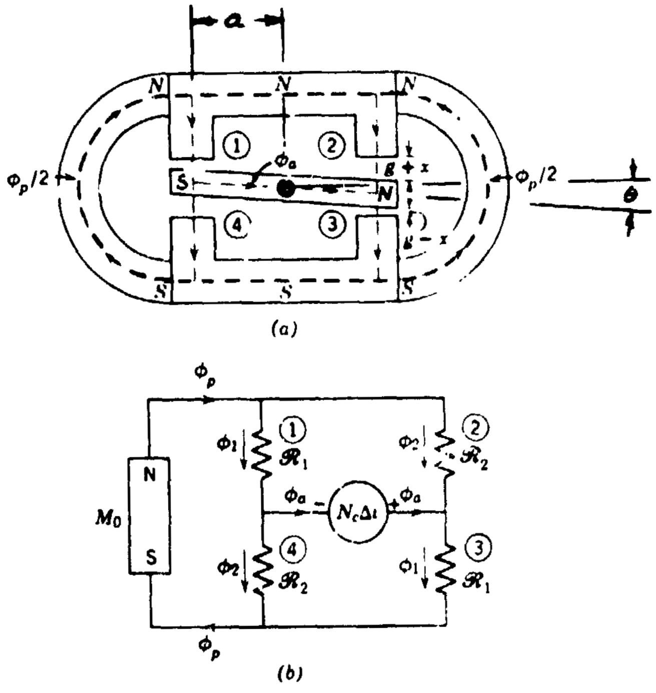
a
N
N
N
①
②
Φp/2
Φa
S
N
g
x
Φp/2
θ
④
③
g
x
S
S
S
(a)
Φp
Φ1
①
ℛ1
Φ2
②
ℛ2
N
Mo
S
Φa
NcΔi
Φa
Φ2
④
ℛ2
Φ1
③
ℛ1
Φp
(b)

Figure 3.1-1. Schematic Diagram of Permanent Magnet Torque Motor

By applying Kirchhoff's first and second laws for electrical circuits to the magnetic circuits of Figure 3.1-1 and forming the Laplace transform, the following equation relating voltage, resistance, inductance and current results:

1) $$2\mu e_g = (R_c + r_p)\,\Delta i + 2\,K_b s\Theta + 2\,L_c s\,\Delta i$$

μ - magnetic permeability

e_g - signal voltage input to amplifier

R_c - resistance of each coil

r_p - internal resistance of amplifier

Δi - current difference between the two coils

K_b - back emf constant for each coil

L_c - self inductance of each coil

Since the attractive force between magnetized parallel surfaces, separated by an air gap is directly proportional to the square of magnetic flux in the gap and inversely proportional to the product of the permeability and the area of the flux path, it can be shown that the torque developed on the armature due to an electrical current input is given by:

2) $$T_d = K_t\,\Delta i + K_m\Theta$$

K_t - torque constant of each coil (in-lb_f-amp)

K_m - magnetic spring constant of torque motor (in-lb_f-amp)

By applying Newton's second law to the armature the equation for the developed torque may be written:

3) $$T_d = J_a \frac{d^2\Theta}{dt^2} + B_a \frac{d\Theta}{dt} + K_a\Theta + T_L$$

J_a - inertia of armature and attached load

B_a - armature viscous damping coefficient

K_a - armature pivot spring rate

T_L - load torque

Equating equations 2) and 3) rearranging and forming the Laplace transform:

4) $$K_t\,\Delta i = J_a\,s^2\Theta + B_a\,s\Theta + (K_a - K_m)\,\Theta + T_L$$

Finally, if the mechanical viscous damping is considered to be small (reasonable assumption in a dry torque motor) by combining equations 1) and 4) the result is the relationship between the input voltage and the angular displacement of the armature.

$$5)\quad \Theta = \frac{K_o e_g - \left[\dfrac{1}{K_a (1 - K_m/K_a)} \right] (1 + \dfrac{s}{\omega a}) T_L}{\dfrac{s^3}{\omega_a \omega_m^2 (1 - K_m/K_a)} + \dfrac{s^2}{\omega_m^2 (1 - K_m/K_a)} + \dfrac{s}{\omega_a (1 - K_m/K_a)} + 1}$$

K_o - static gain constant

ω_a - break frequency of armature circuit

ω_m - natural frequency of armature

Other terms as previously defined.

The above equation will be used to analyze the dynamic response of the torque motor.

3.2 Spool Valve Design Analysis

The analysis of the spool portion of the servovalve is analogous to the torque motor. The flow of fluid to the load is given by:

$$6)\quad Q_L = K_q x_v - K_c P_L$$

K_q - valve flow gain

K_c - valve flow-pressure coefficient

Because the dynamic behavior of the load is intimately related to that of the spool of the valve, both must be considered together. For the purpose of this study a mass-spring-dashpot load with a linear actuator power element has been assumed. The schematic of such a system is shown in Figure 3.2-2.

In Figure 3.2-2 the flow to the load $Q_L = Q_1$:

$$7)\quad Q_L = A_p s X_p + C_{tp} P_L + \frac{V_t}{4\beta_e} s P_L$$

V_t - total volume under compression

β_e - effective bulk modulus of fluid

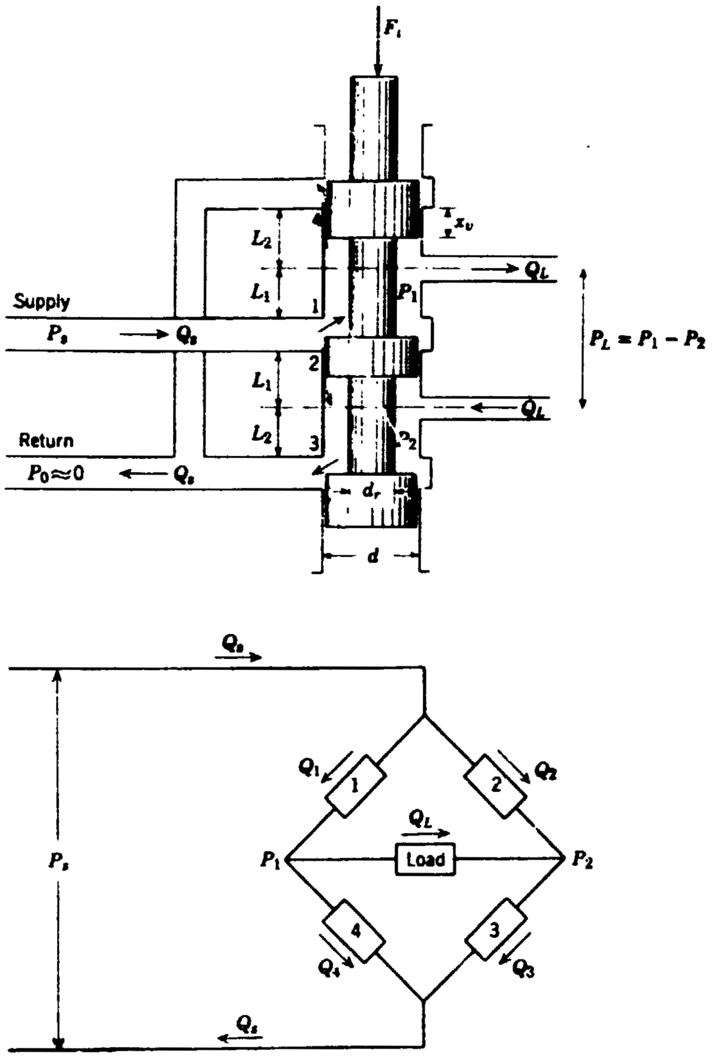
F_i
x_v
L_2
L_1
1
P_1
Q_L
Supply
P_s
Q_s
P_L = P_1 - P_2
2
L_1
L_2
3
P_2
Q_L
Return
P_0≈0
Q_s
d_r
d
Q_s
Q_1
1
2
Q_2
Q_L
P_s
P_1
Load
P_2
4
3
Q_4
Q_3
Q_s

Figure 3.2-1. Schematic of Spool Valve

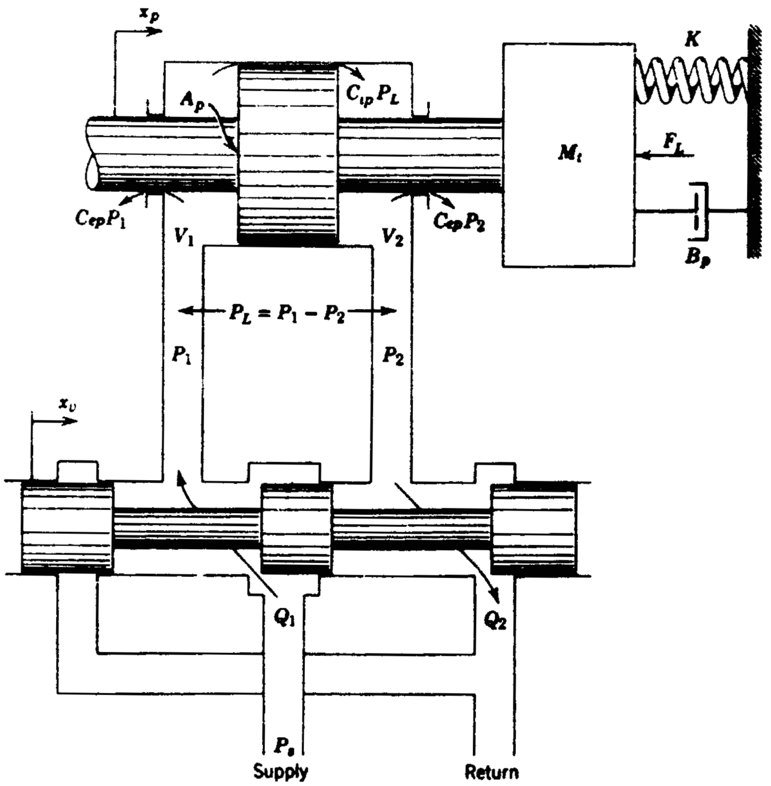
x_p
A_p
$C_{ip}P_L$
M_t
K
F_L
B_p
$C_{ep}P_1$
V_1
V_2
$C_{ep}P_2$
$P_L = P_1 - P_2$
P_1
P_2
x_v
Q_1
Q_2
P_s
Supply
Return

Figure 3.2-2. Schematic of Valve-Actuator-Mass-Spring-Dashpot System

The first term being the flow required to displace the piston; the second term being the total leakage (piston plus rod leakage) and the final term being the flow due to compressibility of the fluid. Applying Newton's second law to the forces on the actuator piston and forming the LaPlace transform yields:

$$8)\quad F = A_p P_L = M_t s^2 X_p + B_p s X_p + KX_p + F_L$$

A_p = net piston area

M_t - total mass of piston and load

B_p - viscous damping coefficient

K - spring rate of load

F_L - load force

If equations 6), 7) and 8) are solved simultaneously the following relationship is obtained:

$$9)\quad X_p = \frac{\dfrac{K_q}{A_p} x_v - \dfrac{K_{ce}}{A_p^2}\left(1 + \dfrac{V_t s}{4\beta_e K_{ce}}\right) F_L}{\dfrac{V_t M_t}{4\beta_e A_p^2} s^3 + \left(\dfrac{K_{ce} M_t}{A_p^2} + \dfrac{B_p V_t}{4\beta_e A_p^2}\right) s^2 + \left(1 + \dfrac{B_p K_{ce}}{A_p^2} + \dfrac{K V_t}{4\beta_e A_p^2}\right) s + \dfrac{K_{ce} K}{A_p^2}}$$

$K_{ce} = K_c + C_{ip} + C_{ep}/2$ - flow-pressure coefficient.

Equation 9) can be used to analyze the spool valve and actuator-load from a linearized standpoint.

Since there are nonlinear characteristics (such as the orifice flow and underlap of spool-sleeve assembly) existing, it was found necessary to model the valve by more exact descriptions. The major effort was on the controlled flow rate response to spool displacement. In the following analysis, both the supply pressure and return pressure were assumed constant.

Figure 3.2-3 depicts the simplified servovalve with a piston and cylinder assembly connected to the control ports. The speed of the piston is a good measure of the controlled flow rate. The orifices at both ends of the spool serve as a damper to the spool motion.

Control Area - The control area or metering area at each land of the spool may be expressed as

$$10)\begin{cases} A_{C1} = WC_1 \\ A_{C2} = WC_2 \\ A_{C3} = WC_3 \\ A_{C4} = WC_4 \end{cases}$$

where

A_{Ci} = metering area, i = 1, 2, 3, 4

W = slot width or control orifice gradient

$$11)\begin{cases} C_1 = C_3 = \sqrt{X_{t1}^2 + C_r^2} \\ C_2 = C_4 = \sqrt{X_{t2}^2 + C_r^2} \end{cases}$$

C_r = radial clearance between spool and sleeve.

$$12)\begin{cases} X_{t1} = \text{MAX}\ (0.,\ (X_S + U)) \\ X_{t2} = \text{MAX}\ (0.,\ (-X_S + U)) \end{cases}$$

U = amount of underlap per land, assumed to be the same for all four lands.

Flow Rate - The flow rate at each opening is determined by metering area and pressure difference. For MIL-H-5606, the following may be written for the right-hand chamber:

$$13)\quad Q_{V1} = \begin{cases} 158 \cdot A_{C1} \cdot Cd\sqrt{P_S - P_{C1}} & \text{if } P_{C1} < P_S \\ -158 \cdot A_{C1} \cdot Cd\sqrt{P_{C1} - P_S} & \text{if } P_{C1} > P_S \end{cases}$$

14)

$$Q_{11} = \begin{cases} 158 \cdot A_{C2} \cdot Cd \sqrt{P_{C1} - Pr} & \text{if } P_{C1} > P_r \\ -158 \cdot A_{C2} \cdot Cd \sqrt{Pr - P_{C1}} & \text{if } P_{C1} < P_r \end{cases}$$

15) $Q_{1d1} = A_p \dot{y}$

16) $Q_{cmp1} = Q_{v1} - Q_{11} - Q_{1d1}$

where Q_{v1} = flow rate into the right-hand chamber or chamber C_1

Q_{11} = flow rate leaving chamber C_1

Q_{1d1} = useful flow rate or load flow rate in chamber C_1.

Q_{cmp1} = flow rate from valve to compensate the compressibility of the fluid in chamber C_1

P_{C1} = pressure in chamber C_1

Cd = discharge coefficient $\simeq$ 0.61

Ap = piston area

y = piston linear displacement

$\dot{y} = \frac{dy}{dt}$

t = time

The rate of change of P_{C1} may be evaluated from equation 17):

17) $\dot{P}_{C1} = (\beta_e Q_{cmp1})/V_{C1}$,

where β_e = bulk modulus of MIL-H-5606

V_{C1} = volume of chamber C_1 and

18) $V_{C1} = Ap\ (y + L)$

L = neutral position of the piston.

A similar procedure may be applied to describe the left-hand chamber or chamber C_2.

The information of $\dot{y}$ in equation 15) is obtained from the piston-load dynamics.

Piston-Load Dynamics - The following expression describes the acceleration of the piston.

$$19)\quad \ddot{y} = [(P_{1C} - P_{2C})\,Ap - B\dot{y} - K_s y]/M_t$$

where

$\ddot{y}$ = piston-load acceleration

B = load damping coefficient

K_S = load spring rate

M_t = total inertia of piston and load.

Orifice Damping for Spool - Due to the highly underdamped characteristic of the spool-spring system, a pair of orifices are used for damping purposes. The pressure at the right end of the spool is described by

$$20)\quad P_1' = \frac{(S_1+Z_1+2C_{12}x_{1d})-S_1\sqrt{1+4S_1(Z_2+C_{12}x_{1d})}}{2C_{12}}$$

and that in the left end of the spool is expressed as

$$21)\quad P_2' = \frac{(-S_2+Z_1-2C_{12}x_{2d})+S_2\sqrt{1+4S_2(-Z_2+C_{12}x_{2d})}}{2C_{12}}$$

where

$Z_1 = 2 \cdot P_S \cdot C_1^2$

$Z_2 = (P_S - Pr)\, C_1^2$

$C_1 = K/(96Ao)$

$C_{12} = C_1 A_s/(96Ao)$

Ao = damping orifice diameter area

$$K = \frac{1.57\, C_r^{\,3}\, [1+1.5(\frac{\varepsilon}{Cr})^2]}{121\mu}$$

ε = distance between the centers of spool and sleeve

l = length of path of viscous flow, see Fig. 3.2-3

μ = viscosity

A_s = spool end area

$S_1 = \text{sign}\left(\dot{X}_S + \frac{K(P_S - Pr)}{A_S}\right)$

$S_2 = \text{sign}\left(\dot{X}_S - \frac{K(P_S - Pr)}{A_S}\right)$

X_{1d} = a function of $\dot{X}_S$, defined as shown in Fig. 3.2-4

X_{2d} = a function of $\dot{X}_S$, defined as shown in Fig. 3.2-5

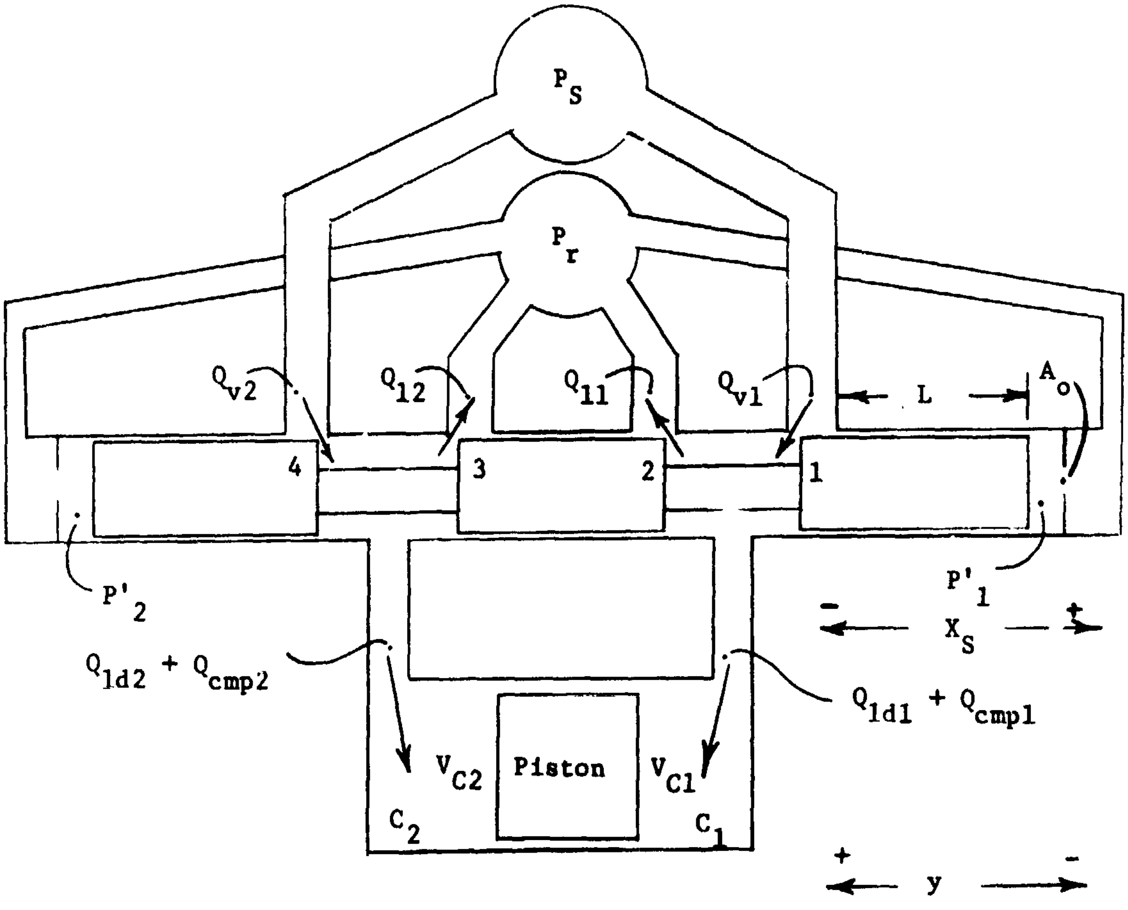
P_S
P_r
Q_{v2}
Q_{12}
Q_{11}
Q_{v1}
L
A_o
4
3
2
1
P'_2
P'_1
-
X_S
+
$Q_{1d2} + Q_{cmp2}$
$Q_{1d1} + Q_{cmp1}$
V_{C2}
Piston
V_{C1}
C_2
C_1
+
y
-

Figure 3.2-3. Flow Paths

The damping (resistive) torque produced by the difference of these pressure is

$$22)\quad T_{dp} = r \cdot A_S\,(P_1' - P_2')$$

In the program that simulates the performance of the servovalve, equations 10), 13), 14), 15), 16), 17), 19), 20), 21), 22) and their associated definitions are implemented.

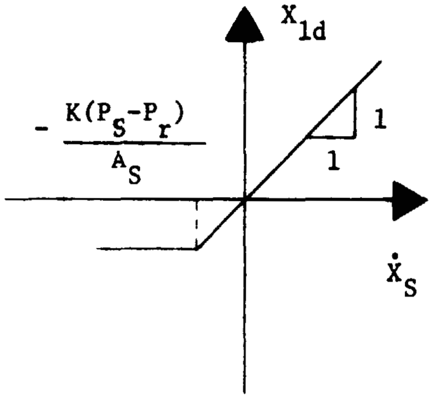

Figure 3.2-4. Geometry for Determining X_{1d}

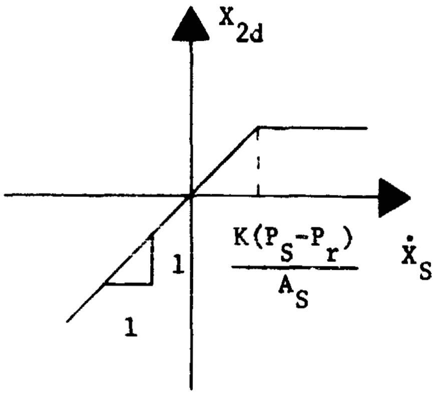

Figure 3.2-5. Geometry for Determining X_{2d}

3.3 Performance Analysis

The system analysis block diagram, which includes the dynamics of the torque motor, spool, actuator and the associated loads, is shown in Figure 3.3-1. The nomenclature used in Figure 1 is described in Table 3.3-I.

Two orifices were used to produce the damping effect needed for satisfactory valve response characteristics. The description of the damping effects were implemented into the computer program for the electro-hydraulic servovalve simulation. Step responses of the valve,

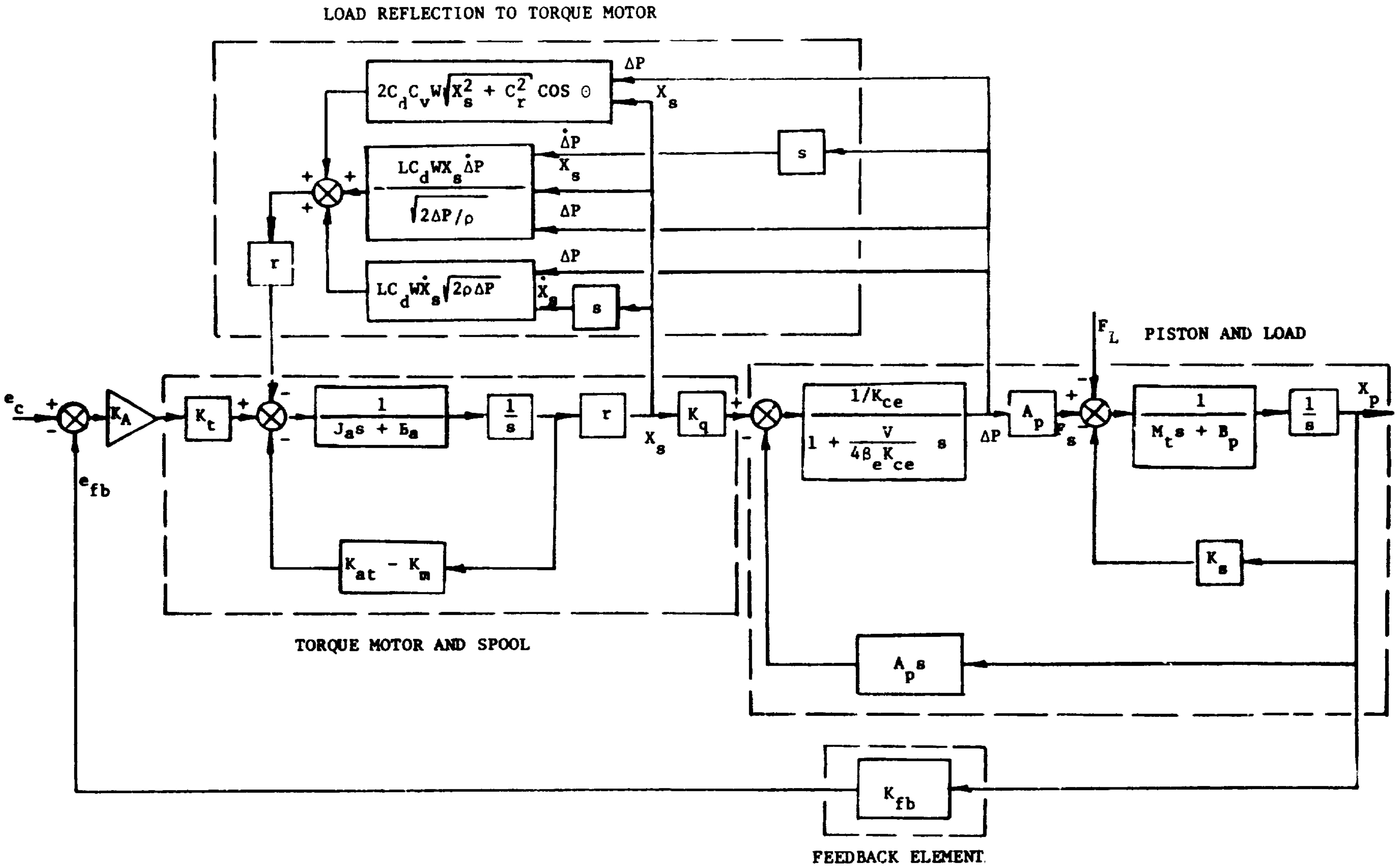
LOAD REFLECTION TO TORQUE MOTOR
$2C_d C_v W\sqrt{X_s^2 + C_r^2}\cos\Theta$
ΔP
X_s
$\frac{LC_d W X_s \dot{\Delta P}}{\sqrt{2\Delta P/\rho}}$
$\dot{\Delta P}$
ΔP
$LC_d W \dot{X}_s\sqrt{2\rho\Delta P}$
$\dot{X}_s$
s
r
e_c
e_{fb}
K_A
K_t
$\frac{1}{J_a s + B_a}$
$\frac{1}{s}$
$K_{at} - K_m$
K_q
TORQUE MOTOR AND SPOOL
F_L
PISTON AND LOAD
$\frac{1/K_{ce}}{1 + \frac{V}{4\beta_e K_{ce}} s}$
A_p
F_s
$\frac{1}{M_t s + B_p}$
X_p
K_s
$A_p s$
K_{fb}
FEEDBACK ELEMENT
+
-

Figure 3.3-1. Block Diagram Representation of the Electro-Hydraulic Servo-Actuator

TABLE 3.3-I

Block Diagram Nomenclature

Symbol	Description	Units	Value
K_A	Amplifier gain	ma/volt	
K_t	Torque motor gain	in-lb$_f$/ma	
K_{at}	Torsion spring constant of pivot	in-lb$_f$/rad	
K_m	Magnetic spring constant of torque motor	in-lb$_f$/rad	
J_a	Inertia of armature and attached load	in-lb$_f$-sec	
B_a	Viscous damping coefficient	in-lb$_f$-sec/rad	
Θ_a	Armature angular rotation	radians	
r	Distance from armature pivot to spool ℄	inches	
X_s	Spool travel	inches	
K_q	Valve flow gain	in^3/sec/in	
Q_v	Valve flow rate	in^3/sec	
K_{ce}	Flow/pressure coefficient	in^3/sec/psi	
V_t	Total volume of fluid under compression	in^3	
β_e	Effective bulk modulus	psi	
A_p	Area of actuator piston	in^2	
F_g	Force generated by actuator	lb$_f$	
F_L	Load force on actuator	lb$_f$	
M_t	Total mass of piston and load	lb$_f$-sec^2/in	
B_p	Viscous damping coefficient of piston	lb$_f$-sec/in	
X_p	Piston travel	in	
K_s	Load spring gradient	lb$_f$	
Q_{DISP}	Displacement flow rate	in^3/sec	
C_d	Orifice discharge coefficient	-	
C_V	Orifice velocity of approach coefficient	-	

TABLE CONTINUED

TABLE 3.3-I (Continued)

Symbol	Description	Units	Value
w	Orifice area gradient	in^2/in	
C_R	Radial clearance between spool and body	in	
Θ	Jet angle	degrees	
L	Damping length	in	
ρ	Fluid density	$lb_f\text{-}sec^2/in^4$	
F_s	Flow forces on spool	lb_f	
T_{La}	Load torque seen by armature	$in\text{-}lb_f$	
K_{fb}	Position feedback gain	volts/in	
e_c	Command voltage	volts	
e_{fb}	Feedback voltage	volts	
s	Laplace operator	sec^{-1}	

with the desirable orifice size (.014 inch dia.) and the diametral clearance (.0005 inch), are shown in Figure 3.3-2 in which the correlation of step control current (amp) and the controlled flow rate (QLD1, in^3/sec) is shown in a time basis. The following information may be drawn from Figure 3.3-2.

Control Current	Settling Time of Flow Rate
0 to 25% (of max. current)	7 ms.
25% to 0	6 ms.
0 to 100%	14 ms.
100 to -100%	19 ms.

The longer settling time for larger step change is due to the non-linearity of the orifice flow.

For the same set of parameters, a set of frequency responses for 1 ampere amplitude was simulated, the results of which were plotted as shown in Figure 3.3-3. These plots indicate that a 90° phase lag occurs at approximately 117 cps and the corresponding amplitude is -3 db.

3.4 Layout

The finalized design layout is shown in Figure 3.4-1.

The assembly envelope is 6 3/8 x 7 1/16 x 9 5/8 inches with an estimated weight of 28 pounds.

All material is non-magnetic, with the exception of torque motor parts requiring magnetic capability.

The armature, torsion bar, and shaft are welded by the electron beam process to comprise a single assembly. During operation, rotation of the armature bar produces a lateral movement of ±0.020 and 200 pound force on the valve spool. Torsion bar reaction will return the spool to null position.

The four pole pieces are adjustable to obtain the 0.135 inch needed clearance between pole piece and armature.

The two magnets are retained between the top and bottom motor plates by compression. The two coils are also retained by compression, utilizing a compressible wrapping material on the coils. These coils, made from No. 17 coil type wire (500 turns), require power of 4 amps and 28 ± 4 volts and approximately 2.5 ohms.

The four major components of the valve are housing, end plugs, sleeve, and spool. The sleeve is sealed to the housing on the outside diameter with nitrile (Buna N) O-rings and has an inside 0.005-0.00075

```
AMP=CONTROL CURRENT,AMPERES.
QLD1=FLUID FLOW RATE(CU. IN.PER SEC) CONTROLLED BY THE VALVE.
RESPONSE OF CONTROLLED FLOW RATE TO CONTROL CURRENT.
```

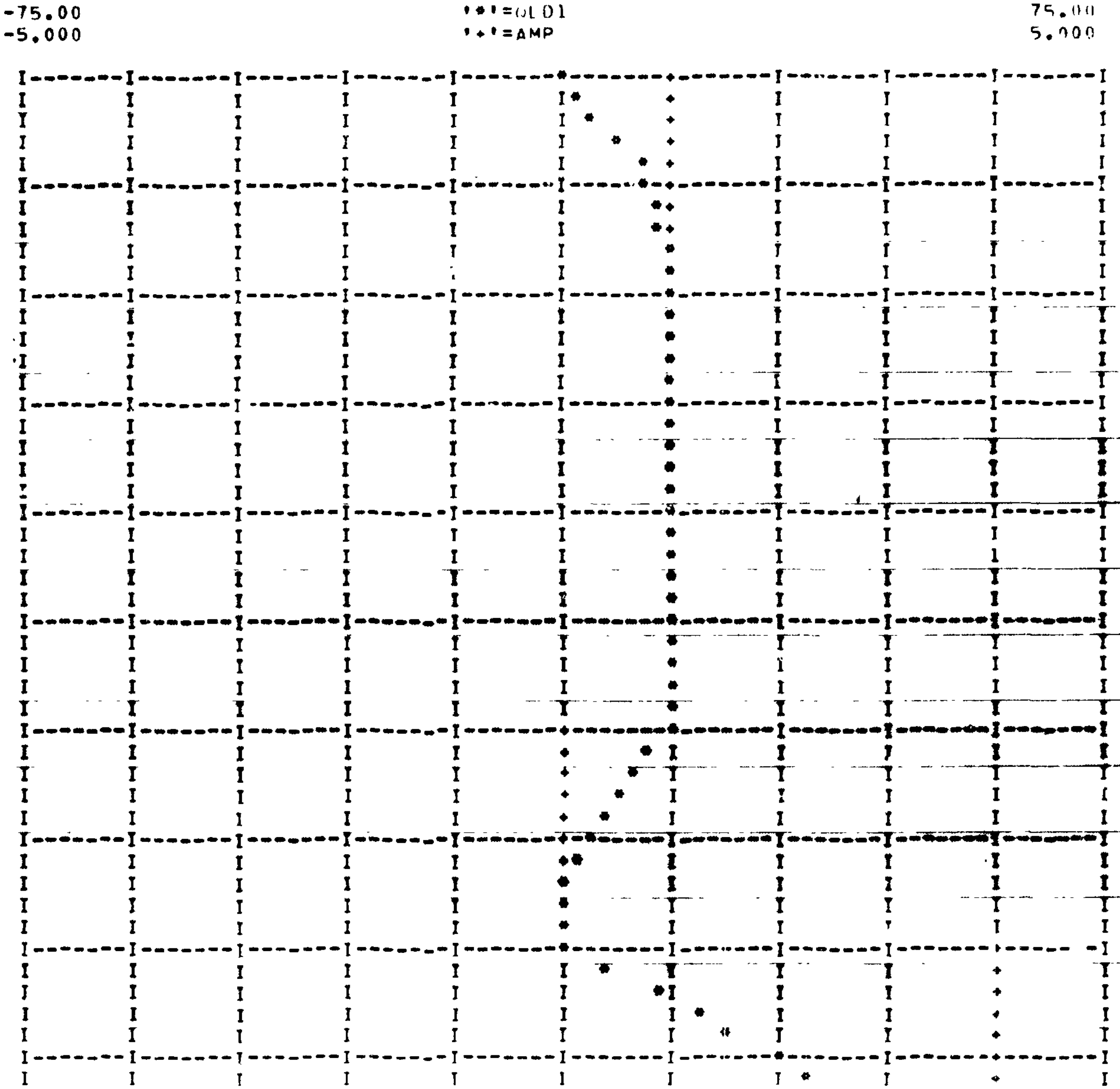

```
    TIME          AMP        QLD1
 .0             1.0010     .0
 1.0000E-03     1.0010     2.2013
 2.0000E-03     1.0010     4.4264
 3.0000E-03     1.0010     7.6513
 4.0000E-03     1.0010     10.281
 5.0000E-03     1.0010     11.886
 6.0000E-03     1.0010     13.268
 7.0000E-03     1.0010     13.288
 8.0000E-03     1.0010     14.366
 9.0000E-03     1.0010     14.417
 1.0000E-02     1.0010     14.967
 1.1000E-02     1.0010     14.470
 1.2000E-02     1.0010     14.507
 1.3000E-02     1.0010     14.677
 1.4000E-02     1.0010     14.471
 1.5000E-02     1.0010     14.324
 1.6000E-02     1.0010     14.670
 [illegible]    1.0010     14.670
 [illegible]    1.0010     14.[illegible]
 [illegible]    1.0010     14.[illegible]
 2.0000E-02     1.0010     14.609
 2.1000E-02     1.0010     14.609
 2.2000E-02     1.0010     14.569
 2.3000E-02     1.0010     14.375
 2.4000E-02     1.0010     14.376
 2.5000E-02     1.0010     14.572
 2.6000E-02     1.0010     14.672
 2.7000E-02     1.0010     14.392
 2.8000E-02     1.0010     14.392
 2.[illegible]E-02     1.0010     14.612
 3.0000E-02     .0         14.612
 3.1000E-02     .0         11.982
 3.2000E-02     .0         9.4608
 3.3000E-02     .0         7.1207
 3.4000E-02     .0         4.9695
 3.[illegible]E-02     .0         3.0826
 3.[illegible]E-02     .0         1.3239
 3.[illegible]E-02     .0         1.3352E-02
 3.8000E-02     .0         .41050
 3.9000E-02     .0         -.47281
 4.0000E-02     4.0000     .23918
 4.1000E-02     4.0000     4.9977
 4.2000E-02     4.0000     12.851
 4.3000E-02     4.0000     19.602
 4.4000E-02     4.0000     23.169
 4.5000E-02     4.0000     30.455
 4.6000F-02     4.0000     33.953
```

Figure 3. -2. Simulated Valve Step Responses

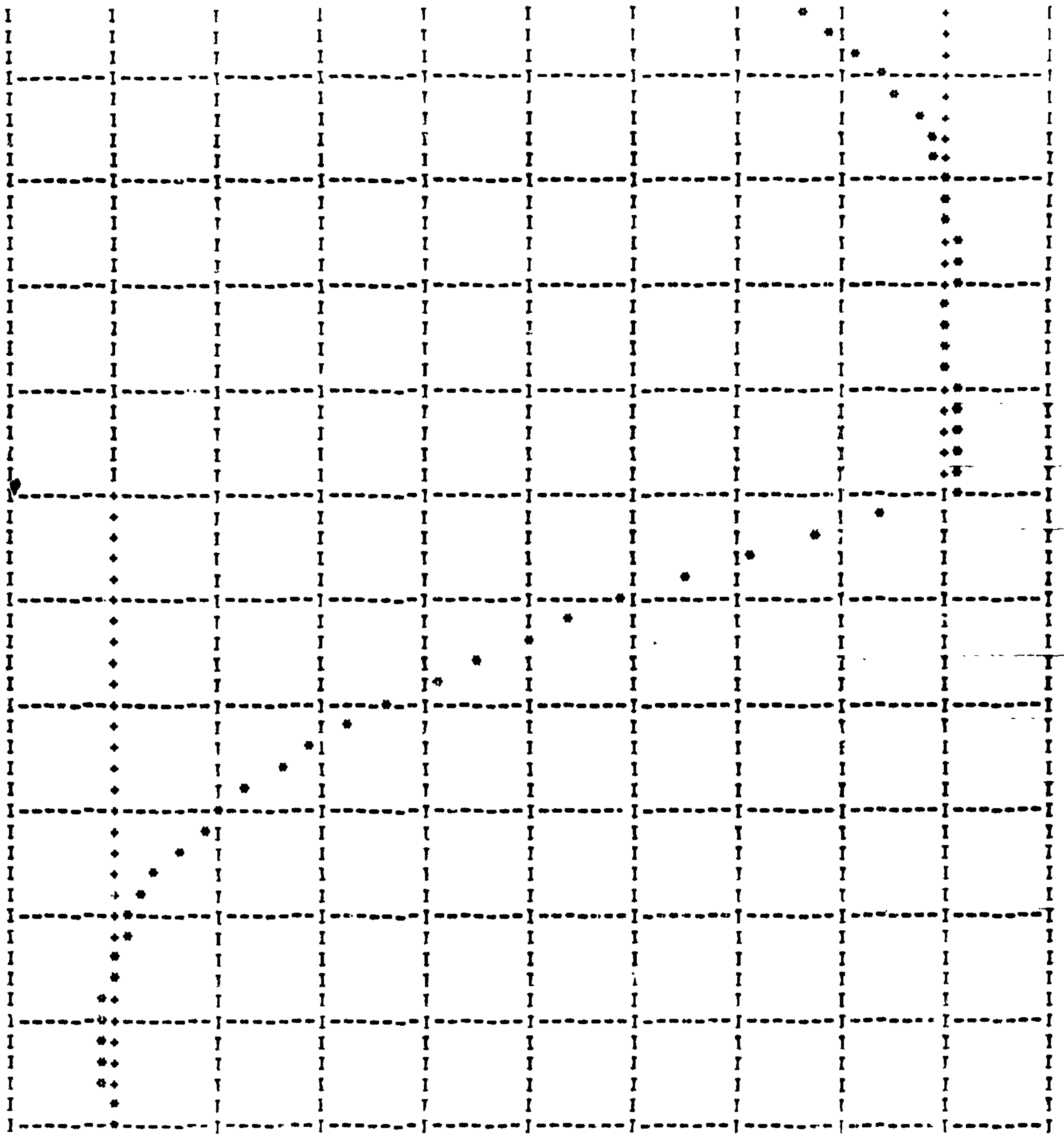

```
4.7000E-02   4.0000    39.155
4.8000E-02   4.0000    43.055
4.9000E-02   4.0000    45.744
5.0000E-02   4.0000    50.13
5.1000E-02   4.0000    52.021
5.2000E-02   4.0000    54.824
5.3000E-02   4.0000    56.572
5.4000E-02   4.0000    57.707
5.5000E-02   4.0000    59.019
5.6000E-02   4.0000    59.981
5.7000E-02   4.0000    60.140
5.8000E-02   4.0000    60.398
5.9000E-02   4.0000    60.398
6.0000E-02   4.0000    60.398
6.1000E-02   4.0000    60.099
6.2000E-02   4.0000    60.099
6.3000E-02   4.0000    60.099
6.4000E-02   4.0000    60.099
6.5000E-02   4.0000    60.228
6.6000E-02   4.0000    60.228
6.7000E-02   4.0000    60.228
6.8000E-02   4.0000    60.228
6.9000E-02   4.0000    60.228
7.0000E-02  -4.0000    60.228
7.1000E-02  -4.0000    49.711
7.2000E-02  -4.0000    40.024
7.3000E-02  -4.0000    30.806
7.4000E-02  -4.0000    22.017
7.5000E-02  -4.0000    13.683
7.6000E-02  -4.0000    5.8574
7.7000E-02  -4.0000   -.42041
7.8000E-02  -4.0000   -7.2092
7.9000E-02  -4.0000   -13.749
8.0000E-02  -4.0000   -19.852
8.1000E-02  -4.0000   -25.508
8.2000E-02  -4.0000   -30.719
8.3000E-02  -4.0000   -35.488
8.4000E-02  -4.0000   -39.817
8.5000E-02  -4.0000   -43.709
8.6000E-02  -4.0000   -47.170
8.7000E-02  -4.0000   -50.202
8.8000E-02  -4.0000   -52.813
8.9000E-02  -4.0000   -55.007
9.0000E-02  -4.0000   -56.796
9.1000E-02  -4.0000   -58.187
9.2000E-02  -4.0000   -59.208
9.3000E-02  -4.0000   -59.911
9.4000E-02  -4.0000   -60.318
9.5000E-02  -4.0000   -60.374
9.6000E-02  -4.0000   -60.374
9.7000E-02  -4.0000   -60.374
9.8000E-02  -4.0000   -60.168
9.9000E-02  -4.0000   -60.068
.10000      -4.0000   -60.068
```

Figure 3.3-2. (Continued)

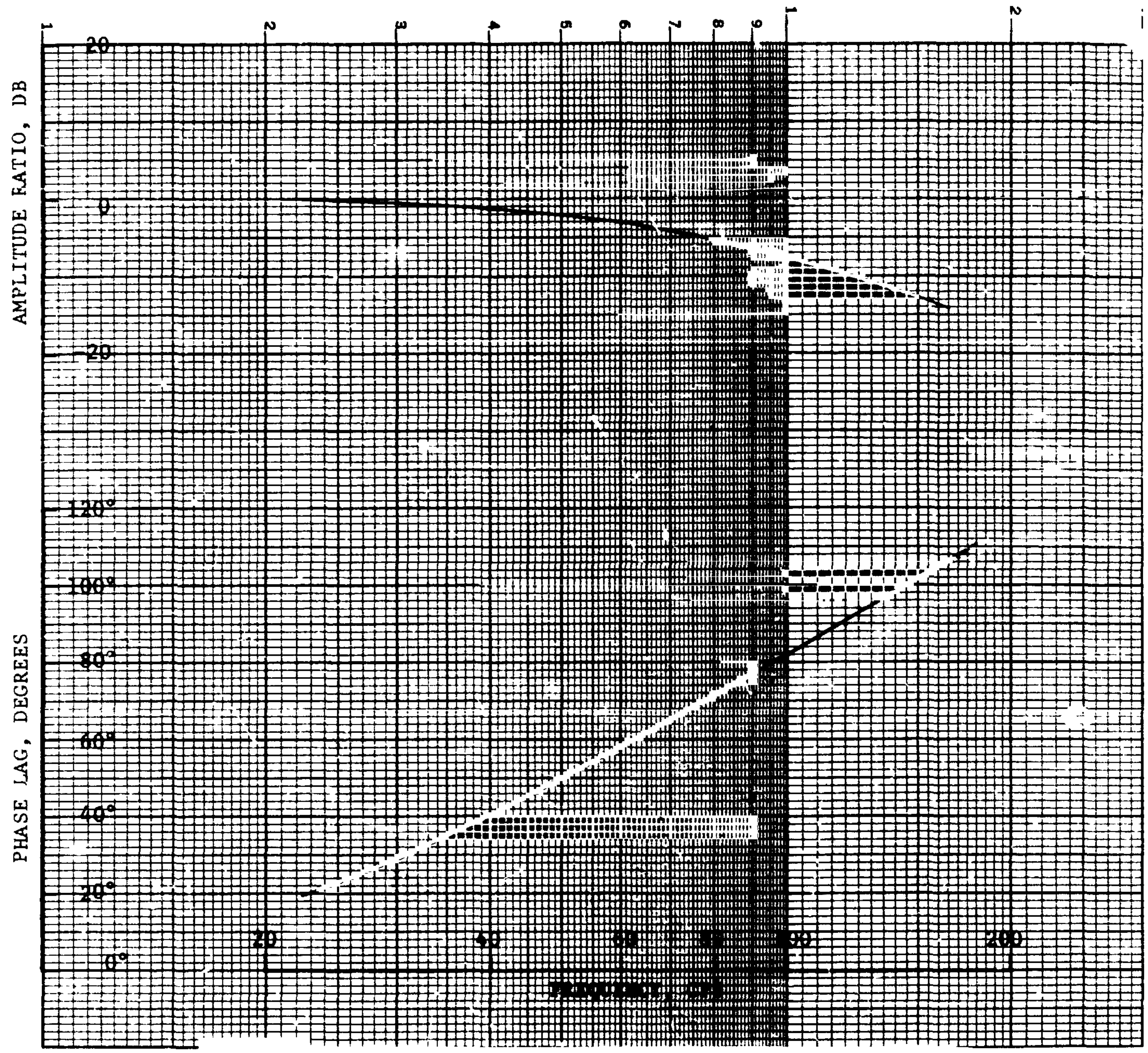

Figure 3.3-3. Predicted Frequency Response

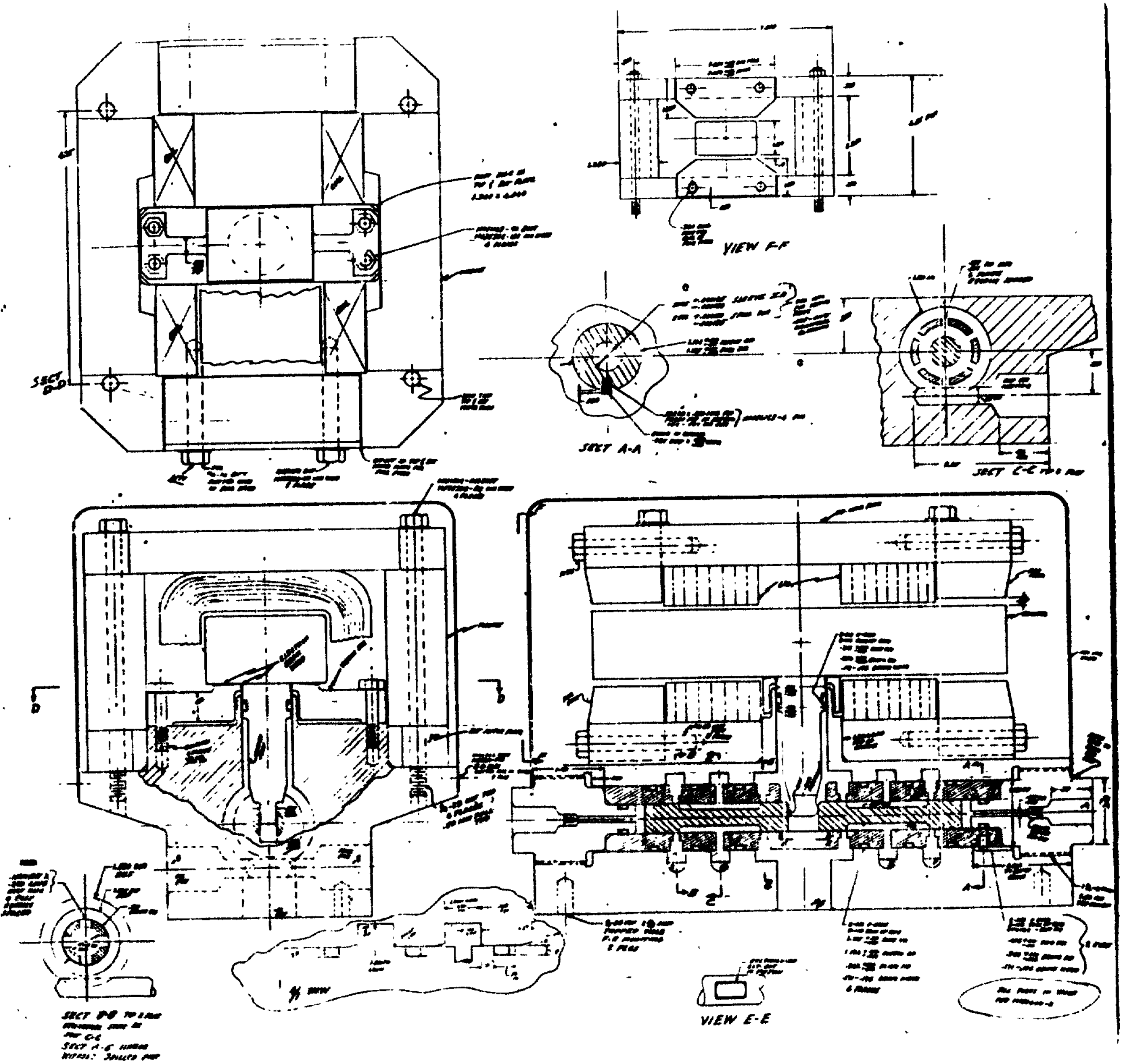
VIEW F-F
SECT A-A
SECT C-C
SECT D-D
VIEW E-E

Figure 3.4-1. Finalized Layout of Valve

inch diametrical clearance fit with the spool. The sleeve is positioned in the housing bore and centered with the null position of the torque motor shaft by adjustment of the end plugs. Rotational position of the sleeve is controlled by an alignment pin. Each end plug contains a 0.014 inch diameter orifice which provides damping for the spool in each direction of travel, and lockwire holes for locking provision.

The spool and sleeve are designed for a 0.001 inch overlap at each sealing surface. Flow grind procedure is required to determine the required overlap/underlap condition at these surfaces.

To facilitate prototype manufacturing, no internal blind passages were designed into the valve housing. External plumbing must be used to connect the respective pressure and return ports, all of which conform to M533649-X.

Suggested order of assembly:

1 Sleeve with required O-rings

2 Spool

3 Bottom motor plate

4 Armature assembly with required O-ring

5 Coils (2)

6 Magnets (2)

7 Top motor plate

8 Pole piece (4)

9 End plugs (2) with required O-ring and orfice

10 Motor cover.

3.5 Design Critique

The design of the electro-hydraulic servo valve was reviewed at Moog, Inc. with Messrs. Jack Williams, George Chenault and Mark Chavas on 30 July 1973.

The present design was generally agreed with Moog's personnel, e.g., based on the present configuration of the torque motor a force of 205 lb_f at spool was predicted from G. Chenault's calculation. Questions were asked and comments and/or suggestions were made. The latter are summarized as follows:

1 Slots inside the sleeve: The present slots are full annulus. A better design is to make four slots rectangular in shape. This design provides better guides for the spool.

This suggestion was taken. Four rectangular slots are used, each of which is 0.22" x 0.1".

2 Spool stroke: A longer stroke of spool tends to make thermal expansion effects less significant. A stroke of 0.012" is used in the present design which corresponds to a movement of the armature of 10% of the air gap. A maximum movement of 30% has been used at Moog. The present spool stroke may be increased provided the related components work out all right.

The stroke of the spool is increased to .020" and the armature movement becomes approximately 24% of the air gap.

3 Effects of thermal expansion on the spool-sleeve neutral position: The sleeve is spring-load at one end against a plug at the other end. Due to the difference of thermal expansion coefficients the relative position of spool and sleeve changes at elevated and lowered temperatures. This causes neutral bias and needs to be solved.

The valve body material will be changed to stainless steel #304.

4 The recommended spool-sleeve diametral clearance is .0005" to .00075". The amount of under-lap is suggested to be .0001" to .0002" per land. This recommendation is being implemented.

5 The back-up rings on the sleeve are used on one side of the "O" ring groove and causes confusion during assembling. This may be eliminated by using two back-up rings in each groove.

The present design is technically correct. Adding back-up rings requires longer sleeve and spool which reduces response speed. No change will be made.

6 The slant ports on the sleeve will not produce sufficient damping effect and a row of normal holes are suggested.

This is agreeable and changes will be made accordingly.

7 Grooves are suggested around spool to eliminate side loading of spool due to difference in pressure.

This suggestion is accepted and changes will be made accordingly.

8 Two screws are suggested to fasten the torsion bar to the valve body rather than one screw.

This suggestion is accepted and changes will be made accordingly.

9 It was suggested to use plugs for both ends of the sleeve for the manufacturing convenience so that the bore of the valve body can be cut through.

This was accepted and changes were made accordingly.

4.0 CONCLUSIONS

The objective of 6° TVC by direct injection of 2000°F gases into a nozzle has been met by the design developed under this contract. Gas flow rates required for control have been minimized by locating injection ports at 60 percent of the distance from the throat to the exit and by injecting the gases supersonically through multiple ports, three in each quadrant. A high margin of safety has been designed into the valve by selecting material capable of 2000°F operation and insulating it to prevent temperatures above 500°F.

Slot injection using a rectangular duct and valve was discarded as a concept because of greater weight than the multiple use of circular valves.

A hydraulic servovalve was designed to accomodate highly contaminated hydraulic fluid. The design consists of a direct drive servo in which the spool is powered directly by the electromechanical device, imparting a spool force of 200 pounds. The valve was orifice damping and has a spool diametral clearance of .0005 inch. The predicted performance provides a settling time of 6 to 19 milliseconds with 90° phase lag occurring at 117 cycles per second.

PRECEDING PAGE BLANK NOT FILMED

5.0 APPENDIX

5.1 References

1. Secondary Gas Injection in a Conical Rocket Nozzle; R. E. Walker, A. R. Stone and M. Shandor; Report CM-1010 Johns Hopkins University Applied Physics Laboratory; February 1962.

2. Basic TVC Experiments with Gas Injection and Probes; R.E. Walker, A. R. Stone and M. Shandor; Dept. TG-537 Johns Hopkins University Applied Physics Laboratory; October 1963.

3. Side Thrust Control by Secondary Gas Injection Into Rocket Nozzles; J. H. Neilson, A. Gilchrist and C. K. Lee; Journal Mechanical Engineering Science, Vol. 10, No. 3 1968, pg 239-251.

4. Experiments on Rocket Thrust Vector Control by Hot Gas Injection; T. Inouye and H.B. Nottage, AIAA Journal of Spacecraft and Rockets, May 1966, pg 737-739.

5. Proportional Solid Propellant Secondary Injection Thrust Vector Control Study, NASA CR-367, November 1966.

6. An Altitude Thrust Vector Control Investigation of Hot Gas and Liquid (N_2O_4) Injections in 300:1 Area Ratio Nozzles; R. E. Smith and B. K. Holmes, AEDC-TR-66-141, September 1966.

7. Basic TVC Experiments with Gas Injection and Probes, R. Walker, A. Stone, M. Shandor, Applied Physics Laboratory, Report TG-537 (AD631-640).

8. Investigation of Secondary Jets on a Cone at a Mach Number of 6, J. Barber and W. Staylor, AIAA Journal of Spacecraft and Rockets, October 1966.

9. Cornell Aeronautical Laboratory, Report No. AA-2267-W-3.

10. Merritt, H.E., Hydraulic Control Systems, John Wiley and Sons, 1967.

11. Blackburn, J.F., et al, Editors; Fluid Power Control. MIT Press, 1960.

5.2 Glossary of Symbols

α = primary nozzle half angle

X/L = ratio of axial position of injection to total primary nozzle length

ε = injection angle from upstream primary nozzle wall

P_{op} = primary total pressure

P_{os} = secondary total pressure

T_{op} = primary total temperature

T_{os} = secondary total temperature

γ_p = ratio of specific heats for primary gas

γ_s = ratio of specific heats for secondary gas

M_s = secondary exit Mach number

Θ = thrust vector control angle

$\dot{m}_s$ = secondary gas mass flow

$\dot{m}_s C_s$ = secondary gas momentum

$\dot{m}_p$ = primary gas mass flow

$\dot{m}_p C^*_p$ = primary gas momentum

C_{fs} = total side force/injectant gas momentum

d^*_s = diameter of injection port

C_{fs} = side force coefficient: Total side force/momentum of injectant gas ($\dot{m}_s c^*_s$).

$\frac{\dot{m}_s c^*_s}{\dot{m}_p c^*_p}$ = momentum ratio: Secondary gas momentum/primary gas momentum

$\frac{P_{os}}{P_{\infty p}}$ = jet pressure ratio: Injection jet total pressure/local undisturbed primary static pressure

$\frac{I}{I_{vac}}$ = specific impulse ratio: Total side impulse/jet impulse exhausting into vacuum conditions

5.3 Detail Drawings - Gas Injection TVC System

REPRODUCIBILITY OF THE ORIGINAL PAGE IS POOR

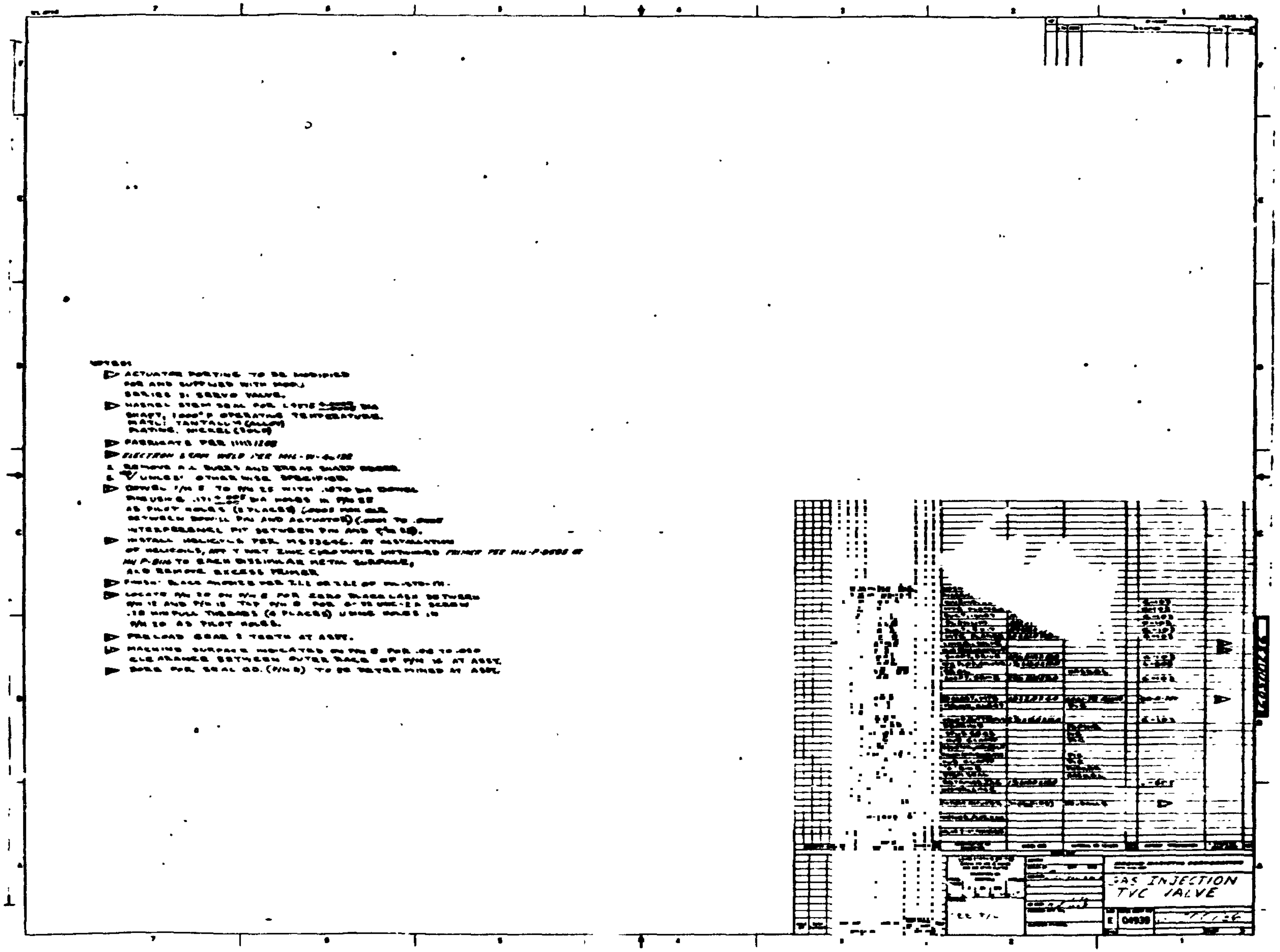
NOTES:
ACTUATOR PORTING TO BE MODIFIED FOR AND SUPPLIED WITH MOOG SERIES 31 SERVO VALVE.
REMOVE ALL BURRS AND BREAK SHARP EDGES.
UNLESS OTHERWISE SPECIFIED.
PRELOAD GEAR 1 TOOTH AT ASSY.
CLEARANCE BETWEEN OUTER RACE OF P/N 16 AT ASSY.
BORE FOR SEAL OD. (P/N 5) TO BE DETERMINED AT ASSY.
GAS INJECTION TVC VALVE

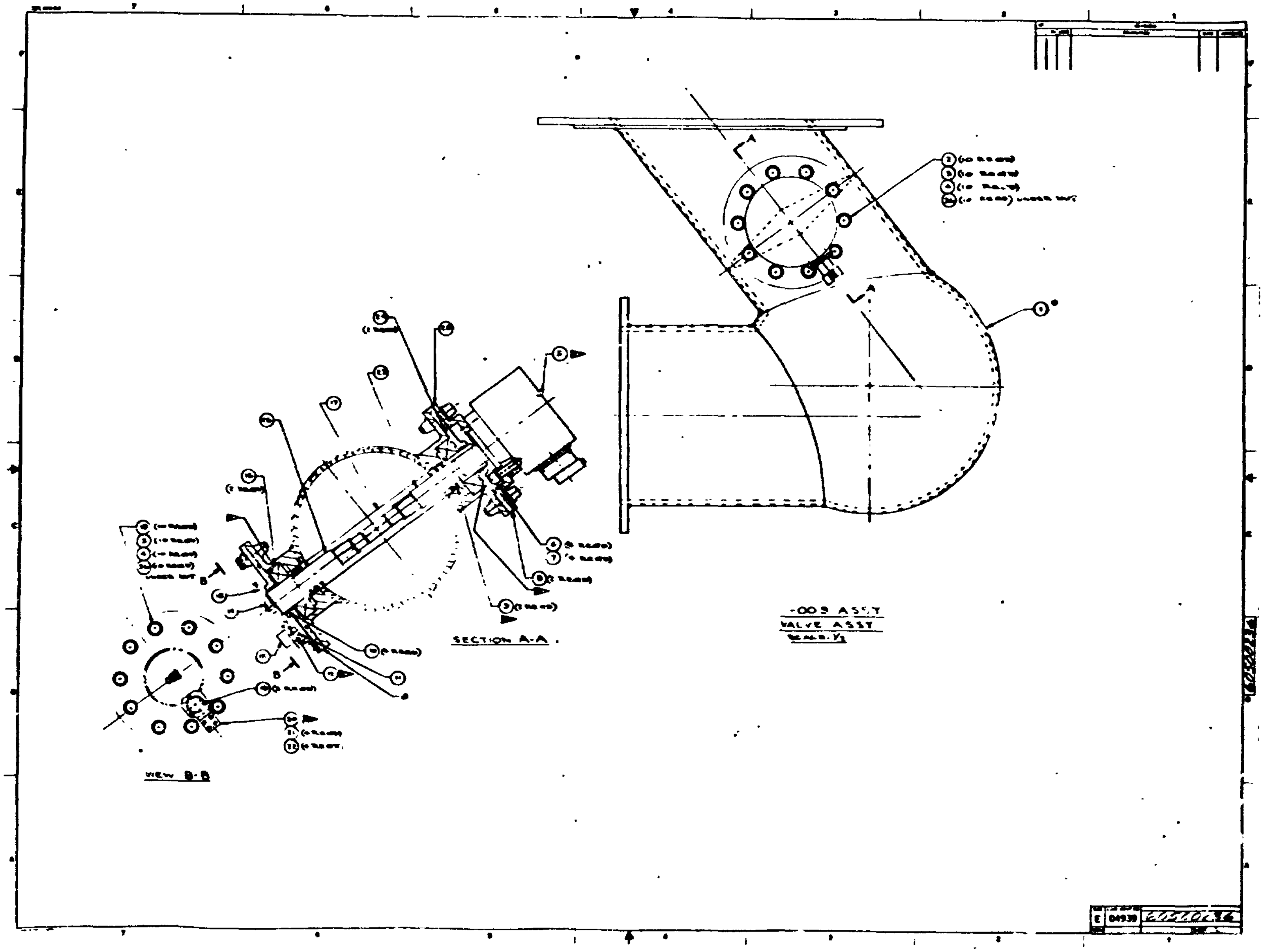
-003 ASSY
VALVE ASSY
SCALE · 1/2
SECTION A-A
VIEW B-B
A
B
E
04939

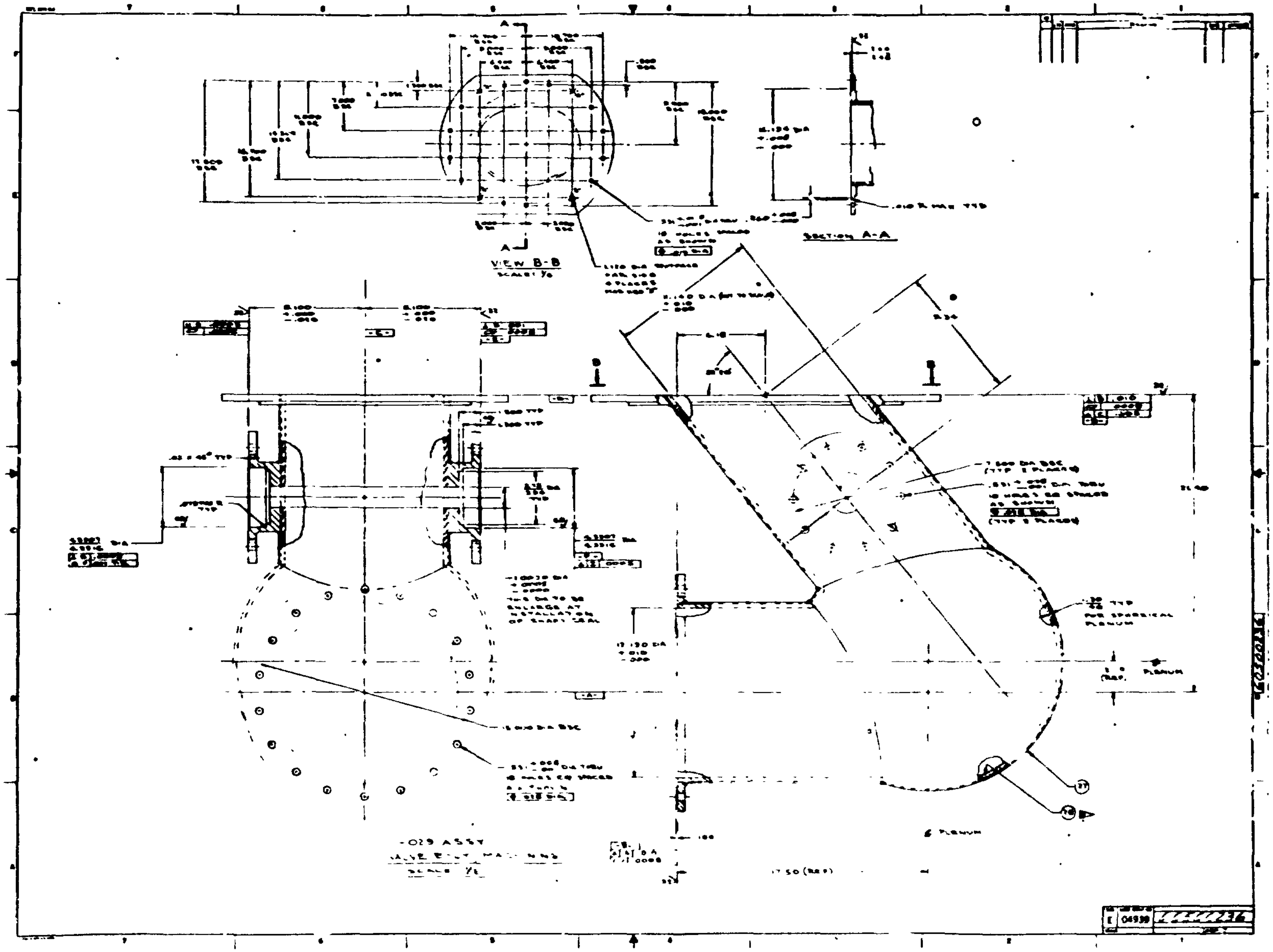
VIEW B-B
SECTION A-A
-029 ASSY
SCALE 1/2
E
04939
PLENUM

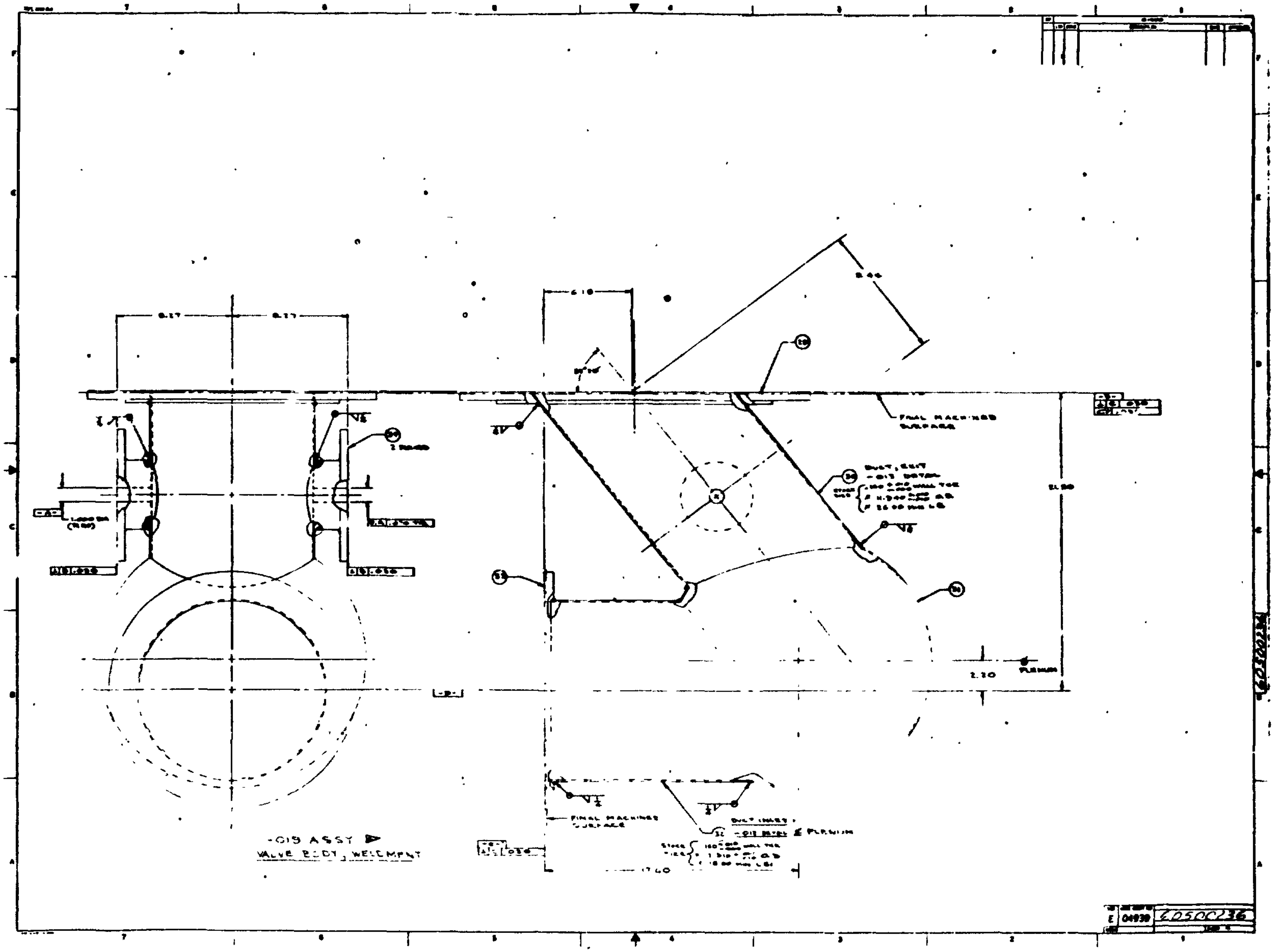

-013 ASSY
VALVE BODY, WELDMENT
FINAL MACHINED SURFACE
FINAL MACHINED SURFACE
DUCT, EXIT
-013 DETAIL
DUCT INLET
-013 DETAIL
℄ PLENUM
STOCK SIZE
6.17
6.17
6.10
8.44
11.80
2.30
17.60
E
04939
Z050C236

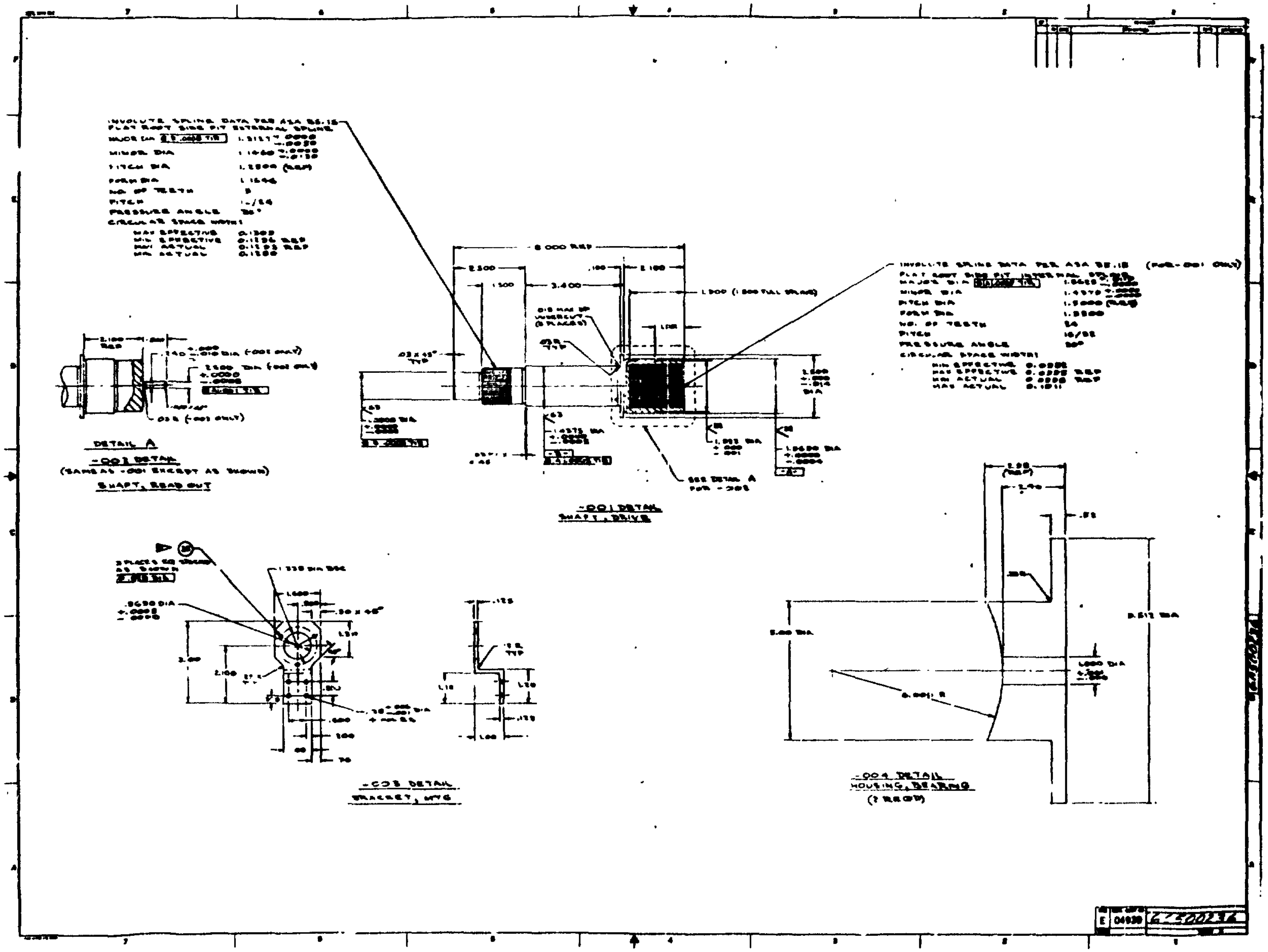
INVOLUTE SPLINE DATA PER ASA B5.15
FLAT ROOT SIDE FIT EXTERNAL SPLINE
MAJOR DIA
MINOR DIA
PITCH DIA
FORM DIA
NO. OF TEETH
PITCH
PRESSURE ANGLE
CIRCULAR SPACE WIDTH
MAX EFFECTIVE
MIN EFFECTIVE
MAX ACTUAL
MIN ACTUAL
INVOLUTE SPLINE DATA PER ASA B5.15 (FOR -001 ONLY)
FLAT ROOT SIDE FIT INTERNAL SPLINE
8.000 REF
2.500
1.500
3.400
.100
2.100
1.500 (1.500 FULL SPLINE)
SEE DETAIL A FOR -002
DETAIL A
-002 DETAIL
(SAME AS -001 EXCEPT AS SHOWN)
SHAFT, READ OUT
-001 DETAIL
SHAFT, DRIVE
-003 DETAIL
BRACKET, MTG
-004 DETAIL
HOUSING, BEARING
(2 REQD)
2.100
3.00
5.00 DIA
E 04939

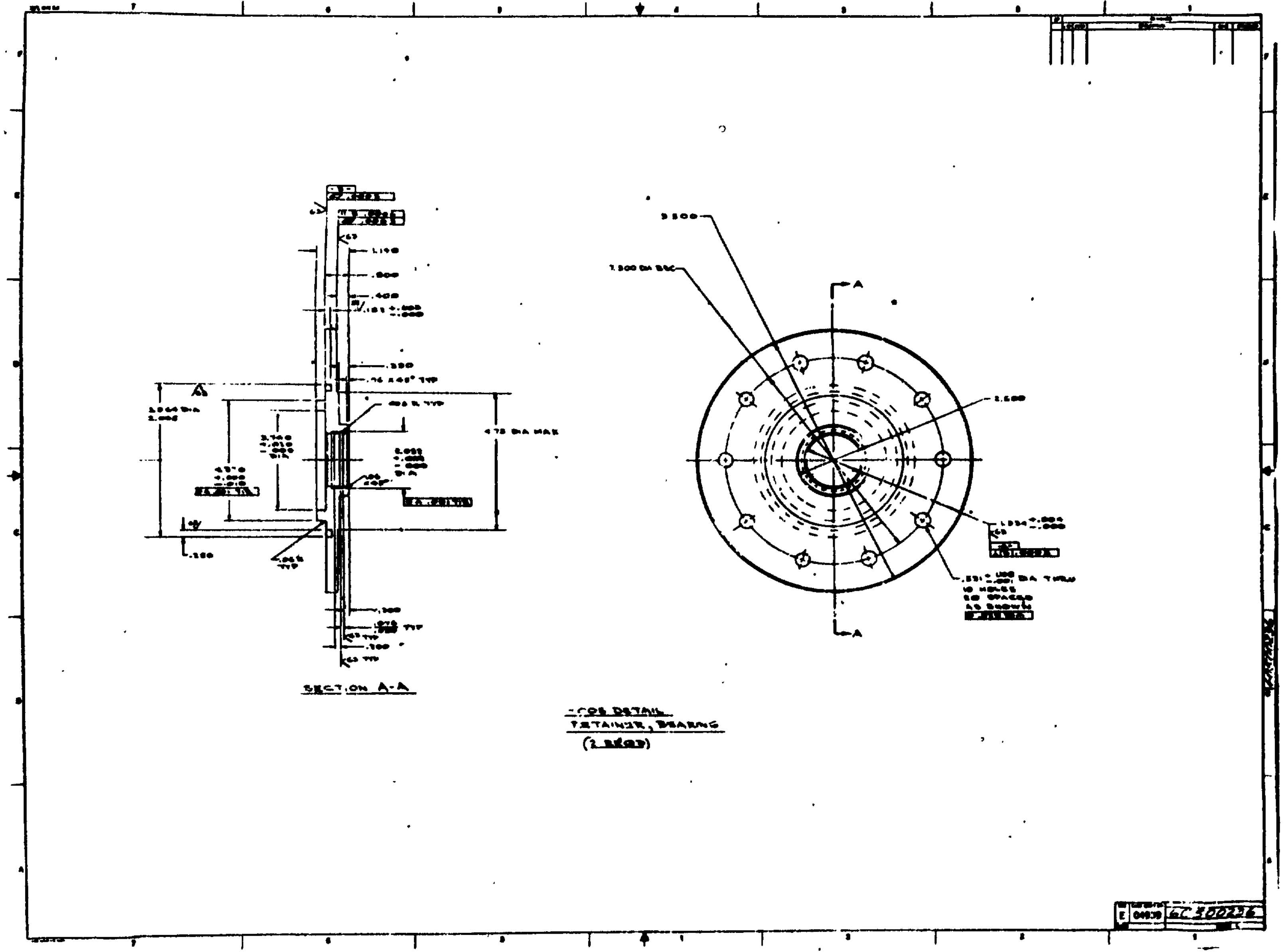
3.500
7.300 DIA BSC
2.500
A
A
1.034 +.004 -.000
10 HOLES
EQ SPACED
AS SHOWN
1.150
.800
.400
.350
.475 DIA MAX
.100
.300
.150
SECTION A-A
-C05 DETAIL
RETAINER, BEARING
(2 REQD)
E
04939
6C300226

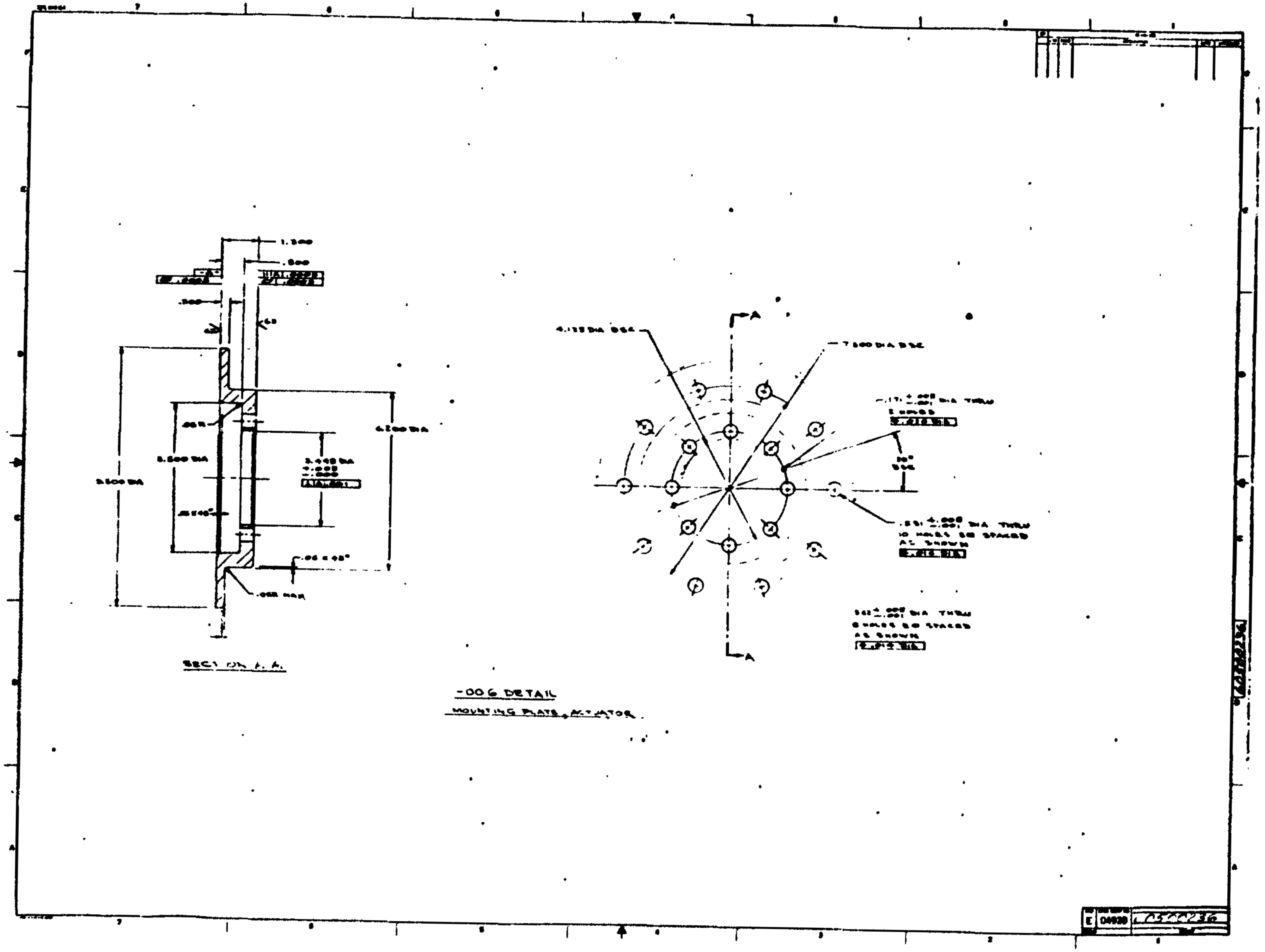
1.300
.500
.300
63
3.500 DIA
4.200 DIA
.06 x 45°
MAX
SECTION A-A
4.125 DIA BSC
7.500 DIA BSC
30° BSC
DIA THRU
10 HOLES EQ SPACED
AS SHOWN
DIA THRU
8 HOLES EQ SPACED
AS SHOWN
A
A
-006 DETAIL
MOUNTING PLATE, ACTUATOR
E

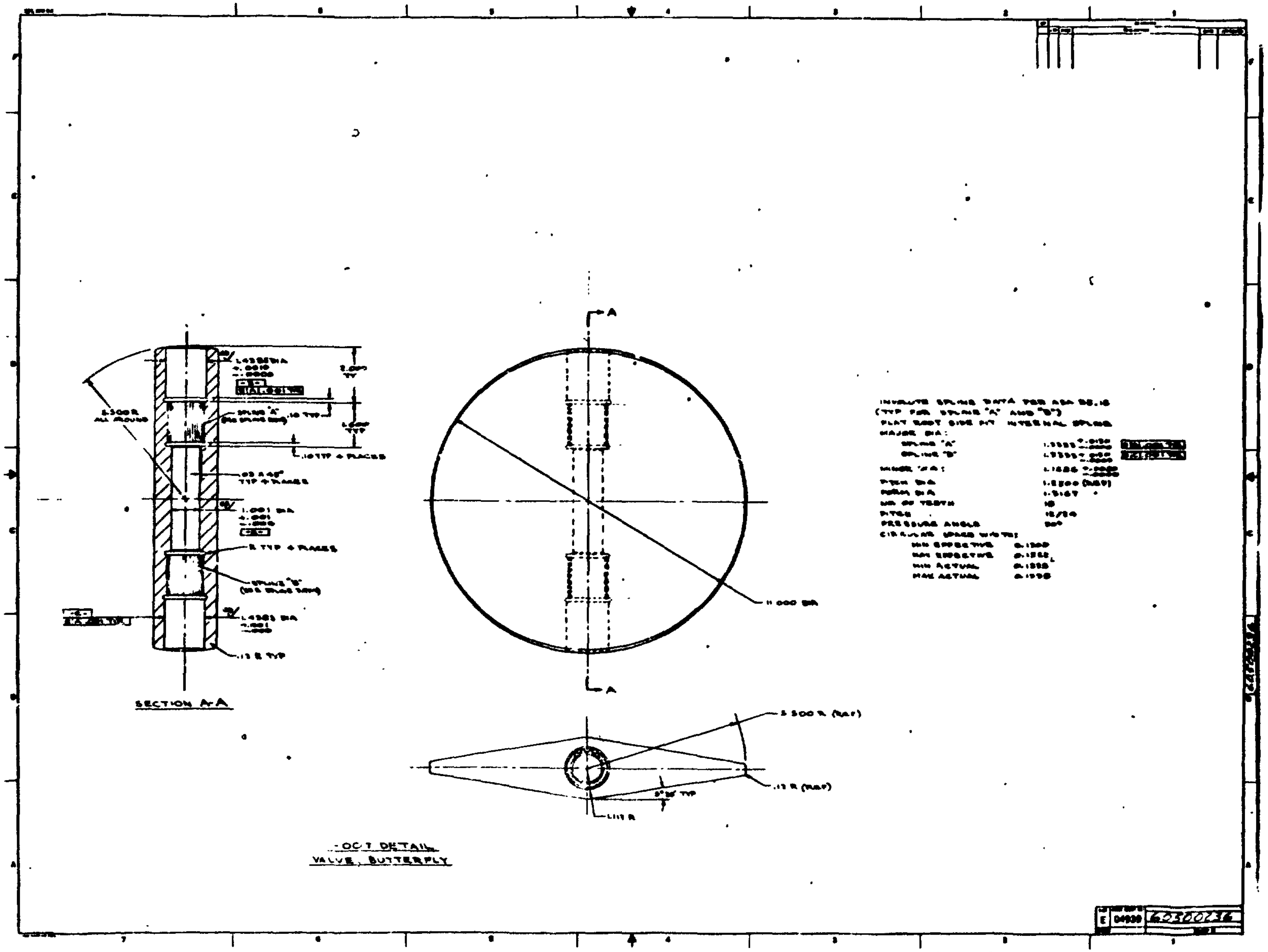
LOX DETAIL
VALVE, BUTTERFLY
SECTION A-A
A
A
11.000 DIA
5.500 R (REF)
.12 R (REF)
5.500 R ALL AROUND
SPLINE "A"
SPLINE "B"
1.001 DIA
.12 R TYP
R TYP 4 PLACES
.10 TYP 4 PLACES
INVOLUTE SPLINE DATA PER ASA B5.15
(TYP FOR SPLINE "A" AND "B")
FLAT ROOT SIDE FIT INTERNAL SPLINE
MAJOR DIA:
SPLINE "A"
SPLINE "B"
MINOR DIA
PITCH DIA
FORM DIA
NO OF TEETH
PITCH
PRESSURE ANGLE
CIRCULAR SPACE WIDTH:
MIN EFFECTIVE
MAX EFFECTIVE
MIN ACTUAL
MAX ACTUAL
60300236

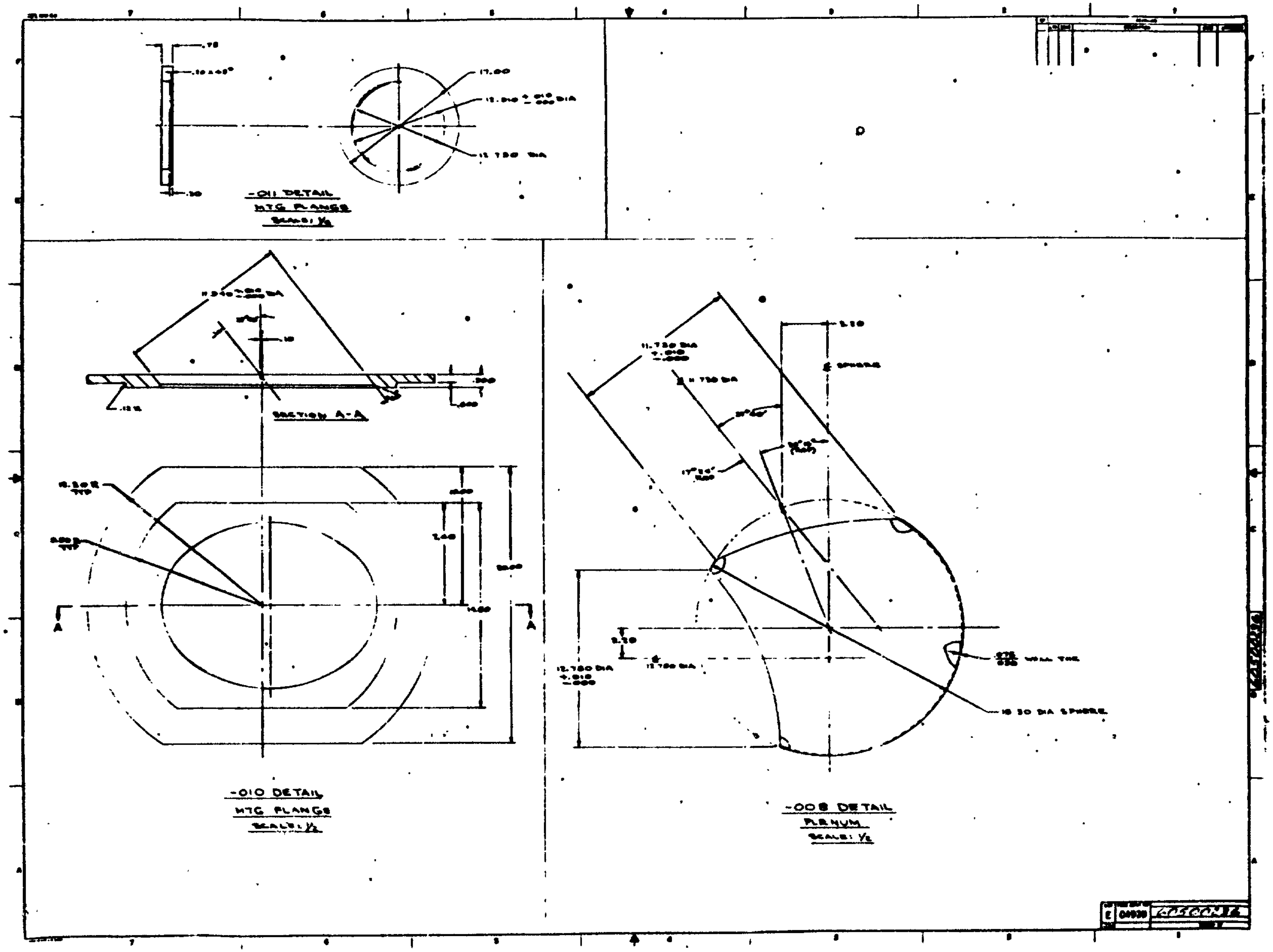
-011 DETAIL
MTG FLANGE
SCALE: 1/2
.75
.10 x 45°
.30
17.00
12.910 +.010 -.000 DIA
12.750 DIA
SECTION A-A
.125
.300
.060
.10
-010 DETAIL
MTG FLANGE
SCALE: 1/2
2.40
14.00
20.00
A
A
-008 DETAIL
PLENUM
SCALE: 1/2
11.750 DIA +.010 -.000
℄ 11.750 DIA
℄ SPHERE
2.10
12.750 DIA +.010 -.000
℄ 12.750 DIA
2.10
WALL THK
18.30 DIA SPHERE
17°24'
E 04939

5.4 Detail Drawings - High Contaminant, Direct Drive Servovalve

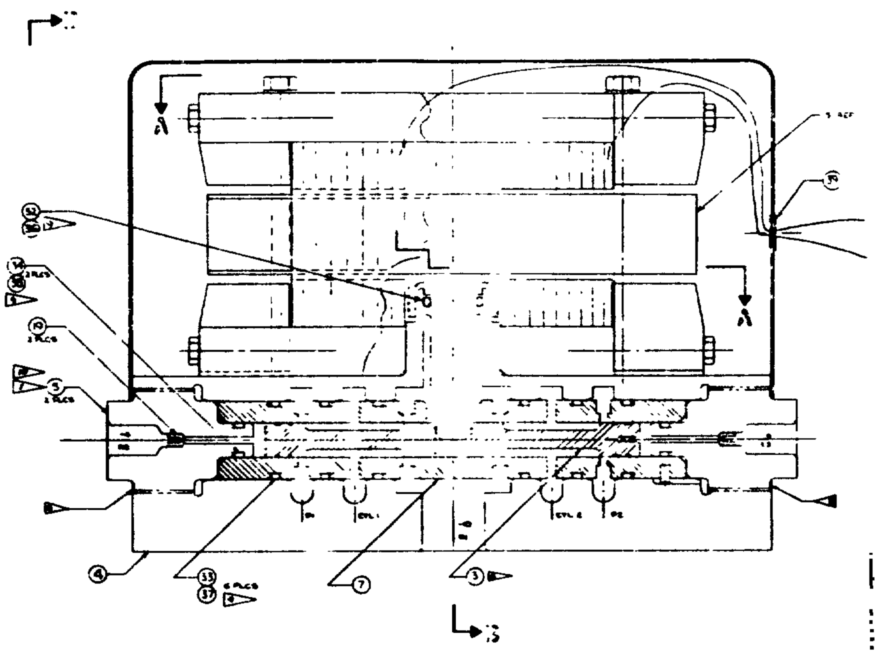

-002 SERVO VALVE ASSY

▷ COAT THDS WITH FLUOROCARBON DRY FILM LUBE
▷ LUBRICATE WITH MIL-H-5606 HYD FLUID UPON INSTALLATION
▷ STAKE 2 PLACES AFTER ADJUSTMENT
▷ TORQUE TO 40-60 IN LBS
▷ INSTALL SPOOL WITH END CONTAINING TAPPED HOLE TO SLEEVE END CONTAINING ALIGNMENT PIN
5 FOR FUNCTIONAL TEST CONNECT WITH EXTERNAL PLUMBING RETURN PORT R1 AND R2. CONNECT PRESSURE PORTS P1 AND P2
4 CLEAN SEAL & PACKAGE PER MIL-STD-794C
3 UTILIZING ADJUSTABLE END PLUGS POSITION SLEEVE TO CENTER FLOW GRIND TO DETERMINE REQD REWORK OF SPOOL (PN 40500253-001) WHICH WILL RESULT IN AN UNDERLAP OF .0004-.0005 AT SPOOL TO SLEEVE SEALING SURFACE. FLOW GRIND PROCEDURE TO BE AT HPS OPTION
2 PRESSURE TEST TO 4500 PSI
▷ SAFETY WIRE PER MS33540
NOTES

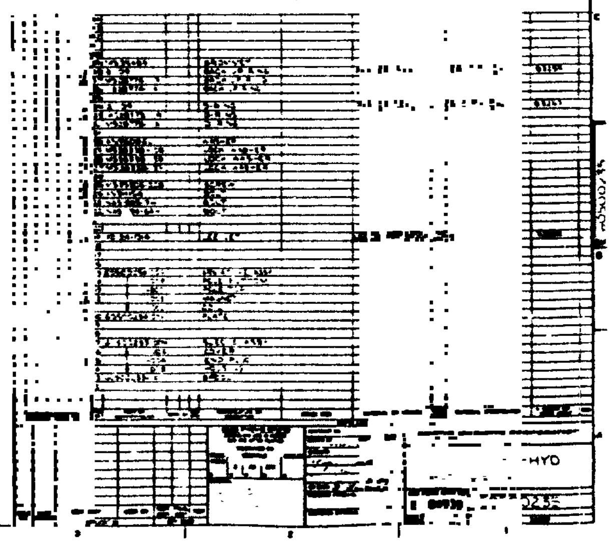

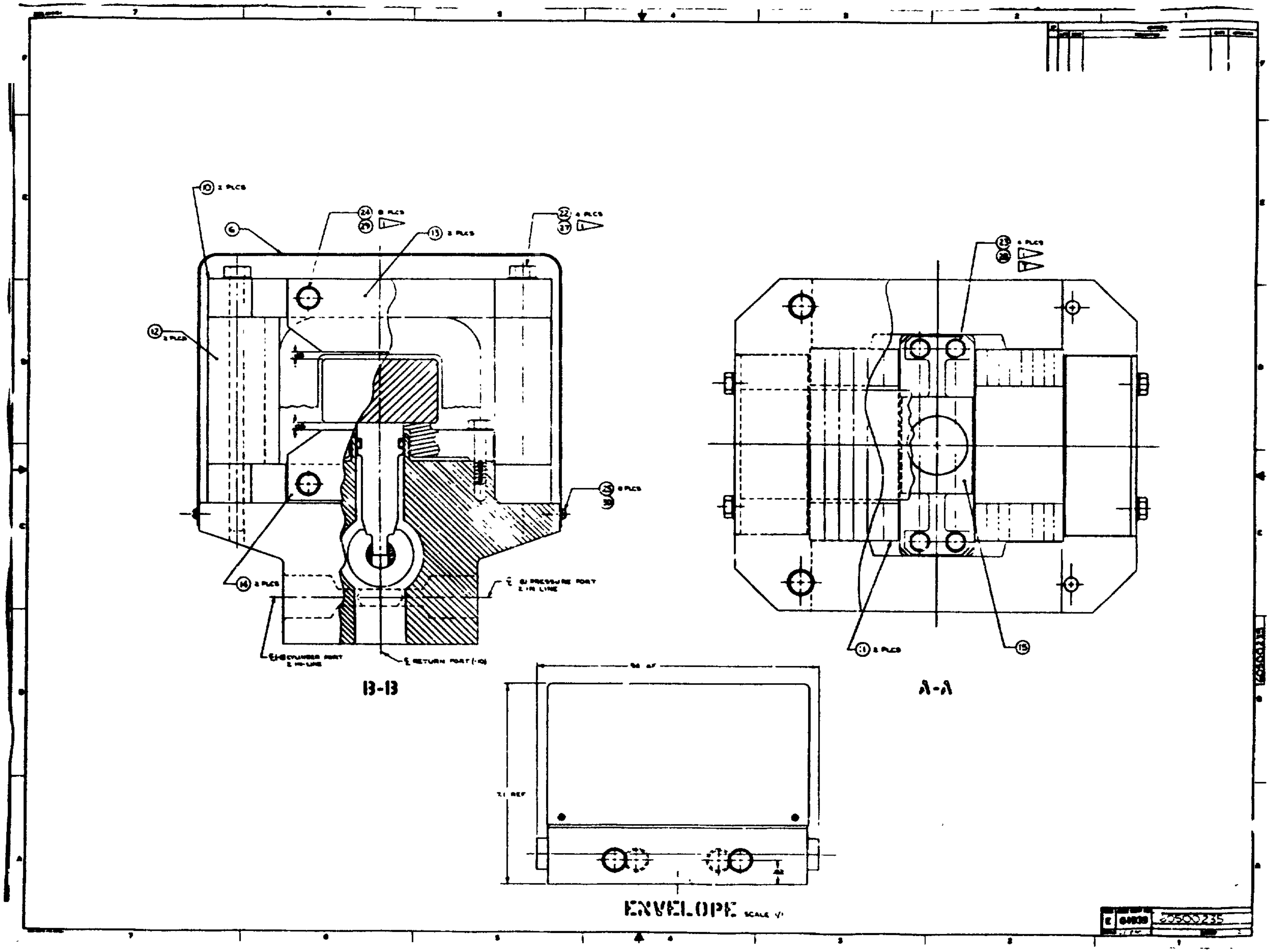
10 2 PLCS
6
24 8 PLCS
29
13 2 PLCS
22 4 PLCS
37
12 2 PLCS
25 8 PLCS
38
14 2 PLCS
℄ PRESSURE PORT
2 IN LINE
℄ CYLINDER PORT
2 IN LINE
℄ RETURN PORT (-10)
B-B
23 4 PLCS
28
11 2 PLCS
15
A-A
7.1 REF
ENVELOPE SCALE 1/1
E
25500235

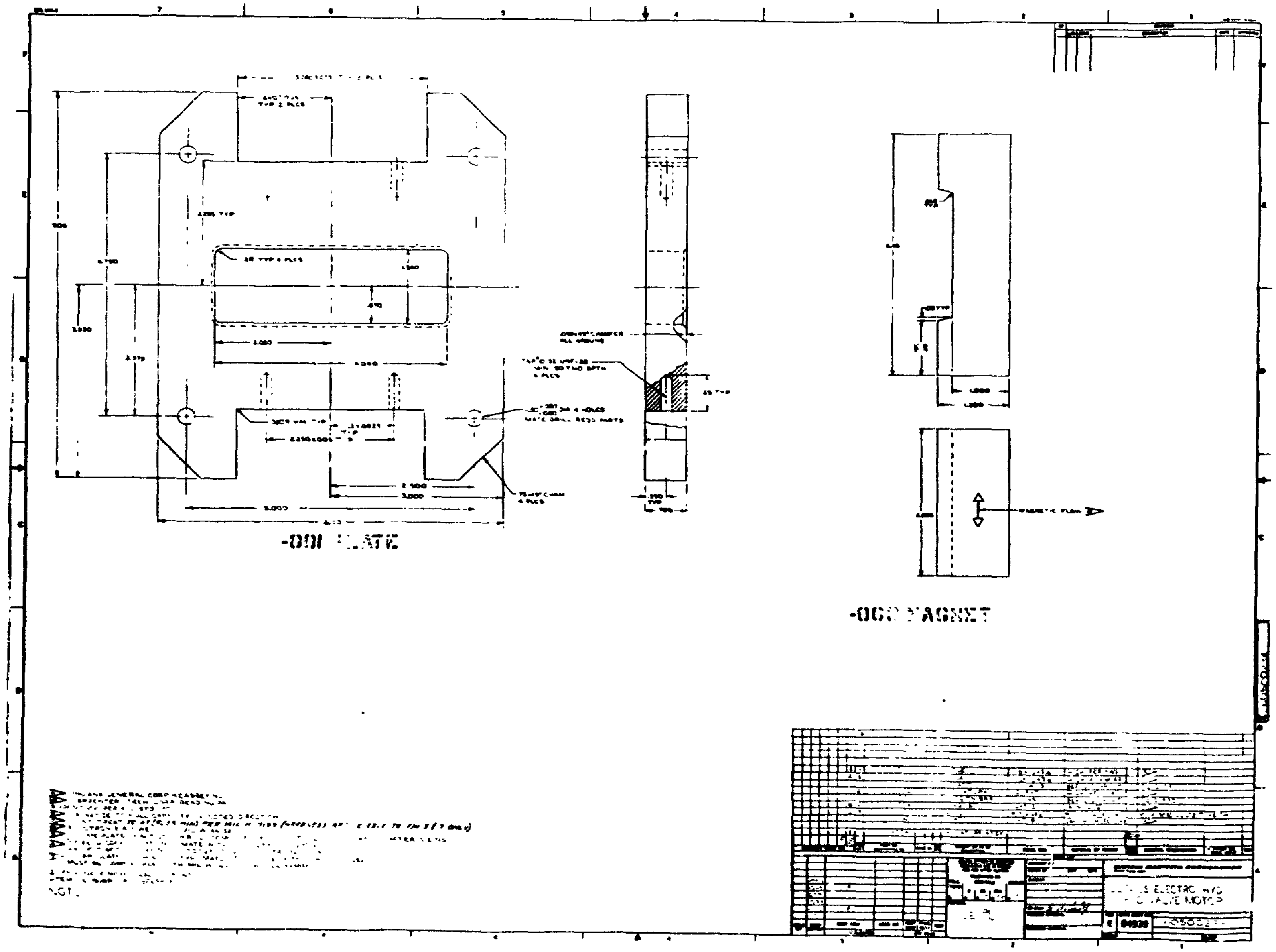-001 PLATE
-002 MAGNET
MAGNETIC FLUX
4.790
2.379
2.350
3.000
2.500
5.000
4.540
2.080
.470
1.360
.250 TYP
45 TYP
TYP 2 PLCS
4 PLCS
CHAMFER ALL AROUND
MATE DRILL
ELECTRO HYD
VALVE MOTOR
94906
NOTE

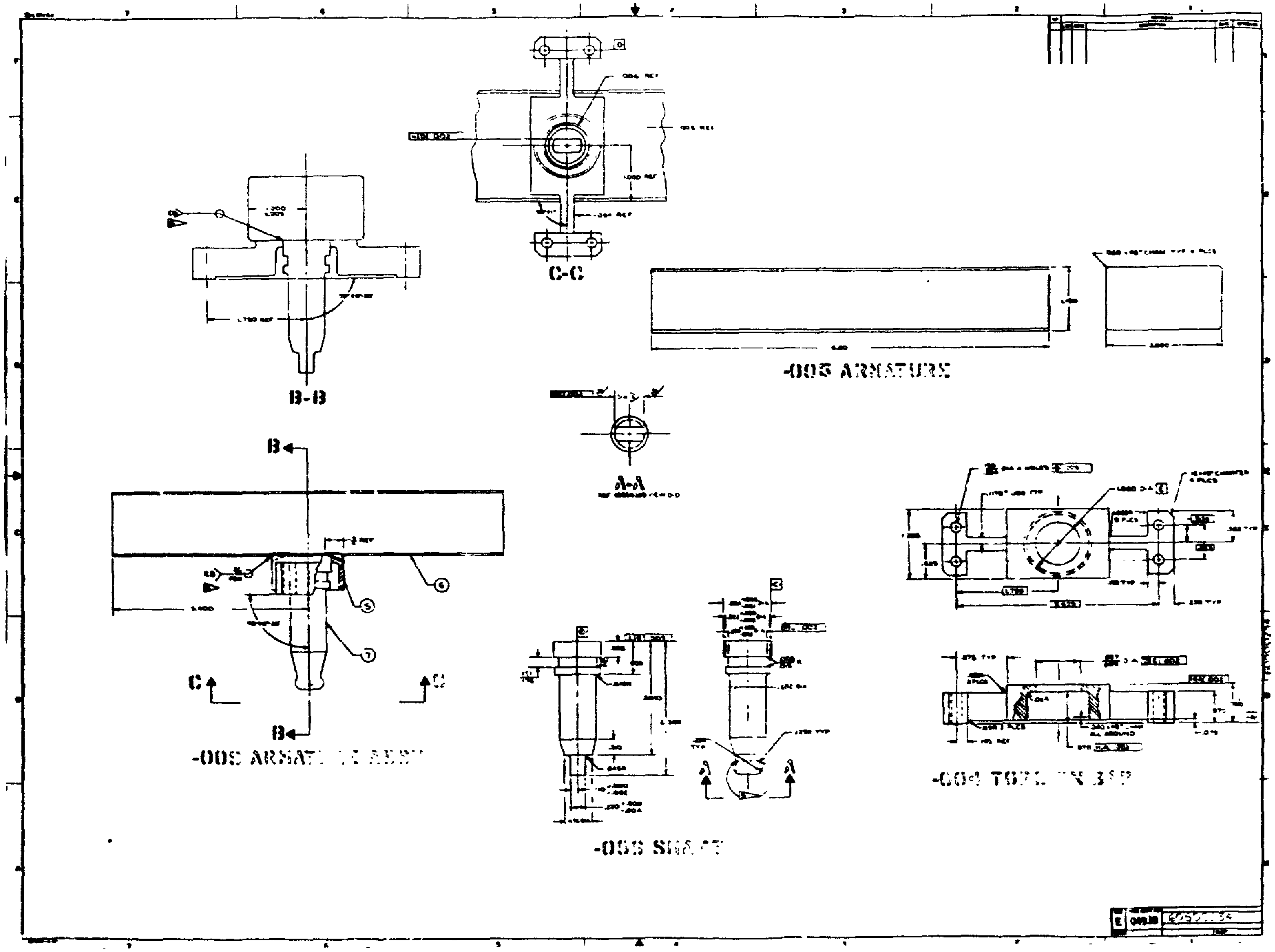
C-C
B-B
-005 ARMATURE
A-A
B
5
6
7
C
-005 SHAFT
E

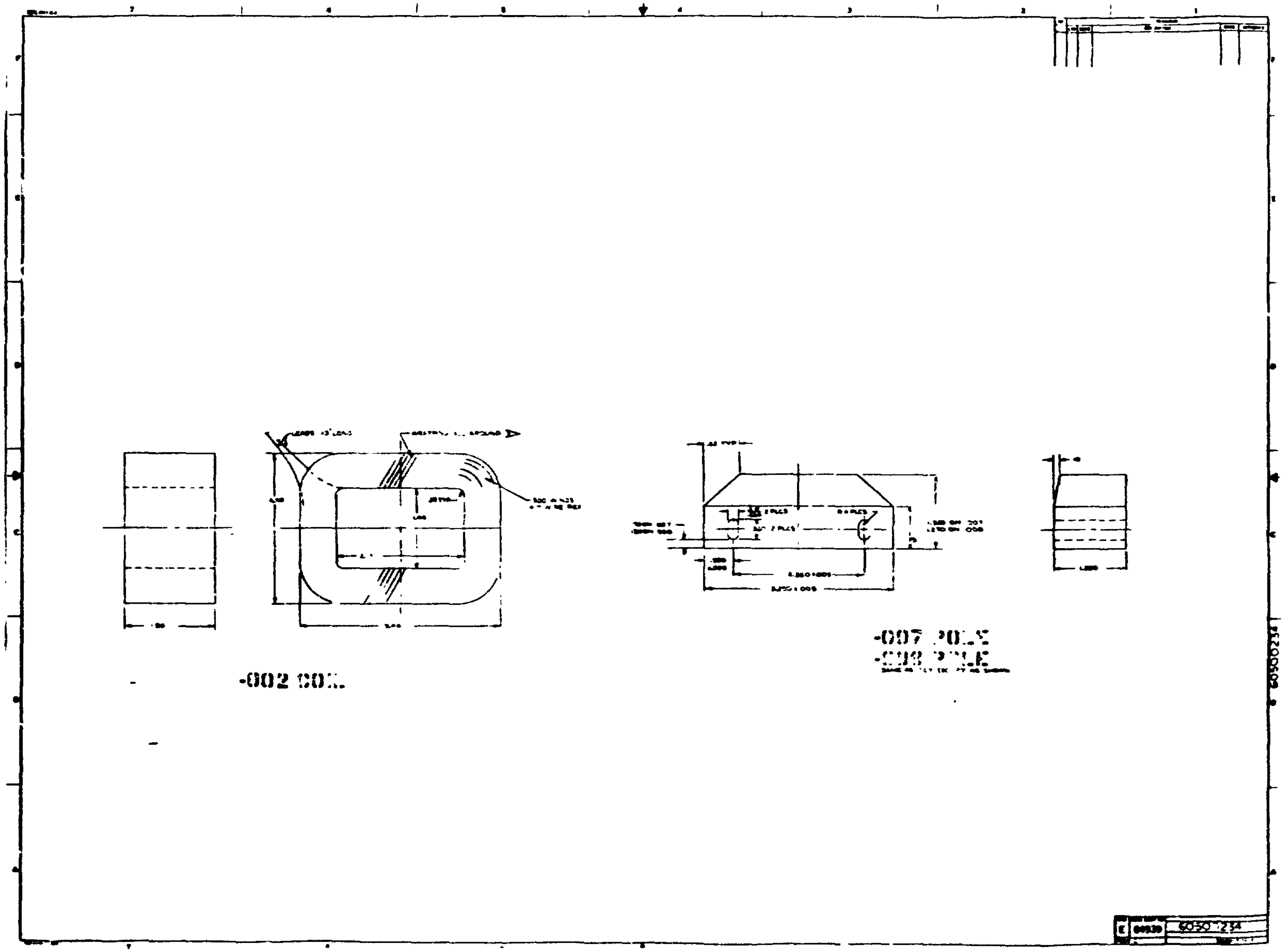
-002 COIL
-007 POLE
-008 POLE
E
6050 234

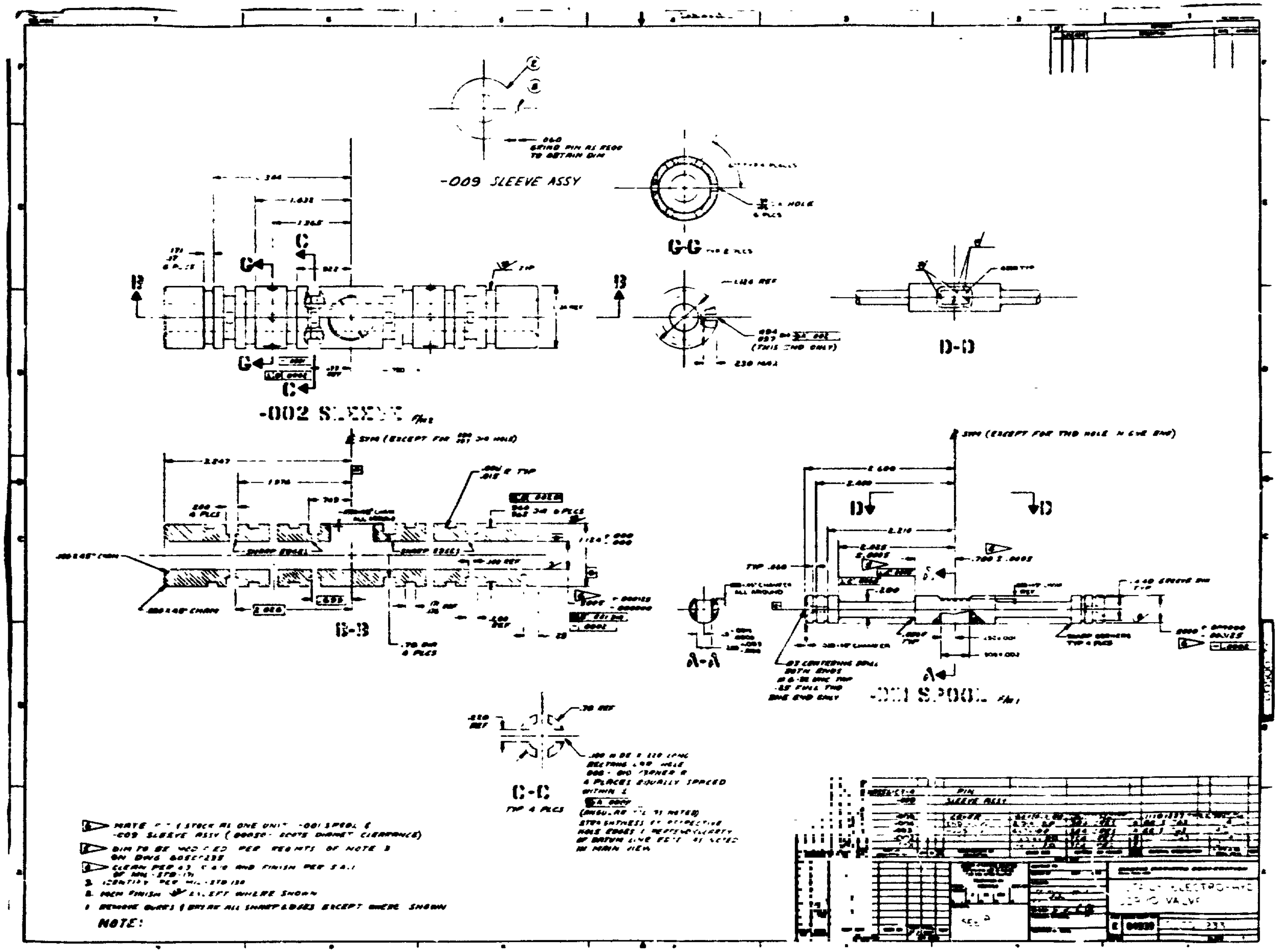
-009 SLEEVE ASSY
GRIND PIN AS REQD TO OBTAIN DIM
G-G
D-D
-002 SLEEVE
B-B
SYM (EXCEPT FOR THD HOLE IN ONE END)
-001 SPOOL
A-A
C-C
TYP 4 PLCS
SHARP EDGE
6 PLACES EQUALLY SPACED
IN MAIN VIEW
6 MATE [illegible] STOCK AS ONE UNIT -001 SPOOL &
-009 SLEEVE ASSY ([illegible] DIAMET CLEARANCE)
5 DIM TO BE [illegible] PER REQMTS OF NOTE 3
ON DWG [illegible]
4 CLEAN PER [illegible] AND FINISH PER [illegible]
OF MIL-STD-[illegible]
3. IDENTIFY PER MIL-STD-130
2. MACH FINISH [illegible] EXCEPT WHERE SHOWN
1 REMOVE BURRS & BREAK ALL SHARP EDGES EXCEPT WHERE SHOWN
NOTE:
SLEEVE ASSY
ELECTROHYD[illegible]
SERVO VALVE

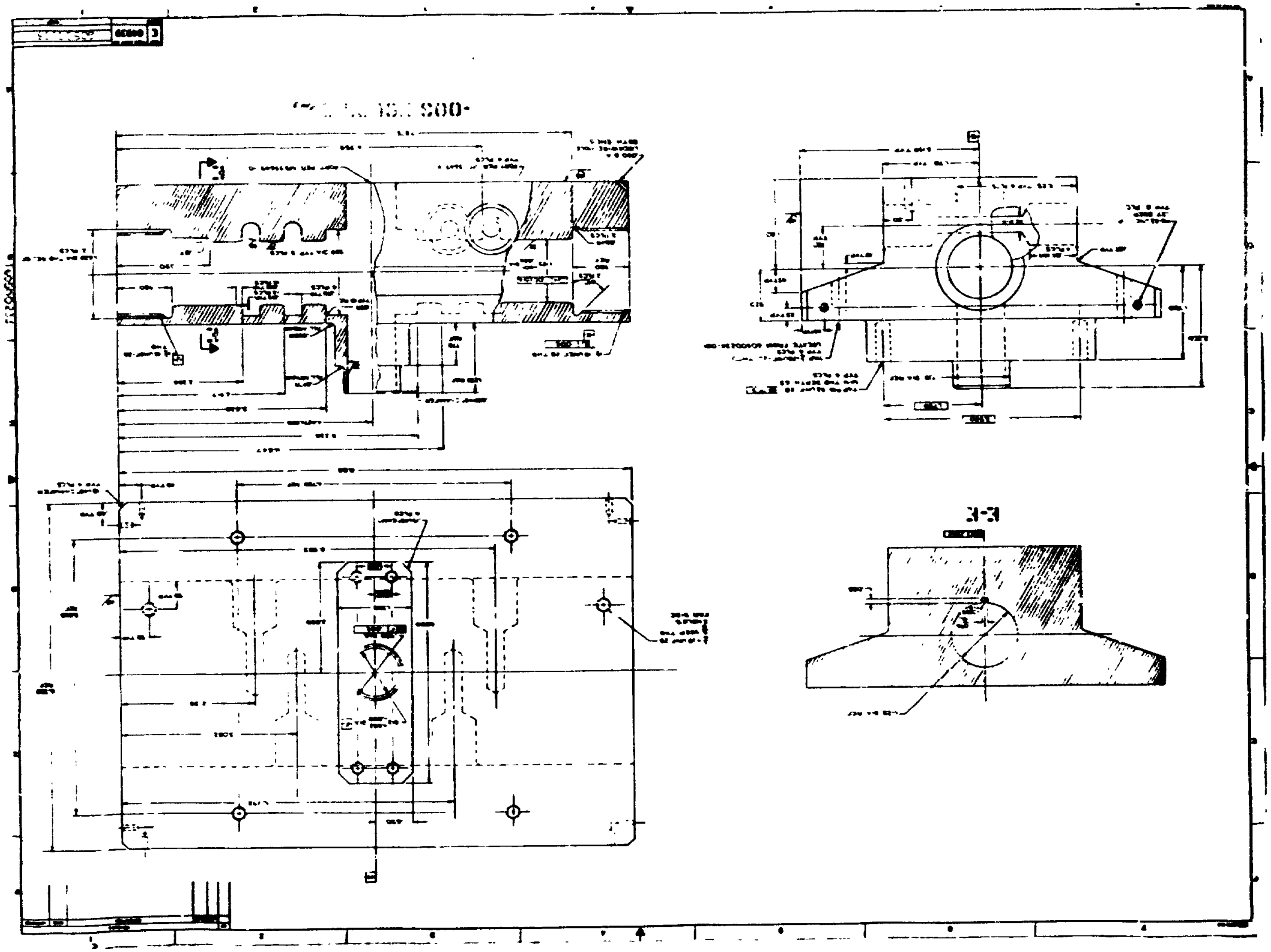
E-E

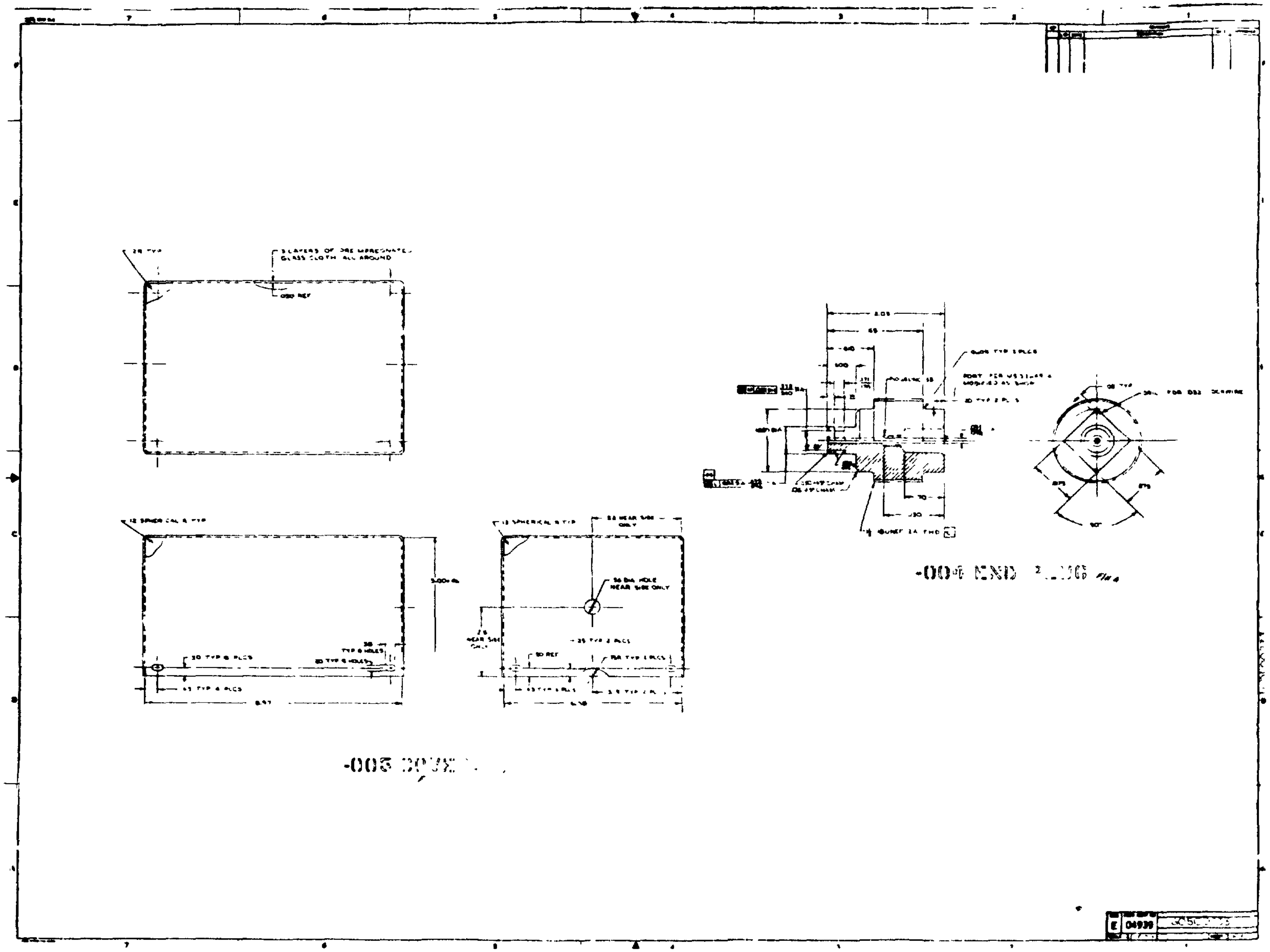
-004 END PLUG
-003 COVER
3 LAYERS OF PRE IMPREGNATED GLASS CLOTH ALL AROUND
.030 REF
.28 TYP
.12 SPHERICAL R TYP
.56 DIA HOLE NEAR SIDE ONLY
NEAR SIDE ONLY
.30 TYP 6 HOLES
.30 REF
5.00
2.03
.65
.640
.500
.70
.230
90°
.875
E
04939